Vortices and Persistent Currents in Rotating Bose Gases - a Diagonalization Approach

Bargi, Sara

2010

Vortices and Persistent Currents in Rotating Bose Gases

—

a diagonalization approach

Sara Bargi

Division of Mathematical Physics, LTH
Lund University 2010

Printed in Sweden 2010
ISBN-978-91-7473-005-0

List of publications

This thesis is based on the following papers. The papers are included in Part II of the thesis.

I *Rotating Bose-Einstein Condensates Confined in an Anharmonic Potential*
S. Bargi, G. M. Kavoulakis, and S. M. Reimann
PHYSICAL REVIEW A **73**, 033613 (2006)

II *Mixtures of Bose Gases under Rotation*
S. Bargi, J. Christensson, G. M. Kavoulakis, and S. M. Reimann
PHYSICAL REVIEW LETTERS **98**, 130403 (2007)

III *Rotational Properties of a Mixture of Two Bose Gases*
J. Christensson, S. Bargi, K. Kärkkäinen, Y. Yu, G. M. Kavoulakis, M. Manninen and S. M. Reimann
NEW JOURNAL OF PHYSICS **10,** 033029 (2008)

IV *Mixtures of Bose Gases Confined in a Ring Potential*
J. Smyrnakis, S. Bargi, G. M. Kavoulakis, M. Magiropoulos, K. Kärkkäinen, and S. M. Reimann
PHYSICAL REVIEW LETTERS **103**, 100404 (2009)

V *Persistent Currents in Bose Gases Confined in Annular Traps*
S. Bargi, F. Malet, G. M. Kavoulakis and S. M. Reimann
Manuscript in preparation to be submitted to Phys. Rev. A

Papers not included in thesis:

1. *Two-component Bose gases under rotation*
S. Bargi, K. Karkkainen, J. Christensson, G. Kavoulakis, M. Manninen, and S. M. Reimann
AIP Conf. Proceedings **995**, 25 (2008)

2. *Vortices in rotating two-component boson and fermion traps*
S. Bargi, J. Christensson, H. Saarikoski, A. Harju, G. Kavoulakis, M. Manninen, and S. M. Reimann
Physica E **42**, 411 (2010)

3. *Coreless Vortices in Rotating Two-Component Quantum Droplets*
H. Saarikoski, A. Harju, J. Christensson, S. Bargi, M. Manninen, and S. M. Reimann
arXiv:0812.3366, accepted for publication in Europhysics Letters

Populärvetenskaplig sammanfattning

Roterande Bose-Einsteinkondensat

Tänk dig en gas instängd i en badringsformad behållare, och tänk dig att du snurrar på denna behållare. På grund av att atomerna eller molekylerna i gasen studsar mot små ojämnheter i behållarens väggar så kommer också gasen börja rotera. Det kanske tar tid för en gas jämfört med exempelvis en vätska, men med lite tålamod så kommer gasen rotera med samma hastighet som behållaren. Tänk nu att du stannar behållaren. Då borde ju gasen till slut också sluta snurra.

Om gasen är till exempel vanlig luft så kommer den också att göra det. Men om det istället är ett Bose-Einsteinkondensat kylt till nästan absoluta nollpunkten - då kommer gasen inte sluta rotera bara för att vi slutar snurra på dess behållare (som fortfarande kan vara badringsformad, men inte består av fast materia utan magnetfält). Istället kommer den fortsätta rotera, och fortsätta och fortsätta i "evighet" - det vill säga så länge någon lyckas hålla alla delar i experimentuppställningen under kontroll. Vilket gör att en "evighet" i dagsläget är tio sekunder lång.[1]

Bose-Einsteinkondensat är de kallaste system människan känner till; de är nästan en miljard gånger kallare än självaste världsrymden (som är cirka -270 grader Celsius). Det är just deras temperatur som är nyckeln till deras speciella egenskaper. Gasens beståndsdelar är nämligen vanliga atomer, som till exempel natrium och kalium - viktiga mineraler som bör ingå in en näringsriktig kost. Den som kan sitt periodiska system vet att dessa ämnen är metaller. Den som dessutom har viss livserfarenhet vet att metaller vid rum-

[1] Vi har för övrigt inte uppfunnit en evighetsmaskin utan bara upptäckt en gas som kan snurra utan friktion. Om vi skulle försöka använda gasen till att driva en motor så skulle den stanna.

stemperatur brukar vara fasta ämnen. Men genom vissa trick kan man hindra atomerna att övergå i fast form. Först hettar upp lite metall så att den övergår i gasform, och sen förtunnar man gasen i en vakuumkammare - den måste bli ungefär en miljon gånger tunnare än luft. Då tar atomerna väldigt lång tid på sig att samla ihop sig och bilda en fast metallbit. Sedan kan man kyla dem med hjälp av laserljus. Det går till ungefär så att man bombarderar atomerna med fotoner som rör sig i motsatt riktning, vilket (långsamt, långsamt - fotoner väger ju ingenting!) bromsar in atomernas rörelse. Till slut blir hela gasen så kall att den blir ett Bose-Einsteinkondensat.

Skillnaden mellan en vanlig gas och ett Bose-Einsteinkondensat påminner om den mellan vanligt ljus och laserljus: i vanligt ljus finns massor av fotoner med olika riktning och våglängd. Medan fotoner i laserljus alla har samma riktning och samma våglängd. Och så är de *koherenta*: varje fotons vågtoppar (och vågdalar) sammanfaller med nästas vågtoppar (och vågdalar).

Likadant är det med atomerna i ett Bose-Einsteinkondensat. Vid så låga temperaturer beter sig nämligen atomer också som vågor; det är ett av fundamenten i kvantmekanik. Och när alla atomernas vågor svänger i takt uppkommer en mängd spännande fenomen, varav evighetsrotationen bara är ett exempel.

Vad ska det vara bra för?

Det vet man inte riktigt än. Forskningen om Bose-Einsteinkondensat - BEC - är mestadels så kallad grundforskning; forskning för forskningens egen skull.[2] Men man har givetvis idéer. Det finns till exempel goda tecken på att Bose-Einsteinkondensat kan användas som mycket små gyroskop. Det har också påpekats att man med ett BEC kan efterlikna elektroniska system och alltså göra datorberäkningar - men i det här fallet är dagens elektroniksystem mycket mindre och det verkar osannolikt att din laptop skulle ersättas med några Bose-Einsteinkondensat.

En möjlig nytta som tilltalar undertecknad är en slags omvänd användning: kanske kan man använda Bose-Einsteinkondensat till att lösa avancerade matematiska ekvationer. Experimenten på BEC är nämligen oerhört reglerbara i flera avsikter; du har ett system helt utan orenheter och det mesta kan kontrolleras av labchefen, såsom huruvida atomerna attraherar eller repellerar varandra, och även hur de växelverkar med sin omgivning. Samtidigt finns det teoretiska modeller som mycket väl beskriver hur systemen beter sig. Om man

[2] Från början visste man inte heller vad elektricitet skulle användas till, och lasern ansågs länge vara en leksaksuppfinning.

utgår exempelvis från kvantmekanik så är den vår "bästa teori" och i princip antas den beskriva de här systemen exakt. Men det betyder bara att vi kan ställa upp exakta ekvationer; inte att vi alltid kan lösa ekvationerna. Här kanske Bose-Einsteinkondensaten kan hjälpa till: om vi har en ekvation vi vill lösa, så kan vi kanske istället göra upp ett experiment som beskrivs av just den ekvationen. Och istället för att försöka hitta lösningen matematiskt, så kan vi studera vårt experiment och se hur atomerna beter sig - det är ekvationens lösning.

I denna avhandling presenterar jag min forskning på roterande bosoner. Jag har bland annat räknat på vad som egentligen krävs för att ett Bose-Einsteinkondensat ska snurra i "evighet" - det gäller att atomerna repellerar varandra tillräckligt starkt. Jag har också hittat flera mycket enkla formler som exakt beskriver energin hos dessa system, vilket är ovanligt för komplicerade kvantmekaniska system. Etcetera etcetera. Jag använder mig av en metod som kallas *diagonalisering*; den bygger på kvantmekanikens lagar och går ut på att lösa ekvationer med hjälp av stora matriser.[3] Metoden är i princip exakt, men då krävs att du kan hantera matriser som är *oändligt* stora, och det är ju praktiskt omöjligt. Men precis som evigheten inte behöver vara längre än tio sekunder så behöver oändligt inte betyda så mycket. Det beror på vad man jämför med. Därför kan diagonaliseringsmetoden, om den tillämpas på små system, ge så gott som exakta resultat.

I dagsläget går det inte att dra slutsatser rakt av från mina beräkningar och applicera dem på experimenten, eftersom jag räknar på några tiotal atomer och experimenten hanterar miljontals atomer. Trots denna diskrepans kan diagonaliseringsmodellen tämligen väl beskriva många egenskaper hos verkliga Bose-Einsteinkondensat. Min förhoppning är att man i framtiden ska kunna göra experiment där man kan studera några få atomer åt gången. Då hade vi fått något som är ganska ovanligt i fysiken: en modell som utan approximationer beskriver ett verkligt system som saknar orenheter. Det är något att arbeta för i framtiden.

[3] Eller i praktiken - metoden går ut på att jag programmerar en dator att lösa ekvationer med hjälp av stora matriser.

Introduction

Bose-Einstein condensation (BEC) is a remarkable state of matter, where quantum mechanics shows up on a macroscopic scale and a range of different counter-intuitive phenomena occur. At zero temperature, non-interacting bosons will "condense" into their quantum mechanical ground state, so that they are all described by the same wavefunction. This was found by Bose and Einstein in the 1920's, and in honor of their contribution, the phenomenon now bears their name. It was first thought to be a curiosity without physical implications, but as it turned out, quite the opposite is true. In 1938 Kapitza, and independently Allen and Misener [1, 2], managed to cool liquid ^{4}He to below the so-called λ point (~ 2.17K) and discovered that it would flow through narrow channels apparently without friction. Kapitza referred to this as "superfluidity", and already the same year London [3] suggested that BEC could be the explanation for the observed phenomena. His model had some success, but liquid helium, being a strongly interacting, highly correlated liquid, is a difficult system to model and the nature of BEC in liquid helium is not yet fully understood.

In 1995 BEC was created in ultra-cold dilute atomic gases [4, 5]. For this achievement, Eric Cornell and Carl Wieman at JILA, and Wolfgang Ketterle at MIT were awarded the Nobel prize in Physics in 2001 [6, 7]. BECs are now predicted to be useful in such diverse areas as atom interferometers and atom lasers [8], for better understanding of condensed matter physics [9], or for example in connection with mathematical problems [10], for precision measurements [11], to do "atomtronics" (an atomic analog of electronics) [12, 13], and many others.

A BEC in a dilute atomic gas has some characteristic features. In order to keep the atoms from solidifying at these low temperatures, the gas must be dilute enough to make three-body collisions infrequent. This means densities are around 10^{13}atoms/cm^3 which is six orders of magnitude lower than the air we normally breathe. The transition temperature at which BEC takes place

is on the order of 100nK and the typical life time of a condensate ranges from seconds to minutes. They can be as large as 0.1mm, and since all atoms occupy the same quantum mechanical state, this means we have a truly macroscopic wavefunction.

These BECs are in several aspects ideal experimental systems, since they can be so well manipulated externally. The BEC is kept in a potential trap created either by a magnetic or optical field, or a combination of the two. The magnetic trap interacts with the hyperfine spin of the atoms, and hence it might not trap all hyperfine components of a given atom. This can be an asset, if one wants a completely pure system with only one hyperfine spin state present, or a problem if one wants to investigate e.g. a spinor condensate. However, optical traps will affect all hyperfine states similarly, and are thus ideal for investigation of spinor condensates. Also the potential form of the trap can be manipulated, and it is possible e.g. to create multiply connected traps.

Another convenient feature is that for atoms showing so-called Feshbach resonances [14, 15], the (effective) interactions between the atoms can be tuned by the experimenter. In fact, one can tune the interactions in real time from weakly repulsive to strongly repulsive, across the resonance to strongly attractive and on to weakly attractive. This is a very unusual feature in any experimental system, and adds to the importance of these systems as testing grounds for various theories.

Bose-Einstein condensates show a range of different counter-intuitive phenomena, and I have concentrated on two particular effects associated with rotational properties: quantized vortices and persistent currents. Vortices, of course, occur also in ordinary fluids - a giant hurricane being one of the most striking examples, where the vortex occurs in plain air. But in a BEC they only occur as quantized vortices, as I will explain in Sec. 2.1. Even more strikingly, if the fluid is set to rotate very fast, the vortices will appear in an ordered lattice, which indeed never happens in any ordinary fluid. Persistent currents can occur if the container in which the fluid is kept has the shape of an annulus. Then, under certain conditions, once the gas is set to rotate it will keep rotating for an "infinite" amount of time.

Counter-intuitive phenomena like these are interesting in themselves. But they are also of importance due to the connections to other fields of research: they are part of the collection of phenomena that go under the name of "superfluidity" which is still today not fully understood. Superfluidity, furthermore, is connected to superconductivity. Through the exploration of (rotating) Bose-Einstein condensation, the hope is that we can apply the knowledge to get a

better view on also other areas of physics.

Though once perhaps met with disbelief, Bose-Einstein condensation of cold bosons is now an accepted consequence of statistical mechanics and a vast field of research. Text books [16, 17] as well as review articles are written on both the general subject of BEC [18, 19], and more specialized subfields; of importance to the results presented in this thesis are particularly the reviews [20, 21, 22, 23].

This thesis is based on five papers referred to as Paper I - V. These are found in Part II of this volume, which also contains a summary of each paper along with a specification of my own contributions. Part I begins with a general introduction to the research field in Chapters 1 and 2. Results from various calculation methods are reported in several of the Papers, but my own contribution is based on the diagonalization method presented in Chapter 3. The results presented in Chapters 4 and 5 are biased towards this method in order to reflect my own work.

More specifically, in Chapter 1 some general results on BECs and the particular requirements of these ultra low temperature experiments (Sec. 1.1) are described. The commonly used Gross-Pitaevskii mean-field equation is introduced in Sec. 1.2, and the ground state of the Bose gas is derived in Sec. 1.3. Sections 1.4 and 1.5 treat two relevant special cases, namely the two-component condensate and the attractively interacting condensate.

Chapter 2 discusses properties of the rotating Bose gas, giving general results on several subjects. The quantization of circulation condition that a BEC must obey is derived in Sec. 2.1, where also vortices are introduced. The two particular regimes of strong interaction (Thomas-Fermi regime) and weak interaction are separately addressed in Secs. 2.2 and 2.3, which include accounts of illustrative experiments. Finally two particular trapping potentials, the anharmonic (Sec. 2.4), and the ring-like (Sec. 2.5), are considered.

Chapter 3 gives an introduction to the method of diagonalization, and the particulars when applying this method to trapped rotating Bose systems. In Chapt. 4 we report our results on vortices in rotating Bose gases, and in Chapt. 5 our results on persistent currents in ring-like traps. Finally, some conclusions and an outlook are given in Chapt. 6.

Acknowledgements

I opened my first book on quantum mechanics when I was 14, and since I did not understand anything of it, I found it extremely interesting. I still open books on quantum mechanics and find it extremely interesting. As to the question of "understanding", I have adopted a more pragmatic approach. If it works, it works. Or in swedish: det är fett när det är fett.

This is my attempt to thank those who helped me escape the complicated domain of Slater determinants and Pauli principles, and introduced me to the peaceful world of bosons. First of all Stephanie Reimann, my supervisor during these four years. I am grateful that you took this time to guide me through the world of Physics, in matters theoretical as well as material. Together we have solved many puzzles large and small, but thankfully, quite a few remain.

I am also indebted to Georgios Kavoulakis, whose vast knowledge in this field has been an invaluable asset. Oh my goodness, where would we be without you!

There are also other people who deserve mentioning. Sven Åberg for his advice on questions big and small. My colleagues. Teachers and students - I have learned a lot from my teachers, but probably even more from the students I have met.

And now I have to change languages. Magnus och Marc, utmärkta kontorskompisar, tack. Monica och Märta, vänner på Fysicum och utanför. Anja och Bengt och alla andra.

Slutligen vill jag tacka min familj, mamma, pappa, Åke, Måns och Sussie - särskilt Sussie, tack så oändligt mycket för all hjälp. Och Spott, som genom hundratals vita hårstrån är den enda som finns med mig på jobbet varje, varje dag.

Contents

Part I

Introduction to Rotating Bose-Einstein Condensates

Chapter 1

General Properties of the Bose Gas

The essence of BEC is the following: bosons do not obey the Pauli principle and there is no restriction to the number of particles occupying any single-particle state. At zero temperature, indistinguishable non-interacting bosons will all be in their lowest-energy state, sharing the same wavefunction, and thus all properties. It is not *a priori* obvious that also interacting bosons at non-zero temperature must "condense" into the same ground state. However, statistical arguments show that below a critical transition temperature, a finite fraction of the total number of bosons will occupy the same state. When it comes to interactions, it can be shown [19] that at least in some limit where they are not too strong these in fact tend to reinforce the formation of BEC, since the exchange interaction between two bosons favors them being in the same single-particle state. If nothing else, the Nobel prize winning experiments [4, 5, 6, 7] clearly showed the condensation of interacting bosons through direct measurements of the momentum distribution of the particles.

Quantum effects become important in a gas when the de Broglie wavelength of the constituents becomes comparable to the typical distance between the particles. A simple order-of-magnitude calculation reveals some of the physics involved in the transition [16, 20]. At a temperature T, the typical thermal energy is $k_B T$, where k_B is the Boltzmann constant. Equating this energy with the kinetic energy of the particles gives the thermal momentum $p_T \sim \sqrt{2Mk_BT}$. Translating into wavelength, we find for the thermal

wavelength λ_T

$$\lambda_T \sim \frac{h}{\sqrt{2Mk_BT}}. \tag{1.1}$$

If the density of the gas is n, then the typical distance between the particles is $n^{-1/3}$ in three dimensions. By equating with the thermal wavelength this gives the critical temperature T_c for when quantum effects become important as

$$T_c \sim \frac{2\pi^2\hbar^2 n^{2/3}}{Mk_B}. \tag{1.2}$$

This form of the dependence explains why we need ultra low temperatures to create a BEC in a gas which is extremely dilute. If we have e.g. $n \sim 2.5 \cdot 10^{12}\text{atoms/cm}^3$ and try to condense ^{87}Rb atoms, then Eq. (1.2) gives a transition temperature $\sim$ 200nK. This is in good agreement with the actual experiment where these figures come from, Ref. [4], where they found a condensate fraction appearing at 170nK. These are exceptional experimental conditions which require particular care in the setup of an experiment.

1.1 Cooling, Trapping and Imaging of BECs

The general experimental procedure in which a dilute gaseous BEC is created requires the three essential elements laser cooling (or sympathetic cooling), magnetic and/or optical trapping, and evaporative cooling. For the present discussion of these I rely on Ref. [16]. The BECs under consideration occur in atomic gases, and the hyperfine interaction splits the ground state energy of the atom. In alkali atoms such as ^{87}Rb, ^{23}Na and ^{7}Li, the nuclear spin is $I = 3/2$, which combines with the electronic spin $J = 1/2$ to give two different hyperfine states with $F = 1$ or $F = 2$, respectively. Each of these multiplets can then be split by the Zeeman effect if an external magnetic field is applied. The energies of some states of the multiplet will decrease with increasing magnetic fields and these atoms cannot be magnetically trapped since it is impossible to create a local maximum of the magnetic field. But some hyperfine spin components can decrease their energy by finding a minimum in the magnetic field and can thus be trapped magnetically. However, since this method only traps certain hyperfine states, it is important to reduce the effects of spin-flipping processes since these can cause atoms to escape the trap. The depth of the magnetic trap is determined by the Zeeman energy, and is usually much smaller than 1K.

Atoms can also be trapped by optical means. The electrical field induced by a focused laser beam creates a dipole moment in the atoms, which shifts

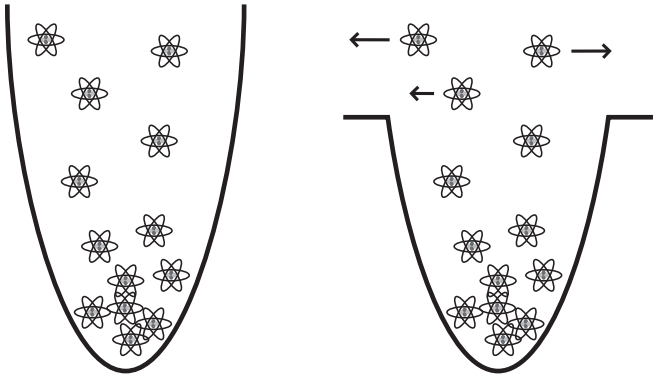

Figure 1.1: Schematic figure of evaporative cooling. If we lower the edges of the trap, as in the figure to the right, then atoms with an energy above the edges can escape. This will decrease the average temperature of the atoms remaining in the trap.

their energy and thus can confine them in a small region of space. The depth of an optical trap is on the order of μK, and thus excessive cooling is required before the atoms can be optically trapped. An advantage of the optical trap is that it affects all hyperfine spin states similarly, and thus spinor condensates can be investigated in such a setup.

Laser cooling is a conceptually simple and appealing idea. Two counter-propagating laser beams are tuned to a frequency slightly smaller than an atomic transition in the atoms to be cooled; these are placed between the two (or six, in a three-dimensional setup) lasers. An atom at rest will absorb equally many photons from both beams. However a moving atom will experience a Doppler shift in the laser frequency, and if it is moving to the right, will absorb more photons that are moving opposite to its direction of motion. In this absorption process, the momentum of the photon is transferred to the atom, and since it is opposite to the direction in which the atom is moving, the atom will be slowed down. This process can cool atoms to a temperature on the order of hundreds of microkelvins.

Laser cooling is generally not enough to achieve high degrees of condensation. Therefore evaporative cooling is used as the final stage of a BEC creation. The process is again conceptually simple: if we let the hottest atoms escape the trap, then the average temperature of the atoms still in the trap is lowered. Schematically, we can draw a trap with flat edges at a given energy; atoms above this energy will then be able to escape, as illustrated in Fig. 1.1.

Finally a method is needed to somehow detect the condensate. Since the

BECs are so "big" - up to several hundreds of micrometers - they can be imaged by ordinary laser light. There are possibilites to do non-destructive imaging, but when investigating e.g. vortices the vortex cores are too small to be resolved. Usually one instead turns off the trap and lets the condensate expand, and then images the enlarged cloud.

1.2 The Gross-Pitaevskii Equation

The Gross-Pitaevskii (GP) equation is the most widely used tool to model BECs, and it has been applied with considerable success to explain various phenomena related to BEC. Detailed accounts are given in e.g. the textbooks [16, 17]; following here is a recapitulation weighted towards what is needed to understand rotation.

Modelling a BEC in a dilute gas is simplified because for many situations, we can assume that all particles indeed reside in the ground state (this approximation will be justified towards the end of this section). We consider zero temperature. With all particles in the condensed state, one can make an ansatz for the many-body wavefunction as a simple product state, which is the mean-field approximation. If we call the single-particle wavefunction of the ground state ϕ_0 and the (spatial) coordinate of the ith particle $\mathbf{r}_i$, then the many-body state Φ is a simple product function such that

$$\Phi(\mathbf{r}_1, ..., \mathbf{r}_N) = \prod_{i=1}^{N} \phi_0(\mathbf{r}_i). \tag{1.3}$$

We can make a drastic reduction of the number of variables from $3N$ to 3 through the concept of a *condensate wavefunction,* Ψ. This is defined as

$$\Psi(\mathbf{r}) = \sqrt{N}\phi_0(\mathbf{r}), \tag{1.4}$$

and as we see it is normalized to the number of particles N. This is the macroscopic wavefunction which is often referred to in the context of BEC. Also the term *order parameter* is frequently used.

Neutral atoms are considered to interact via the van der Waals interaction, $-\alpha/(\mathbf{r} - \mathbf{r}')^6$, plus a hard-core repulsion at short distance. With a density n, the typical distance between the particles is $\sim n^{-1/3}$. If the gas is so dilute that the scattering length is much smaller than this distance,

$$|a_s| \ll n^{-1/3}, \tag{1.5}$$

then short-wavelength oscillations can be safely neglected.

Now consider a system with very low energy. If the temperature is e.g. well below the critical temperature for BEC, then from Eq. (1.2), we find that the momenta p always satisfy

$$\frac{p}{\hbar n^{1/3}} \ll 1. \tag{1.6}$$

Again $n^{-1/3}$ is the typical distance between particles. It can be shown that for such small momenta, the scattering is independent of the exact scattering energy, and furthermore isotropic. It is characterized by one single parameter, the s-wave scattering length a_s, which is positive for repulsive interactions and negative for attraction. Under these circumstances it is sufficient to model interactions with a simple "pseudo-potential" contact interaction

$$U_0\delta(\mathbf{r}-\mathbf{r}') = \frac{4\pi\hbar^2 a_s}{M}\delta(\mathbf{r}-\mathbf{r}'), \tag{1.7}$$

where M is the atomic mass. References [16, 24] discuss in detail the subject of interactions in cold atom gases.

Using the δ function for the interaction greatly simplifies things. Including the usual kinetic energy term and a potential $V(\mathbf{r})$, the Gross-Pitaevskii energy functional for the condensate wavefunction Ψ is

$$E[\Psi] = \int d\mathbf{r}\left(\frac{\hbar^2}{2M}|\nabla\Psi|^2 + V(\mathbf{r})|\Psi|^2 + \frac{U_0}{2}|\Psi|^4\right), \tag{1.8}$$

where we have used $N-1 \sim N$ in the limit of large particle numbers; i.e., terms of order $1/N$ have been ignored. By minimizing this expression with respect to Ψ^*, with the normalization constraint $N = \int |\Psi|^2 \,\mathrm{d}\mathbf{r}$, we can derive the widely used Gross-Pitaevskii (GP) equation which reads

$$\left(-\frac{\hbar^2}{2M}\nabla^2 + V(\mathbf{r}) + U_0|\Psi(\mathbf{r})|^2\right)\Psi(\mathbf{r}) = \mu\Psi(\mathbf{r}), \tag{1.9}$$

where μ is the chemical potential. The GP equation is a non-linear Schrödinger-like equation, where interactions are treated in a mean-field approximation. Thus we do not expect it to do well if correlations between individual atoms are strong. It may be solved self-consistently. One way of doing this is by transforming it into a diffusion-like equation and propagate in imaginary time [25], a method which can find a local or global energy minimum.

The Gross-Pitaevskii equation as presented in Eq. (1.9) relies on one single-particle state being macroscopically occupied, i.e., the number of particles in the condensed state $N_0 \approx N$. In reality an interacting condensate will always be *depleted* to some extent, i.e., a number of particles will occupy other states.

A small amount of depletion can be accurately accounted for employing a Bogoliubov approach [16, 17]. This indeed shows the fraction of particles out of the condensate to be $(N - N_0)/N_0 \sim (na^3)^{1/2}$. The gas parameter na^3 was already assumed to be small in order to be able to use the mean-field approximation. This is in marked contrast to superfluid liquid helium; a system which is not dilute and has a condensate fraction N_0/N typically smaller than 10%.

1.3 Ground State of the Bose Gas

A Bose-Einstein condensate in a trap behaves very differently from the homogeneous condensate - one striking example of this will is the attractively interacting condensate which cannot even exist without the trap, as explained in Sec. 1.5. The potential traps that confine the atoms can be tailored to have a number of different shapes, but the simplest is the harmonic trap potential

$$V(\mathbf{r}) = \frac{1}{2}M\left(\omega_x^2 x^2 + \omega_y^2 y^2 + \omega_z^2 z^2\right), \tag{1.10}$$

which in the most general case has three different trapping frequencies. However it is now sufficient to consider the isotropic case and thus we set all trapping frequencies equal, $\omega_x = \omega_y = \omega_z = \omega$. In an isotropic harmonic potential, the dimensionless parameter which characterizes the solutions to the GP equation is $Na_s/a_{\rm osc}$, where $a_{\rm osc} = \sqrt{\hbar/M\omega}$ is the oscillator length. If $Na_s/a_{\rm osc}$ is large we are said to be in the Thomas-Fermi regime, and if it is small the system is said to be weakly interacting. We start by considering this latter case.

If the condensate density $n(\mathbf{r}) = |\Psi(\mathbf{r})|^2$ is slowly varying over the extent of the condensate, R, then the potential energy per particle is of the order $M\omega^2 R^2/2$. From Heisenberg's uncertainty principle, we find that the momentum of a particle in its ground state is $\sim \hbar/R$ and thus its kinetic energy is $\hbar^2/(2MR^2)$. So for a non-interacting condensate, the total energy varies as R^{-2} for small R, and R^2 for large R, with an energy minimum for

$$R = \sqrt{\frac{\hbar}{M\omega}} \equiv a_{\rm osc}, \tag{1.11}$$

where we have defined the standard oscillator length $a_{\rm osc}$. So, unsurprisingly, for a non-interacting condensate in a harmonic trap we find that the condensate size is the oscillator length. This result is also obvious from inspecting the GP equation (1.9): without interactions, it reduces to the Schrödinger

equation for a particle in a harmonic potential, and the solutions are familiar. The non-interacting case can thus be solved exactly and analytically also for a many-particle system.

In the following we will study rotational symmetry in the xy plane and thus we set $\omega_x = \omega_y = \omega$. We will assume ω_z to be very large. A large trapping frequency means a tight confinement in the z direction; thus the condensate will be of oblate shape. Furthermore, if $\hbar\omega_z$ is much larger than the typical strength of the interaction, then we can consider the condensate to be in its z direction ground state, and thus the system is effectively two-dimensional. The wavefunction in the z direction is the Gaussian

$$\phi_0(z) = \frac{1}{(a_z^2\pi)^{1/4}} e^{-z^2/2a_z^2}, \tag{1.12}$$

where $a_z = \sqrt{\hbar/(M\omega_z)}$ is the oscillator length in the z direction. Going from three dimensions to two is done by integrating over the z direction, which will change all energies by an offset which is equal to $\hbar\omega_z$ and rescale the interaction strength such that $U_{2D} = U_{3D}/(\sqrt{2\pi}a_z)$. For notational simplicity we will write $U_{2D} \equiv U_0$.

Our non-interacting Hamiltonian is simply a sum of single-particle operators,

$$H = \sum_{i=1}^{N} \left(-\frac{\hbar^2}{2M}\nabla_i^2 + \frac{1}{2}M\omega^2\rho_i^2 \right), \tag{1.13}$$

where we have introduced cylindrical coordinates (ρ, φ) and assumed all particles to be of equal mass M. The eigenfunctions of the Hamiltonian are known to be

$$\phi_{nm}(\rho,\varphi) = \sqrt{\frac{2n_r!}{(n_r+|m|)!}} \rho^{|m|} \mathcal{L}_{n_r}^{|m|}(\rho) e^{-\rho^2/2a_{\text{osc}}} \frac{e^{im\varphi}}{\sqrt{2\pi}}, \tag{1.14}$$

where $\mathcal{L}_{n_r}^{|m|}(\rho)$ are the associated Laguerre polynomials, and the oscillator length in the radial direction $a_{\text{osc}} = \sqrt{\hbar/M\omega}$. We have two quantum numbers n_r and m, where n_r is the number of radial nodes, and $\hbar m$ is also the eigenvalue of the angular momentum operator L_z and is thus important for rotation.

The energy of the system is just the sum of the single-particle energies,

$$E = \hbar\omega \sum_{i=1}^{N} \left(2n_{r,i} + |m_i| + 1\right). \tag{1.15}$$

This energy is obviously minimized by putting $n_{r,i} = m_i = 0$, in which case we have simply $E = N\hbar\omega$.

If interactions are sufficiently weak, $nU_0 \ll \hbar\omega$, where now n is the density, they can be treated as a perturbation. Approximate wavefunctions can be found e.g. by the variational principle; a reasonable trial wavefunction is a Gaussian with the width $\alpha a_{\rm osc}$ as a variational parameter. Weakly repulsive interactions will then slightly expand the condensate, but its width will still be on the order of $a_{\rm osc}$.

For completeness I will also briefly discuss the so-called Thomas Fermi limit, where the interactions are strong, $Na_s/a_{\rm osc} \gg 1$, implying that the kinetic energy term in Eq. (1.9) can be ignored. Solving the Gross-Pitaevskii equation Eq. (1.9) is now greatly simplified and one finds for the density $n = |\Psi(\mathbf{r})|^2$:

$$n(\mathbf{r}) = \frac{\mu}{g} - \frac{M\omega^2}{2g} r^2 = n(0)\left(1 - \frac{r^2}{R_0^2}\right), \tag{1.16}$$

with $r^2 = x^2 + y^2 + z^2$, the central density $n(0) = \mu/g$, and the condensate radius $R_0 = 2\mu/M\omega^2$. This is the so-called Thomas-Fermi density profile, an inverted parabola. Most experiments are performed in this limit and indeed fits of the experimental profile to Eq. (1.16) are used to calculate e.g. the temperature of the condensate.

1.4 Two-Component Condensates

The versatility of the BEC experiments in dilute alkali gases allow for exploration of multi-component condensates; see e.g. the review [21] and references therein. A mixture could be made by trapping different atoms [26] or by trapping more than one internal spin state of the atom. Depending on the experimental setup, the particle number in each species could be conserved [27], or spin dependent interactions could be allowed in which case one has a spinor condensate [28]. More generally it is also possible to mix fermions and bosons [29].

The behavior of a two-component Bose gas is not trivial, but the generalization of its theoretical modelling is straightforward. We label the two components A and B, there are N_A and N_B atoms of each kind, and if the particles are distinguishable there will be two separate condensate wavefunctions Ψ_A and Ψ_B. Each of these is defined as in Eqs. (1.4) and (1.3) and normalized such that $\int |\Psi_A|^2 \, d\mathbf{r} = N_A$ and $\int |\Psi_B|^2 \, d\mathbf{r} = N_B$. If the two different species are distinguishable, the new interaction term that arises in the Hamiltonian

is

$$V_{AB} = U_{AB} \sum_{k=1}^{N_A} \sum_{l=1}^{N_B} \delta\left(\mathbf{r}_k - \mathbf{r}_l\right), \tag{1.17}$$

where U_{AB} is the parameter for the interspecies interaction (since the two species are distinguishable, there is no double counting in the sum and thus no factor of 1/2). The GP equation (1.9) can be readily generalized to describe a system of two or more components [16]. Generalizing Eq. (1.8) and minimizing, we get two coupled equations

$$\begin{aligned} \left(-\frac{\hbar^2}{2m}\nabla^2 + V + U_{AB}\left|\Psi_B\right|^2\right)\Psi_A + U_{AA}\left|\Psi_A\right|^2\Psi_A &= \mu_A\Psi_A, \\ \left(-\frac{\hbar^2}{2m}\nabla^2 + V + U_{AB}\left|\Psi_A\right|^2\right)\Psi_B + U_{BB}\left|\Psi_B\right|^2\Psi_B &= \mu_B\Psi_B, \end{aligned} \tag{1.18}$$

where U_{AA} and U_{BB} are the intraspecies interaction parameters. The expression within parentheses indicates that the density of one component yields an effective "external potential" on the other component.

In a two-component condensate, the question arises whether the two components will be overlapping in space or whether they will separate. In the case of a uniform condensate in a box potential, it is known [16] that the two species are miscible if $U_{AB}^2 < U_{AA}U_{BB}$; otherwise they will separate. For the trapped condensate, the situation is more intricate and regions of phase separation or overlap depend non-trivially on the parameters of the system [30, 31, 32, 33].

1.5 Attractive Condensates

Bose-Einstein condensates with repulsive interactions have gained more attention than their attractive counterparts. However ^{7}Li has a negative scattering length, and for species that exhibit Feshbach resonances, the scattering length can be externally tuned to become negative [34]. As already mentioned, the trap plays a particularly important role for the attractively interacting quantum gas: in a homogeneous setting, even if the gas is originally perfectly isotropic, any perturbation will cause the particles to aggregate and eventually collapse. Also with the trap present, the absolute lowest-energy state in the GP description will always be a collapsed state, but there can be regions of metastability for the existence of an attractively interacting condensate: if the size of the condensate is $\sim R$, then the kinetic energy scales as R^{-2},

for a three-dimensional system the interaction energy scales as R^{-3}, and in a harmonic potential, the trap energy scales as R^2.

Following Ref. [17], let us be more specific. For a three-dimensional system in a harmonic trap we make an ansatz for the condensate wavefunction

$$\Psi = \left(\frac{N}{R^3 \pi^{3/2}} \right)^{1/2} e^{-r^2/2R^2}, \tag{1.19}$$

where again R is the typical extension of the atomic cloud. We evaluate the terms of the GP energy functional Eq. (1.8) to find the kinetic energy

$$E_{\rm kin} = \frac{3\hbar^2 N}{4MR^2}, \tag{1.20}$$

the potential energy of the trap

$$E_{\rm trap} = \frac{3}{4} N M \omega^2 R^2, \tag{1.21}$$

and the interaction energy

$$E_{\rm int} = \frac{N^2 U_0}{\sqrt{32\pi} R^3}. \tag{1.22}$$

For attractive interactions the scattering length is negative and thus $U_0 = 4\pi\hbar^2 a_s/M < 0$. We can express the size of the condensate in terms of the oscillator length, $R = \alpha a_{\rm osc}$ and find the total energy as a function of α,

$$E(\alpha)/N\hbar\omega = \frac{3}{4}\frac{1}{\alpha^2} + \frac{3}{4}\alpha^2 - \frac{1}{\sqrt{2\pi}} \frac{N\left|a_s\right|}{a_{\rm osc}} \frac{1}{\alpha^3}. \tag{1.23}$$

This function is plotted in Fig. 1.2 for different values of the dimensionless parameter $N\left|a_s\right|/a_{\rm osc}$. The dotted lines correspond to the homogeneous case with no trap present; clearly there is no stable condensate size here. The full-drawn lines include the trap term which can stabilize the system in a local minimum of $E(\alpha)$ if the dimensionless parameter $N\left|a_s\right|/a_{\rm osc}$ is not too large. Interestingly, under rotation the centrifugal force further helps to balance the negative interaction energy, so that there can be a metastable condensate at even larger magnitudes of the scattering length.

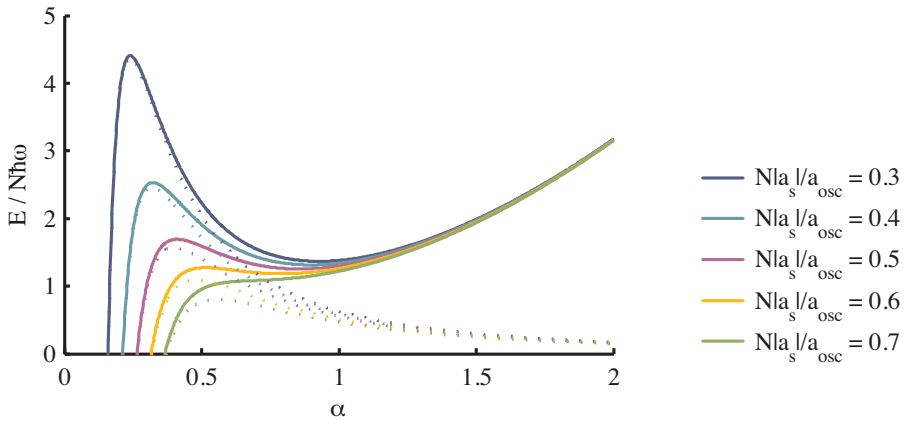

Figure 1.2: Energy per particle as a function of the dimensionless parameter α which determines the size of an attractive condensate. The energy for a condensate in a spherical trap is plotted as solid lines, and the dotted lines give the result for the corresponding homogeneous Bose gas. If the dimensionless parameter $N\left|a_s\right|/a_{\mathrm{osc}}$ is not too large, and attractively interacting condensate can exist in a metastable state in a harmonic trap.

Chapter 2

Properties of the Rotating Bose Gas

The Bose gas under rotation is of particular interest since it shows many counter-intuitive phenomena such as quantized vortices, vortex lattices and persistent currents. In the fast rotating limit, there are connections to the quantum Hall effect; see e. g. Refs. [22, 35, 36]. Other rotational aspects which have received attention recently are "quantum turbulence" [39, 40, 41], the Sagnac effect [42], the "vortex pump" [37, 38], dipolar gases in toroidal traps [43], and vortex dipoles [44]. All these effects originate from the requirement that the condensate wavefunction be single-valued, which puts restrictions on the rotational motion that the condensate can acquire.

2.1 Quantization of Circulation in a Bose-Einstein Condensate

One of the most remarkable properties of BEC is the quantization of circulation, which follows rather straightforwardly from the Gross-Pitaevskii equation [16]. A condensate wavefunction $\Psi(\mathbf{r}, t)$ can always be written in terms of a density n and a phase S:

$$\Psi(\mathbf{r}, t) = \sqrt{n(\mathbf{r}, t)} e^{iS(\mathbf{r},t)}, \tag{2.1}$$

where we have included the time dependence of the variables. If we insert this expression into the time-dependent Gross-Pitaevskii equation, we can derive two so-called *hydrodynamic* equations, similar to the hydrodynamic equations

of ordinary fluid mechanics. The force-type (Bernoulli) equation is

$$M\frac{\partial \mathbf{v}_s}{\partial t} = -\nabla\left(\tilde{\mu} + \frac{1}{2}Mv_s^2\right), \tag{2.2}$$

where $\mathbf{v}_s$ is the superfluid velocity which we will return to soon, and

$$\tilde{\mu} = V + nU_0 - \frac{\hbar^2}{2M\sqrt{n}}\nabla^2\sqrt{n}. \tag{2.3}$$

The other equation given by this procedure has the form of a continuity equation

$$\frac{\partial n}{\partial t} + \nabla\cdot\mathbf{j} = 0, \tag{2.4}$$

where $\mathbf{j}(\mathbf{r}, t)$ is the current density; in quantum mechanics it is written as

$$\mathbf{j}(\mathbf{r}, t) = -\frac{i\hbar}{2M}\left(\Psi^*\nabla\Psi - \Psi\nabla\Psi^*\right), \tag{2.5}$$

and if we apply this to the condensate wavefunction written in the form of Eq. (2.1), we find

$$\mathbf{j}(\mathbf{r}, t) = n\frac{\hbar}{M}\nabla S. \tag{2.6}$$

Since the current is a density times a velocity, it is reasonable to define the superfluid velocity as

$$\mathbf{v}_s = \frac{\hbar}{M}\nabla S. \tag{2.7}$$

The fact that the velocity is the gradient of the phase has far-reaching consequences when combined with the requirement that the condensate wavefunction must be single-valued at any given point in space. If we integrate the phase along a closed contour in space, it must change by an integer multiple of 2π,

$$\Delta S = \oint \nabla S \cdot d\mathbf{l} = 2\pi m. \tag{2.8}$$

The integer m is called the *winding number.* We see from Eqs. (2.7) and (2.8) that the circulation of the superfluid velocity has to be quantized as

$$\oint \mathbf{v}_s \cdot d\mathbf{l} = \frac{\hbar}{M}2\pi m. \tag{2.9}$$

If m is zero the flow is irrotational. If $m > 0$, then there is a singularity inside the encircled area. This singularity must be accompanied by a density

node, because if there is a point where the velocity goes to infinity, then the density at that same point must be zero. From Eqs. (2.8) and (2.9) we see that this vanishing density is accompanied by a phase change of $2\pi m$. This is exactly the definition of a quantized vortex: a density node around which the circulation is quantized.

A general solution to the GP equation, which has a vortex line on the z axis, can be written

$$\Psi(\mathbf{r}) = e^{im\varphi} \left|\Psi(\rho, z)\right|, \tag{2.10}$$

where we have used cylindrical coordinates (ρ, φ, z) and m is an integer. Note that in the case of more complicated wavefunctions, this "m" is not necessarily the same as in Eq. (2.8), as we will later see. The superfluid velocity is tangential and from Eq. (2.7) given by

$$v_s = \frac{\hbar}{M}\frac{m}{\rho}. \tag{2.11}$$

This expression is fundamentally different from rigid-body rotation where

$$\mathbf{v} = \mathbf{\Omega} \times \mathbf{r}, \tag{2.12}$$

i.e., the further from the center of rotation, the greater the speed. For a single vortex, however, the speed of rotation is proportional to the *inverse* of the distance from the center of rotation. In a condensate rotating at high speed, we can retrieve again the rigid-body result. In this case, the bosonic cloud will be pierced by many vortices forming a lattice, and on a larger scale as we take the average, the velocity field will follow Eq. (2.12) [16, 20].

Consider a wavefunction of the type Eq. (2.10), and assume that Ψ has one single node, at the origin. The angular momentum per particle is then equal to $m\hbar$. (A two-dimensional analysis suffices for our purposes, and thus we identify the expectation value of the angular momentum operator with its z component, $\langle L\rangle \equiv L_z$). If $m = 1$, this is a singly quantized vortex state, and for $m > 1$ the vortex is multiply quantized. In a harmonic trap, the energy of several singly quantized vortices is always lower than the energy of any multiply quantized vortex [16, 45] - a hand-waving argument is that the energy (in the Thomas-Fermi limit) of a vortex depends on the winding number m as m^2. Thus, the system can save energy by having several vortices with unit winding number, rather than one with higher circulation. In a weakly interacting condensate, Refs. [46, 47] showed that again, in the harmonic potential, singly quantized vortices are always favored. It has also been shown experimentally [48] how a doubly quantized vortex spontaneously splits into two.

The state where there is a singly quantized vortex at the center of the trap, with $\hbar$ units of angular momentum per particle, is often called a *unit vortex*. Note though that the requirement in Eq. (2.9) that the circulation be quantized, does not necessarily imply there is quantized angular momentum *per particle*. For a non-central singly quantized vortex, the angular momentum per particle is less than $\hbar$, and it depends on the vortex position in a non-trivial way. The situation is clarified in e.g. Ref. [20]; see also references therein.

2.2 Rotation in the Thomas Fermi Regime

Most experiments are performed in the Thomas Fermi regime which we briefly discussed in Sec. 1.3, where $Na_s/a_{\rm osc} \gg 1$ and the condensate density profile has the shape of an inverted parabola. Because of this, I will go through some of the results for a rotating condensate in this limit, but I would like to stress that these results are not necessarily valid in the weakly interacting system.

In a rotating condensate in the Thomas-Fermi regime, the vortex core size is on the order of the so-called healing length ξ. The healing length is found by comparing the kinetic energy term in Eq. (1.9) with the interaction energy term $U_0 n$, which gives

$$\xi = \frac{\hbar}{\sqrt{2MU_0 n}} = \frac{1}{\sqrt{8\pi a_s n}}, \tag{2.13}$$

where we have used $U_0 = 4\pi\hbar^2 a_s/M$. It can be shown that in the Thomas-Fermi regime [16, 20], we have a clear separation of length scales $\xi \ll a_{\rm osc} \ll R_0$, i.e., the the vortex core size is small compared to the oscillator length, which in turn is small compared to the size of the condensate R_0. We want to emphasize that this is not true in a weakly interacting condensate, where both the condensate size, and the size of the vortex core, are of the same order of magnitude as the oscillator length.

By allowing for the trapping potential to be rotated in the GP description, one can study the energetic stability of a vortex in a harmonic trap [20]: the energy of the vortex can be calculated as a function of its position in the condensate. If the external rotational frequency $\Omega = 0$, then the energy for a vortex as a function of its displacement from the trap center is monotonically decreasing, i.e., if a vortex is somehow created at the trap center, the condensate can decrease its energy if the vortex is moved out of the condensate. In practice, it will spiral outwards since a vortex moves with the local velocity of the fluid [49, 50, 45, 51]. However, the energy of a vortex at the trap center decreases as Ω is increased, and at a specific critical frequency, the energy of a

vortex at the center of the condensate has the same energy as a vortex outside of the condensate (i.e. a non-rotating condensate). Importantly, there is an energy barrier between these two states, so if there is a vortex created at the center, moving it out of the condensate would instead cost energy. This implies that at this critical rotational frequency, a central vortex is energetically stable.

Turning to the experimental achievements, the first vortex state that was realized in a dilute gaseous BEC was created in a two-component system [52]. The scheme had been proposed shortly before [53], and used external fields to induce a coupling between internal states of the atoms and the spatial wavefunction. The successfully created vortex was *coreless*, meaning that only one component was rotating, while its core was filled by the other component. It was also possible to remove the non-rotating component, and the vortex would remain. More importantly, it was possible to image the phase difference between the two components. The non-rotating one must have a constant phase so the phase difference image in effect showed the phase of the rotating component, which verified that indeed the phase varied from 0 to 2π around the core. This is evidence of a quantized vortex.

Subsequently, new methods were developed to induce rotation in a BEC. One way is to make the trapping potential slightly anisotropic, and then rotate this potential [54]. This is more similar to how superfluidity is observed in experiments on liquid helium, where the fluid is kept in a container which is rotated, and the surface roughness of the container walls exert forces on the fluid to set it in motion. Madison *et al.* [54] used a laser beam to mimic such a 'rotating bucket' experiment. They observed the formation of first one vortex in the condensate, and then as the rotational speed was increased, the stable states contained two, three, or four vortices. However, their measured frequencies of external rotation where the vortices occurred, did not match the current theoretical predictions which stated at which rotational frequency a certain state would have a lower energy. To explain this difference, one needs to dynamically study how the vortices actually nucleate in the condensate. Sinha and Castin [55] showed how dynamical instabilites could be a source of vortex nucleation: for a frequency $\Omega/\omega_{\text{osc}} \approx 1/\sqrt{2}$, where Ω is the external rotation frequency and ω_{osc} is the trap frequency (in the absence of anisotropic modification), the stirring resonantly excites a quadrupole mode of the condensate, such that the condensate starts to oscillate. Since this mode is dynamically unstable, it grows and then vortices can appear.

The existence of vortex lattices has also been verified experimentally [56]; as many as 130 vortices were noticed in these first experiments. It is important

to note that in the fast-rotating regime $\Omega \to \omega$ the condensate will become effectively unconfined since the centrifugal force competes with the trapping potential to give an effective confinement

$$V_{\text{eff}} = \frac{1}{2} M \rho^2 \left(\omega^2 - \Omega^2\right). \tag{2.14}$$

The fast-rotating regime introduces interesting physics [22, 35], but the loss of confinement has made it difficult to reach experimentally. This is one motivation for the investigation of other confining potentials, as will be discussed in Sec. 2.4.

2.3 Rotation in the Weakly Interacting Regime

In the weakly interacting regime $Na_s/a_{\text{osc}} \ll 1$ (with $a_{\text{osc}} = a_z$ if the z degree of freedom is "frozen out") the length scales are very different from the Thomas-Fermi regime, as mentioned in the previous section. Nevertheless, the way vortices occur in the condensate is qualitatively similar [46, 47]. For all external rotational frequencies below a critical value Ω_{c1}, the nonrotating state $L = 0$ remains lowest in energy. The implication is that in an experiment, if the rotation frequency is below Ω_{c1}, the condensate will not be set to rotate. Above Ω_{c1}, the lowest-energy state is a single vortex at the center of the trap. This state again remains the lowest-energy state for a range of rotational frequencies, until at a second critical rotational frequency where instead two singly quantized vortices appear as the lowest-energy state. Similarly, this remains lowest in energy until a third vortex appears, and so on. The vortices will arrange symmetrically in the condensate and as the rotational is further increased they will arrange to form a lattice. This sequence of events is qualitatively similar to what has been seen in experiments performed in the Thomas-Fermi regime [54, 56].

To understand a weakly interacting two-dimensional condensate under rotation, we start from the purely non-interacting system and its energy Eq. (1.15). The total angular momentum for a system rotating about the z axis is $\hbar L = \hbar \sum_{i=1}^{N} m_i$. For a given L, the energy Eq. (1.15) is minimized by choosing $m \geq 0$ and $n = 0$. This restriction is called the lowest Landau level (LLL) approximation, and it is also appropriate for a condensate under fast rotation. The non-interacting energy in LLL is

$$E = \hbar\omega \left(N + \sum_{i=1}^{N} |m_i| \right) = \hbar\omega(N + L), \tag{2.15}$$

i.e., it is only dependent on the total particle number, and the total angular momentum. It does not depend on how the angular momentum is distributed among the particles. There is a high degree of degeneracy associated with this: a configuration where one particle carries all the angular momentum has exactly the same energy as a configuration where the angular momentum is evenly distributed among the particles. This is a very particular feature of the harmonic oscillator. For a discussion of this "partition space", see Ref. [57].

The eigenfunctions of the Hamiltonian Eq. (1.13) in LLL are (again omitting the z direction wavefunction; see Sec. 1.3)

$$\phi_{0m}(\rho,\varphi) \equiv \phi_m(\rho,\varphi) = \sqrt{\frac{2}{|m|!a_{\rm osc}^2}} \left(\frac{\rho}{a_{\rm osc}}\right)^{|m|} e^{-\rho^2/2a_{\rm osc}^2} \frac{e^{im\varphi}}{\sqrt{2\pi}}. \tag{2.16}$$

Note that these are of the general form Eq. (2.10) and have angular momentum $L = \hbar m$. The non-rotating state $m = 0$ is a pure Gaussian. However, $m = 1$ gives a vortex state. The vortex is characterized by a vanishing density at the vortex core, which is guaranteed by the factor $\rho^{|m|}$ (the core is at the origin), and around this point a phase shift from 0 to 2π, which is implied in the factor $e^{im\varphi}$. A multiply quantized vortex is present for $m > 1$; then the phase shift is a multiple of 2π. We see also from the factor $\rho^{|m|}$ that a multiply quantized vortex has a larger vortex core, since the density rises more slowly for small ρ.

The states which have the lowest energy for a given angular momentum are in nuclear physics terminology called "yrast" states [58], which in Swedish means the most dizzy states. Because of Eq. (2.15), it is the interaction energy that determines the behavior of the system. Interestingly, both mean-field methods as well as diagonalization (see Chapt. 3) give that in the angular momentum region $2 \leq L \leq N$ the interaction energy is linear in L [47, 59]. The mean-field expression in Ref. [47] agrees up to order $1/N$ with the diagonalization result [59]

$$E_{\rm int} \propto \frac{N(2N - L - 2)}{2}, \tag{2.17}$$

which was found to be true to machine precision. In fact, the full energy spectrum for $0 \leq L \leq N$ has been studied and partly characterized, and the wavefunctions of the yrast states are known [90, 60, 61, 62, 63]; see also Ref. for a recent connection to the "composite fermion" construction.

The condensate wavefunctions for the vortex states can be expressed in terms of the wavefunctions ϕ_m [46, 47]. For the unit vortex, it is simply the oscillator eigenfunction ϕ_1 as defined in Eq. (2.16) (apart from the normalization to N). The next energetically stable state has two singly quantized

vortices displaced from the trap center and, including only leading contributions, the condensate wavefunction is of the form

$$\Psi(\mathbf{r}) = c_0\phi_0(\mathbf{r}) + c_2\phi_2(\mathbf{r}) + c_4\phi_4(\mathbf{r}), \tag{2.18}$$

where the c:s are constants with $|c_2|^2$ dominating over the other two [47]. The angular momentum per particle in the two-vortex state is less than $2\hbar$, since the two vortices are displaced from the trap center. Three singly quantized vortices have a condensate wavefunction with the states $m = 0$, $m = 3$, and $m = 6$ giving leading contributions. This pattern continues with other vortex states with some rotational symmetry which can be described in a similar way [46, 47].

2.4 Anharmonic Traps

Introducing an anharmonic perturbation to the harmonic potential, as suggested by Fetter [65] and Lundh [66], is done for two reasons. One is to approach the fast-rotating limit: for a harmonically trapped condensate, as the external rotational frequency Ω approaches the trapping frequency ω, the effective centrifugal potential will win over the trapping potential and the condensate will fly apart. Thus it is difficult experimentally to reach really high rotation frequencies in a harmonically trapped condensate [67, 68]. An attempt to create an anharmonic potential, via addition of a Gaussian laser beam, and rotate above the limit $\Omega/\omega = 1$ showed a distorted vortex lattice at high rotation frequency and a density depression at the trap center [69]. The interpretation of this experiment has not been evident; a recent suggestion is given in Ref. [70].

The other reason to change the trapping potential is that physically new phenomena emerge: multiply quantized vortices can be energetically stable in an anharmonically trapped condensate [66, 71]. To understand how multiply quantized vortices appear we investigate first a non-interacting system with a trapping potential of the following form:

$$V(\rho) = \frac{1}{2}M\omega^2\rho^2\left(1 + \lambda\frac{\rho^2}{a_{\mathrm{osc}}^2}\right), \tag{2.19}$$

where λ is a small dimensionless parameter governing the strength of the anharmonicity. A perturbative calculation, starting from the LLL wavefunction ϕ_m of Eq. (2.16) gives the energy

$$E = \hbar\omega\left(|m| + 1 + \frac{\lambda}{2}(|m|+1)(|m|+2)\right). \tag{2.20}$$

This energy is quadratic in the single-particle momentum m, as opposed to the harmonic oscillator energy Eq. (1.15) which is linear in m. Thus the high degree of degeneracy of the harmonic oscillator is broken, and it becomes energetically unfavorable to involve states with high single-particle angular momentum. This means e.g. that the two-vortex configuration in Eq. (2.18) becomes unfavorable as compared to a doubly quantized vortex, since the two off-center vortices involve the state with $m = 4$. It can be shown [65] that this faster-than-linear dependence of the energy on m is a general feature of potentials that are steeper than harmonic.

In experiments, multiply quantized vortices have been created via phase-imprinting [72] and an "evaporative spin-up technique", where evaporation of slow atoms makes a rapidly rotating condensate rotate even faster [73]. Theoretical results for a weakly interacting condensate in an anharmonic trap will be discussed in relation to the diagonalization results in Sec. 4.1.

2.5 Ring-Like Traps and Persistent Currents

Other than quantized vortices, there are two striking superfluid effects that can appear in connection to rotation: the Hess-Fairbank effect [74], and metastability of persistent currents [19, 75]. Both are most easily considered in an annular geometry.

We start by discussing the Hess-Fairbank effect. Consider a superfluid *above* the transition temperature to superfluidity, and consider it kept in an annular container with a radius much larger than the width of the annulus. If the container is set to rotate, the fluid will rotate along with it. Assume the rotational frequency to be very low. Then cool the system below the transition temperature to superfluidity and wait. It is found that even though the container is kept rotating (slowly), the fluid will come to a rest.

For a Bose-condensed system, this effect can be explained as follows. We consider a quasi one-dimensional system by assuming fixed wavefunctions in all but the azimuthal direction. The condensate is unconfined in the angular direction and periodic boundary conditions apply. If R is the radius of the annulus, and S its cross sectional area, we can assume the condensate wavefunction to be

$$\Psi_m(\rho, \varphi, z) = \sqrt{N}\frac{e^{im\varphi}}{\sqrt{2\pi}}\frac{1}{\sqrt{RS}}. \tag{2.21}$$

This wavefunction has the kinetic energy $Nm^2\hbar^2/(2MR^2)$ and angular momentum $Nm\hbar$. To find the energy in the rotating frame of reference, we

subtract $L\Omega$ and find (ignoring interactions)

$$E(m)/N = \frac{m^2\hbar^2}{2MR^2} - m\hbar\Omega. \tag{2.22}$$

The value of m that minimizes this expression is the integer which comes closest to $MR^2\Omega/\hbar \equiv \Omega/\omega_c$, where $\omega_c = \hbar/MR^2$. So for an external rotational frequency small enough, $-\omega_c/2 < \Omega \leq \omega_c/2$, the system will stay in the non-rotating ground state. It can be shown that in different geometries and with interactions present, the phenomenon can still occur [19].

The Hess-Fairbank effect has been studied in the context of a rotating Bose gas by several authors; see e.g. Ref. [76]. Unluckily it is sometimes also referred to as a "persistent current". However the Hess-Fairbank effect concerns which state is the lowest-energy state at a given rotational frequency. As such, it is different from the metastable persistent flow we describe below.

Metastable persistent flow is another extraordinary effect related to superfluidity. Again consider a fluid in an annular container, rotating above the transition temperature this time at a significant speed. If this system is cooled below the transition temperature, the fluid will keep rotating. The remarkable thing happens if we stop the external rotation: the fluid will not stop, but keep on rotating. It is not in its absolute ground state (which still is the non-rotating state), but it is in a metastable state with a very long lifetime.

The dispersion relation is the key to understanding meta-stability of persistent flow [19]. Assume a dispersion relation $E(L)$ with a local minimum for some value L_c. Through external rotation we can bring angular momentum to the system, and if the value is close to L_c, then the system will relax to this angular momentum rather than $L = 0$ since there is an energy barrier between these two states. So it is clear that a necessary condition for persistent currents to occur, is that the dispersion relation has a negative curvature at some point.

Bloch [77] proved some general features of the dispersion relation of a bosonic system in a one-dimensional ring. The particles are free in the direction along the ring, which has a radius R. A solution to the Schrödinger equation (which only includes the kinetic energy term) separates into center of mass and relative coordinates,

$$\Phi = e^{iL(\sum_i \varphi_i)/N\hbar}\chi(\varphi_i - \varphi_j), \tag{2.23}$$

where $L = RP = R\sum_i p_i$ is the total angular momentum of the system (p_i is the linear momentum of each particle), φ_i is the angle coordinate along the ring of the ith particle, N is the total number of particles and $\chi(\varphi_i - \varphi_j)$ is

the relative wavefunction which only depends on the relative position of the atoms. Inserting Eq. (2.23) into the Schrödinger equation yields an equation for χ,

$$H\chi = e\chi. \tag{2.24}$$

The total energy E for the system is

$$E = \frac{L^2}{2NMR^2} + e(L), \tag{2.25}$$

i.e., it is parabolic in the total angular momentum L but also contains the contribution $e(L)$.

The wavefunction Φ must be single-valued, i.e., $\Phi(\varphi_1, ..., \varphi_i, ...) = \Phi(\varphi_1, ..., \varphi_i + 2\pi, ...)$. This condition is satisfied if

$$\chi(\varphi_1, ..., \varphi_i + 2\pi, ...) = e^{-2\pi i L/N\hbar}\chi(\varphi_1, ..., \varphi_i, ...). \tag{2.26}$$

Furthermore, if all variables φ_i are augmented by 2π, then their relative position remains unaltered and thus χ must be unaltered by this modification. This in turn requires that $\left(e^{-2\pi i L/N\hbar}\right)^N = 1$, which is satisfied if $L/\hbar = m$, where m is an integer.

The condition on χ, Eq. (2.26), does not change if L is increased by an amount $N\hbar$, as can be seen from the original wavefunction Eq. (2.23). This means that the wavefunction χ itself cannot change due to such an increment. This in turn implies that its eigenvalues must satisfy $e(L) = e(L + N\hbar)$; thus the function $e(L)$ is periodic in $N\hbar$. It is also symmetric around $L = 0$, since the sense of rotation cannot affect the energies of a function which depends only on relative position of the particles.

To summarize, we find that the dispersion relation Eq. (2.25) consists of one part which is quadratic in L, and a periodic part with periodicity $N\hbar$. The periodic part has minima at $L = 0$ and $L = N\hbar$, and thus here local minima in the dispersion relation can occur. The dispersion relation is shown schematically in Fig. 2.1. We note that since it is the periodic part that can cause local minima, and the periodic part arises due to internal motion of the condensate, it is the interactions that cause the local minima to appear. If interactions are sufficiently weak, there will be no local minima and no persistent currents.

In more specific studies related to BEC in dilute alkali gases, energy barriers in the Thomas-Fermi regime have been investigated in Refs. [78, 79], which confirmed the possibility of having persistent currents in such a system. Also their lifetime has been calculated [80] and found to be long enough for the

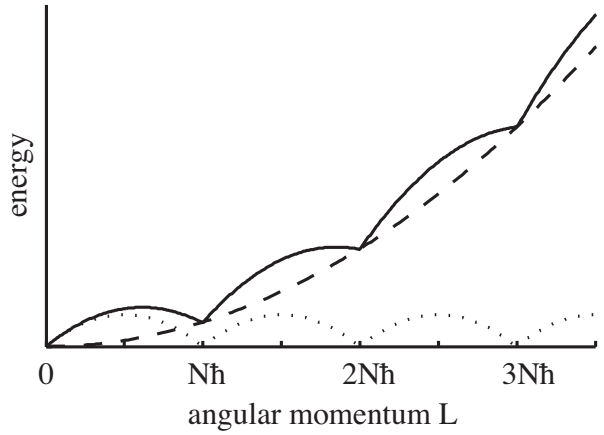

Figure 2.1: Schematic figure of dispersion relation for N bosons in an annular trap. The dashed line is the envelope part $\propto L^2$ and the dotted line the periodic part; the full-drawn line is their sum i.e. the dispersion relation. Since there are local minima this system could show persistent currents.

phenomenon to be observable. Even in presence of disorder, these currents can exist [81].

Experimentally, persistent currents in a Bose gas have been successfully achieved [82]. A BEC was kept in a harmonic trap which could be made toroidal through an additional laser beam, and angular momentum could be transferred to the atoms via a Laguerre-Gaussian laser beam. *In situ* imaging showed a condensate with a hole in the middle, but images taken after the trap was switched off and the condensate had expanded were dependent on the original state of the system. If the condensate was non-rotating at the stage when the trapping potential was turned off, then in the time-of-flight (TOF) image there was no hole; it had been filled during expansion. If however the angular momentum transfer had been performed, then the TOF image showed a clearly visible hole in the condensate density. This provided means to detect the rotation.

By measuring the decay of the rotation as a function of time, the persistent flow could be verified to last for up to 10 seconds. In contrast, transferring angular momentum to a condensate in the purely harmonic trap resulted in a vortex, which decayed in only 0.5 seconds. The limitation of the lifetime of the persistent flow was attributed to technical factors - the alignment of the

laser creating the hole in the potential was not perfect and after 10 seconds the drift would be noticeable, causing the decay of the current.

The authors were also able to create persistent flow with an angular momentum of $2\hbar$ per particle. As a means of detecting this higher angular momentum, it was seen that removing the plug beam caused the density hole to split into two singly quantized vortices.

Finally, we would like to mention that the attractively interacting Bose gas in a toroidal potential has been investigated [83, 84, 85] to reveal an interesting phase diagram. In fact, it has some similarities to that for the anharmonic potential in Fig. 4.5, to be discussed later. For weak attraction, there are lobe-shaped areas where the density is homogeneous along the ring, and the wavefunction is composed of only one function of the type Eq. (2.21). I.e., it has a quantized circulation m. At stronger interaction, the condensate wavefunction contains contributions from more m states and a soliton is expected to develop.

Chapter 3

Diagonalization Approach to the Many-Body Problem

By writing the Hamiltonian in matrix formulation and diagonalizing, we can - in principle - find all exact eigenstates of the system. This is the main reason to use the diagonalization method. Unsurprisingly, it is usually not this simple: first of all, to exactly describe a system we must know its Hamiltonian exactly, and secondly, for the solutions to be exact an infinite number of basis states is needed. Therefore the method is only usable when one can motivate a truncation of the basis. Since the many-body basis size is strongly dependent on particle number, one is usually restricted to the study of "small" systems.

We discussed the Gross-Pitaevskii equation in Sec. 1.2. This is a widely used mean-field method, where the wavefunction is written as a simple product of single-particle states, and as such it cannot incorporate correlations between individual atoms. On the other hand, one is not restricted to small particle numbers - rather the particle number has to be much larger than 1 since terms of order $1/N$ are neglected in its derivation. Due to the two methods' compensating strengths and weaknesses, combined together they make a good tool to explore the behaviors of BECs [86].

We first give an overview of the "exact" diagonalization method; in the literature one often also encounters the name "configuration-interaction method". The eigenvalue equation for the Hamiltonian H is

$$H\Phi = E\Phi, \tag{3.1}$$

where Φ is the (many-body) eigenfunction and E is the eigenenergy. Because of the completeness of these eigenstates, any "real" state that the system can

have can be written as a superposition of these eigenstates.

We expand the wavefunction in a complete basis $\{\psi_n\}$ with expansion coefficients α_n,

$$\Phi = \sum_{n=1}^{\infty} \alpha_n \psi_n. \tag{3.2}$$

The first difficulty of the method is finding a suitable basis, and a suitable truncation of the basis. We can then write the Hamiltonian in matrix representation using the same basis; the matrix is

$$\begin{pmatrix} \langle\psi_1|H|\psi_1\rangle & \langle\psi_1|H|\psi_2\rangle & \cdots \\ \langle\psi_2|H|\psi_1\rangle & \langle\psi_2|H|\psi_2\rangle & \\ \vdots & & \ddots \end{pmatrix}. \tag{3.3}$$

This is the next potential difficulty; to calculate the integrals of the matrix elements $\langle\psi_i|H|\psi_j\rangle$. For actually solving Eq. (3.1), we can make use of efficient numeric diagonlization algorithms such as the Arnoldi/Lanczos algorithm [87]. Let us now investigate the different steps in more detail, starting with the basis.

A complete basis for a many-body problem with N particles, is built up in terms of a complete single-particle basis $\{|\lambda\rangle\}$. We use the Fock notation for the many-body basis states,

$$\psi = |n_\lambda\, n_\mu\, n_\nu ...\rangle\,, \tag{3.4}$$

where n_λ is the number of particles occupying the state $|\lambda\rangle$ and so on. For bosons, the n_ks can take any non-negative number, as opposed to fermions which obey the Pauli principle and thus are restricted to occupations 0 or 1. Other choices are possible, but since we consider weak interaction, it is convenient to take the eigenfunctions of the single-particle Hamiltonian H_{sp} as basis states. These are calculated by numerically solving the single-particle Schrödinger equation

$$\left(-\frac{\hbar^2}{2M}\nabla^2 + V(\mathbf{r})\right)\phi = E\phi, \tag{3.5}$$

with eigenfunctions ϕ $(= \langle\mathbf{r}|\lambda\rangle)$ and an appropriate potential $V(\mathbf{r})$ for the problem at hand. This calculation is performed using the 'shooting' method with a fourth-order Numerov stepping scheme.

We write the Hamiltonian in second quantization to facilitate computer calculations. So we introduce the usual bosonic annihilation and creation

operators for the state $|\lambda\rangle$, $\hat{a}_\lambda$ and $\hat{a}_\lambda^\dagger$ (denoted with hats to avoid confusion with other quantities). The action of these operators on the many-body basis in Fock notation is

$$\begin{aligned}\hat{a}_\lambda^\dagger \left|n_1\, n_2 ... n_\lambda ...\right\rangle &= \sqrt{n_\lambda + 1}\left|n_1\, n_2 ... (n_\lambda + 1) ...\right\rangle, \\ \hat{a}_\lambda \left|n_1\, n_2 ... n_\lambda ...\right\rangle &= \sqrt{n_\lambda}\left|n_1\, n_2 ... (n_\lambda - 1) ...\right\rangle,\end{aligned} \tag{3.6}$$

and they obey the bosonic commutation rules

$$\left[\hat{a}_\lambda^\dagger, \hat{a}_\mu^\dagger\right] = \left[\hat{a}_\lambda, \hat{a}_\mu\right] = 0, \tag{3.7}$$

$$\left[\hat{a}_\lambda, \hat{a}_\mu^\dagger\right] = \delta_{\lambda\mu}. \tag{3.8}$$

The kinetic and trap energy many-body operators T and V are simple sums of the corresponding single-particle operators t and v. Since we work in a basis of eigenfunctions of the single-particle Hamiltonian, the kinetic energy can be written

$$T = \sum_{\lambda\mu} \langle\lambda|\, t\, |\mu\rangle\, \hat{a}_\lambda^\dagger \hat{a}_\mu = \sum_\lambda \epsilon_{\mathrm{kin},\lambda} \hat{a}_\lambda^\dagger \hat{a_\lambda}, \tag{3.9}$$

where $\epsilon_{\mathrm{kin},\lambda}$ is the single-particle kinetic energy in the state $|\lambda\rangle$. The trap energy reads

$$V = \sum_{\lambda\mu} \langle\lambda|\, v\, |\mu\rangle\, a_\lambda^\dagger a_\mu = \sum_\lambda \epsilon_{\mathrm{trap},\lambda} a_\lambda^\dagger a_\lambda, \tag{3.10}$$

with $\epsilon_{\mathrm{trap},\lambda}$ being the single-particle trap energy for the state $|\lambda\rangle$.

For the interaction energy, however, we have a two-body operator $u = u(\mathbf{r}_i - \mathbf{r}_j)$. For bosons, this can generally be expressed in second quantization as

$$U = \frac{1}{2} \sum_{\lambda\mu\nu\rho} \langle\lambda\mu|u|\nu\rho\rangle\, \hat{a}_\lambda^\dagger \hat{a}_\mu^\dagger \hat{a}_\rho \hat{a}_\nu, \tag{3.11}$$

where the matrix element now is a double integral:

$$\langle\lambda\mu|u|\nu\rho\rangle = \int d\mathbf{r} \int d\mathbf{r}'\, \phi_\lambda^*(\mathbf{r}) \phi_\mu^*(\mathbf{r}') u(\mathbf{r}, \mathbf{r}') \phi_\nu(\mathbf{r}) \phi_\rho(\mathbf{r}'). \tag{3.12}$$

Conservations laws often put restrictions on the number of matrix elements that are non-zero. Calculation of the integral is simplified when the δ interaction is appropriate, but for e.g. Coulomb or dipolar interactions, this is a more difficult task.

To recapitulate, the specific Hamiltonian used in our work is

$$H = \sum_{i=1}^{N} \left(-\frac{\hbar^2}{2M} \nabla_i^2 + V(\rho_i) \right) + \frac{U_0}{2} \sum_{i,j;i\neq j}^{N} \delta(\mathbf{r}_i - \mathbf{r}_j). \tag{3.13}$$

The potential $V = V(\rho)$ is rotationally symmetric around the z axis and since the angular momentum operator $L = L_z$ commutes with the Hamiltonian, we can diagonalize in a subspace which has definite angular momentum. This greatly reduces the basis size: for each value of L separately, we find the eigenstates and eigenenergies of the system.

To model rotation, it is most convenient to work in the rotating reference system, since then the variables are time-independent. The real system will find equilibrium in the state where it has the lowest energy according to its own frame of reference. Standard mechanics give the transformation of energy in the rotating frame of reference. For a system having angular momentum L, rotating with frequency Ω, we find the energy in the rotating frame of reference E_{rot} from the energy in the laboratory frame of reference E_{lab} through the following transformation [19]:

$$E_{\text{rot}} = E_{\text{lab}} - L\Omega. \tag{3.14}$$

This simple form of the relation is valid for a two-dimensional system.

We calculate the dispersion relation $E(L)$ in diagonalization, but in experiments (and usually in GP calculations), it is the external rotational frequency Ω which can be controlled and fixed. From Eq. (3.14) we see that the dispersion relation is tilted when we introduce external rotation, and a new state (other than $L = 0$) can become the lowest in energy.

The many-body eigenfunctions Φ which solve the eigenvalue equation Eq. (3.1) are functions of many variables, even if we are restricted to small particle numbers due to numerical limitations. To analyze its content of different single-particle states, we calculate the occupation number n_λ for the single-particle state $|\lambda\rangle$ according to

$$n_\lambda = \left\langle a_\lambda^\dagger a_\lambda \right\rangle. \tag{3.15}$$

These numbers can be used to identify different types of vortex states as follows. Using single-particle wavefunctions of the form Eq. (2.16), a single vortex at the center of the trap is represented by the state with $m = 1$. So if the occupation number for this state is very much higher than all others, we call it a vortex state. A doubly quantized vortex will have a high occupation

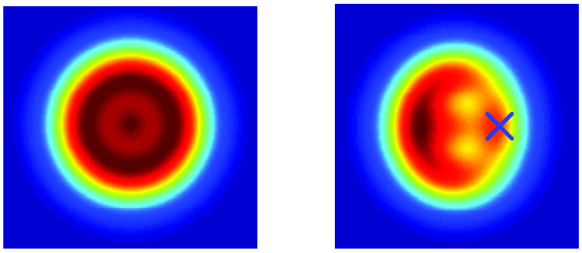

Figure 3.1: "Color plots" in the x, y plane of the density (left panel) and the pair correlation Eq. (3.16) (right panel). Blue corresponds to zero density, and each plot is "normalized" so that red is the maximum value in that particular plot. The pair correlation reveals the internal structure of a many-body state. The density to the left is rotationally symmetric. It shows no trace of the two vortices which appear in the right panel, which shows the pair correlation with a particle fixed at the marked point $x_A = 1.2\, a_{\rm osc}$. Both panels extend from $-3.5 \leq x/a_{\rm osc} \leq 3.5$. For consistency, these values are used in all the following plots of this kind.

of the state $m = 2$, and so on. Two singly quantized vortices are composed of the three states with $m = 0$, 2 and 4, similarly to the condensate wavefunction Eq. (2.18).

In the GP approach, a central "unit" vortex will have macroscopic occupation only of the $m = 1$ state. In a finite-size system, this will not occur due to finite-size effects, which in comparison with GP are of order $1/N$ [16]. However, for small N it is not always easy to distinguish between terms of order N, 1, and $1/N$. Another possibility is to check the occupancy dependence on the particle number, and thus investigate which states would be occupied in the limit of large particle numbers. This we showed explicitly in Paper I, and it has been done when appropriate also in the other studies.

If the Hamiltonian is rotationally symmetric, so will be the solutions we find. This complicates the identification of the vortex states and the comparison with mean-field calculations (which need not give solutions with symmetric density). In order to map out the internal structure of the diagonalization eigenstates, we introduce pair correlation functions, calculated (in coordinate space) as

$$P(\mathbf{r}; \mathbf{r}_A) = \frac{\sum_{i \neq j} \langle \Phi | \, \delta(\mathbf{r} - \hat{\mathbf{r}}_i) \delta(\mathbf{r}_A - \hat{\mathbf{r}}_j) \, | \Phi \rangle}{(N-1) \sum_j \langle \Phi | \, \delta(\mathbf{r}_A - \hat{\mathbf{r}}_j) \, | \Phi \rangle}. \tag{3.16}$$

Here Φ is the many-body state whose internal symmetry we wish to reveal,

and $\mathbf{r}_A$ is a parameter: $P(\mathbf{r};\mathbf{r}_A)$ is the probability of finding any particle at position $\mathbf{r}$, given that one particle is fixed at the position $\mathbf{r}_A$. The location of the fixed particle should be chosen with some care. It is reasonable to fix it at a point where the density is high. Before making definite statements, one should also check that the pair correlation function does not depend sensitively on the exact location of the fixed particle. An example of a two-vortex state for 10 atoms in a harmonic trap is shown in Fig. 3.1. In our plots of this kind, blue corresponds to zero density, and each plot is "normalized" so that red is the maximum value in that particular plot. We will in the following always choose $x_A = 1.2\,a_{\mathrm{osc}}$, and we have confirmed that in the figures we show, the plots are not sensitive to the exact choice of x_A. The left panel of Fig. 3.1 shows the density, which is rotationally symmetric. The right panel shows the pair correlation function Eq. (3.16), with a particle fixed at the point marked in the figure. Now, two vortices appear as minima in the pair correlation.

Chapter 4

Exploring Vortices in a Bose Gas Using Diagonalization

We have already given a flavor of the rich structure of quantized vortices that a single-component Bose gas in a harmonic trap exhibits. Now we will investigate two particular systems which add even more to this picture: a Bose gas in an anharmonic trap, and systems consisting of two components. We focus on diagonalization results but compare with other methods when appropriate.

4.1 Rotation in an Anharmonic Trap

In Sec. 2.4 we discussed some features of a BEC rotating in an anharmonic trap. Several theoretical studies have been performed investigating a weakly interacting system using a mean-field approach, for both attractive and repulsive condensates. We first summarize their findings, considering first the case of repulsion [66, 88, 89], in order to compare with the diagonalization results.

The behavior of the system is determined by the interplay between the interaction energy strength and the energy associated with the anharmonicity. To keep the number of parameters limited, we consider a fixed, weak anharmonicity parameter and variable external rotational frequency and interaction strength. Then, for weak enough interaction, the stable states are multiply quantized vortices. This is due to the quadraticity of the single-particle energies, as discussed in Sec. 2.4: e.g. the two-vortex state implies involvement of the $m = 4$ single-particle state, which is unfavorable if the energy is quadratic in m. By increasing the interaction strength, the weak anharmonic term can

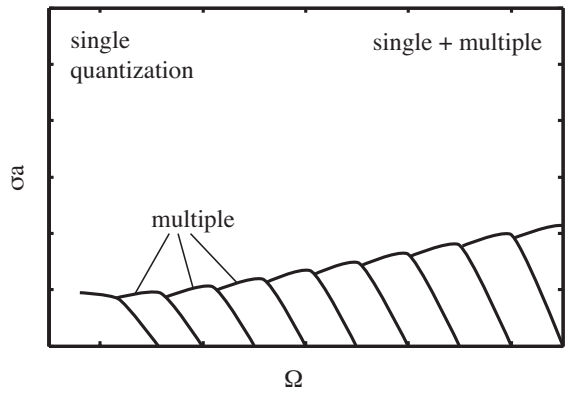

Figure 4.1: Schematic phase diagram of a weakly repulsive Bose gas in an anharmonic potential. For sufficiently weak interaction multiply quantized vortices are energetically favorable. At stronger interaction, singly quantized vortices appear. When both rotational frequency and interaction strength are significant, states appear where a multiply quantized vortex is surrounded by singly quantized ones.

be made less important and at some point, the system will again prefer to form singly quantized vortices. It is also found that the stronger the interaction, the easier it is to set the condensate rotating. This is because the rotation pulls the atoms further apart, thus decreasing the interaction energy. When both rotational frequency is high and the interaction strength is large, states appear where there is one central, multiply quantized vortex surrounded by several singly quantized vortices. A schematic phase diagram of this is shown in Fig. 4.1.

Our diagonalization approach goes beyond previous mean-field calculations [66, 88, 89]. Results from both methods are in general consistent: multiply quantized vortices are energetically stable when the interaction is weak enough, and singly quantized vortices appear where the interaction is stronger and the rotational frequency is kept moderate. The numeric values agree well with mean-field results though they do not coincide exactly, since in the diagonalization calculation there are finite-size effects which are absent in a GP approach.

To be specific, we have diagonalized the following Hamiltonian

$$H = \sum_{i=1}^{N} \left(-\frac{\hbar^2}{2M}\nabla_i^2 + \frac{1}{2}M\omega^2\rho_i^2 \left(1 + \lambda\frac{\rho_i^2}{a_{\rm osc}^2}\right)\right) + \frac{U_0}{2}\sum_{i\neq j=1}^{N}\delta(\mathbf{r}_i - \mathbf{r}_j), \quad (4.1)$$

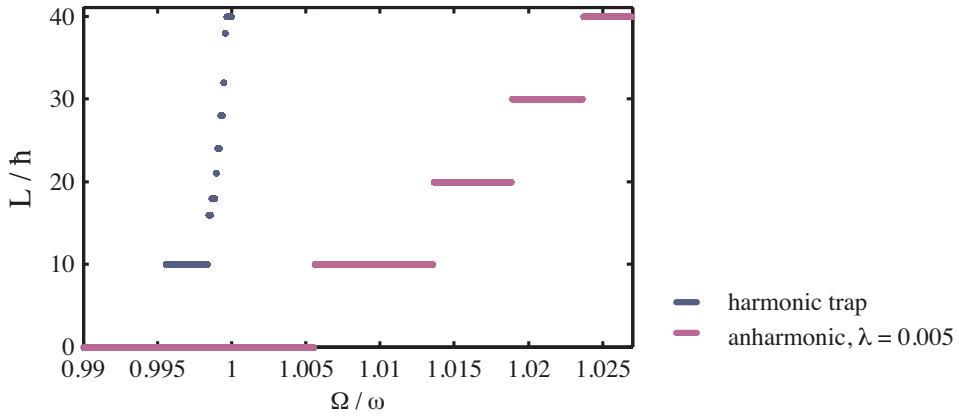

Figure 4.2: Angular momentum of the lowest-energy state as function of rotational frequency for 10 bosons, in a harmonic trap (blue), and in a weakly anharmonic trap (purple). The plateaus are the energetically stable states, which apart from the first at $L = 10$ differ for the two potentials. Note that the critical velocity for rotation is greater than 1 in the anharmonic condensate, for this given set of parameters. Both graphs show diagonalization results with $\sigma a_s = 0.008$; anharmonicity $\lambda = 0.005$ for the purple curve.

in the lowest Landau level and in a two-dimensional setting, as motivated in Sec. 2.3. To map out the "phase diagram", we vary the interaction strength, measured by the dimensionless quantity σa_s, where $\sigma \sim N/a_z$ is the density in the z direction and thus $\sigma a_s = (N-1)U_0/(4\pi a_z a_{\text{osc}}^2 \hbar\omega)$. We calculate eigenenergies and eigenfunctions for a range of angular momenta $\hbar L$, and subtract $L\Omega$ to find the lowest energy of the system in the co-rotating frame for a given rotation frequency Ω. Thus we find the mechanically stable states at each rotational frequency. For notational simplicity, we will in the following always measure the angular momentum in units of $\hbar$, unless explicitly mentioned otherwise.

In Fig. 4.2 we show the total angular momentum L as a function of Ω, measured in units of the trap frequency ω, for a condensate in a harmonic trap (blue curve), and a condensate in a weakly anharmonic trap with $\lambda = 0.005$ (purple curve). The plateaus correspond to the energetically stable states, and we see that apart from the first plateau - the unit vortex - the stable states have different angular momenta in the two potentials. Since in the harmonic trap, all vortices except the first are non-central, they do not have integer angular momentum per particle $l = L/N$, but rather $l \approx 1, 1.7, 2.1, ...$ corresponding

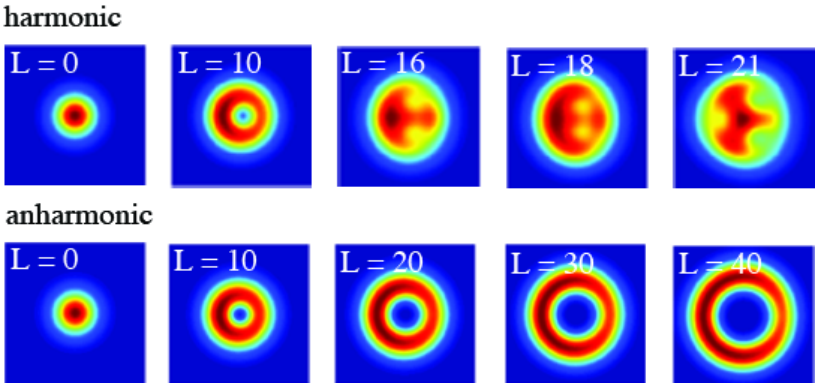

Figure 4.3: Pair correlation plots (as explained in Fig. 3.1) for bosons trapped in a harmonic potential (upper row), and anharmonic potential (lower row). The five first energetically stable states are shown for each trapping potential, i.e. the states corresponding to a plateau in Fig. 4.2. The unit vortex at $L = 10$ is similar for the two systems, but at higher angular momenta, the difference is striking: in the harmonic trap, singly quantized vortices appear, while with a small quartic contribution $\lambda = 0.005$, instead vortices of multiple quantization are the energetically stable states. The diagonalization was performed for 10 atoms with interaction strength $\sigma a_s = 0.008$, and each panel has a spatial extension from $-3.5\, a_{\mathrm{osc}}$ to $3.5\, a_{\mathrm{osc}}$; one particle is fixed at $x = 1.2\, a_{\mathrm{osc}}$.

to states with 1, 2 and 3 vortices respectively. In the anharmonic case, there are plateaus for $l = 1, 2, 3$ which are multiply quantized vortices located at the center of the trap. These results agree well with those of Refs. [66, 88, 89]. Pair correlation figures for the five first stable states are shown in Fig. 4.3. The upper row shows for comparison the singly quantized vortices in the harmonic trap, which are remarkably different from the multiply quantized vortex states in the anharmonic trap as shown in the lower row.

For a larger interaction strength, we find that singly quantized vortices appear as stable states alongside the multiply quantized ones. Figure 4.4 shows pair correlation plots for the energetically stable states at $\sigma a_s = 0.08$, which clearly include singly as well as multiply quantized vortices.

We now move on to study the attractively interacting gas. For such a system in a harmonic trap, vortices are never stable - the rotational frequency at which they could be exceeds $\Omega/\omega = 1$, which is unachievable with harmonic confinement. Instead, a rotating attractively interacting Bose gas takes up angular momentum in center of mass motion [57, 90]. This is due to the fact

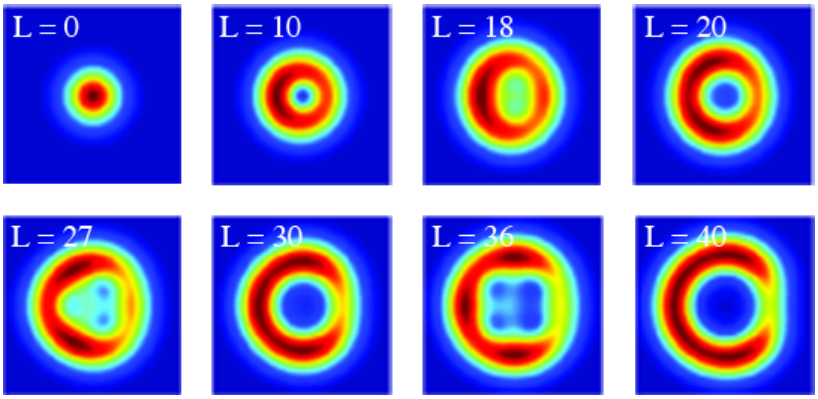

Figure 4.4: Pair correlation functions for energetically stable states in a weakly anharmonic trap with $\sigma a_s = 0.08$, i.e. stronger interaction than in Fig. 4.3. All other parameters are the same as in that figure, apart from the angular momenta which are given in each panel. We note that in comparison to the weaker interaction, we now have states with singly quantized vortices as well as multiply quantized ones.

that in an attractive condensate, any excitations out of the ground state will increase the interaction energy [16]. Thus these are energetically unfavorable as compared to exciting the center of mass, which will set the condensate rotating as a lump around the trap without changing the relative position of the particles, and thus without affecting the interaction energy.

The wavefunction for center of mass rotation may be written exactly for any angular momentum L, and it is

$$\Phi(z_1, ..., z_N) \propto z_c^L \prod_{j=1}^{N} e^{-z_j^2/2a_{\rm osc}^2}, \tag{4.2}$$

where $z_j = x_j + iy_j$ are complex coordinates of particle j, and $z_c = \sum_{j=1}^{N} z_i/N$ is the center of mass. We note that this mode exists also in the repulsive condensate, but it then has higher energy than all states which involve modifying the internal structure of the system. The occupation numbers $n_m(N, L)$ for the center of mass mode can be derived analytically [90] which gives

$$n_m(N, L) = \frac{(N-1)^{L-m} L!}{N^L (L-m)! m!}. \tag{4.3}$$

We can compare this formula with the occupation numbers found by diagonalization to identify the center of mass rotation.

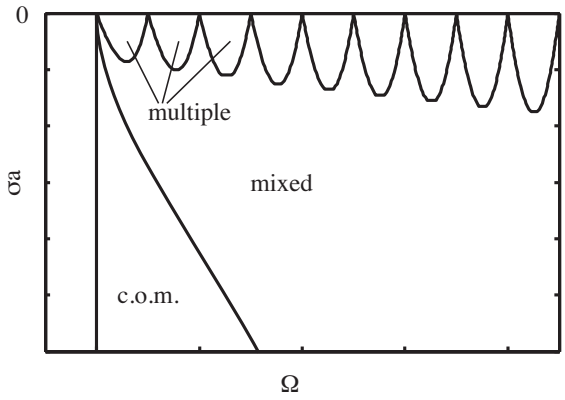

Figure 4.5: Schematic phase diagram of a weakly attractive Bose gas in an anharmonic potential. To the left of the vertical line the gas is non-rotating. In the upper lobes multiply quantized vortices are energetically stable. The area marked c.o.m. is where the center of mass rotation phase is lower in energy than the multiply quantized vortices, and in between the system tries to balance between center of mass rotation and vortices; we name this phase "mixed".

The introduction of a weak anharmonic term to the trapping potential again changes the behavior of the gas drastically. In the anharmonic trap, for weak attractive interactions, vortices can in fact be stable [91, 92, 93, 94]. The quartic contribution to the potential guarantees that the condensate remains trapped even at high rotational frequencies. The vortices are generally multiply quantized, similarly to the repulsive case and for the same reason. A schematic phase diagram is shown in Fig. 4.5. For small rotational frequencies (i.e. to the left of the vertical line) the condensate is non-rotating. For weak enough interaction, the stable states are multiply quantized vortices. For stronger interactions, the condensate absorbs angular momentum in center of mass rotation. In the intermediate region, we have "mixed" states, where there is macroscopic occupancy of several single-particle states, but the occupancies do not exactly coincide with those at "pure" center of mass rotation.

The diagonalization results confirm that the energetically stable states for sufficiently weak interaction are successive states with vortices of multiple quantization. In Fig. 4.6 we plot the angular momentum as a function of the rotational frequency. The blue curve is for $\sigma a_s = -0.001$ and the green for $\sigma a_s = -0.0025$. In contrast to the repulsive case, which showed discrete

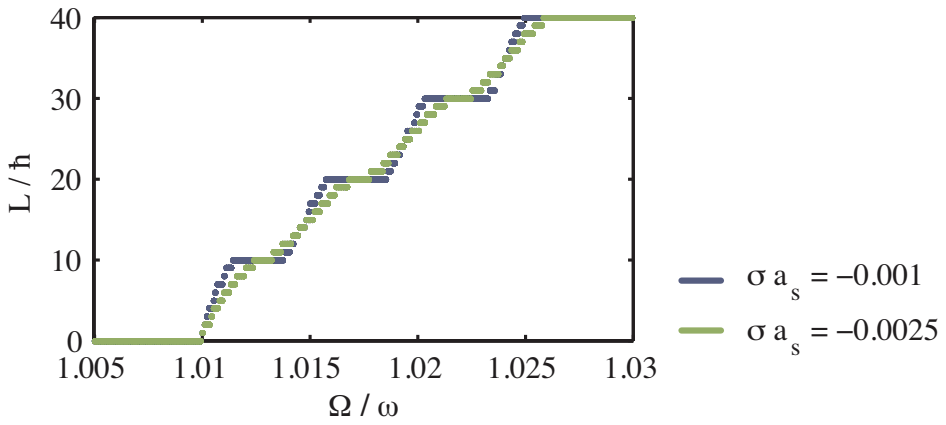

Figure 4.6: Angular momentum of the lowest-energy states as a function of rotational frequency, for an attractive condensate in a weakly anharmonic trap. There are plateaus where the multiply quantized vortices occur, but the function $L(\Omega)$ is continuous between the plateaus (apart from the steps induced by the finite particle number; here $N = 10$). We see that for the blue curve, where $\sigma a_s = -0.001$, the plateaus are slightly wider than for the green curve, where $\sigma a_s = -0.0025$. This agrees with the phase diagram in Fig. 4.5; the regions of stability for multiply quantized vortices becomes narrower for larger magnitude of the interaction.

jumps between the vortex plateaus, the transition is now continuous. The stronger the interactions (purple curve), the narrower these plateaus. This agrees well with the phase diagram of Fig. 4.5: the regions where multiply quantized vortices are stable become narrower for stronger interactions.

In Ref. [91] a boundary between the multiply quantized vortex state and the center of mass rotation state was calculated. However this was only an upper bound, showing where the center of mass phase is energetically favorable as compared to a multiply quantized vortex. In fact, there are many intermediate states where the wavefunction involves occupancy of many single-particle states. Our study confirms this conclusion, and puts the limit where center of mass rotation occurs at much stronger interaction strengths than were found in Ref. [91]. The center of mass mode was detected via the occupation numbers Eq. (4.3), and as can be seen from Fig. 4.7 the diagonalization results reproduce these almost perfectly for low angular momenta at $\sigma a_s = 0.03$. For the same interaction strength, but at higher angular momenta the system is no longer in center of mass rotation but in a "mixed" state, as can be seen from

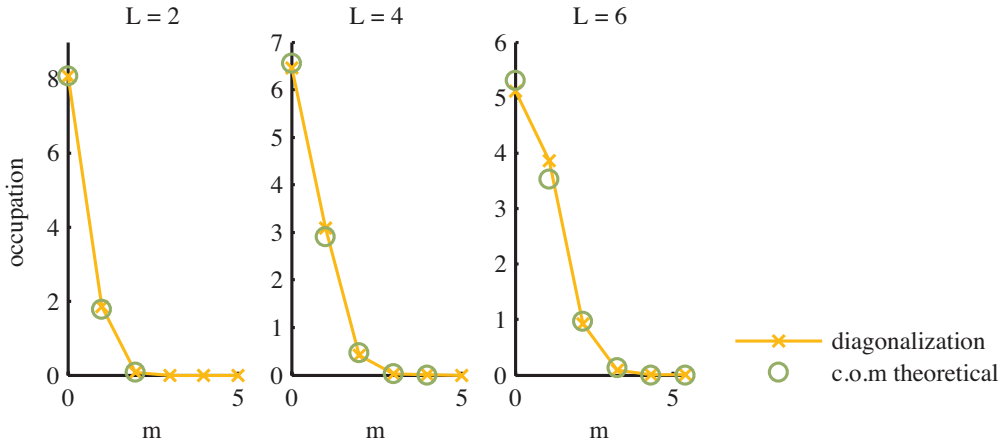

Figure 4.7: Occupation numbers for $N = 10$ atoms in a weakly anharmonic trap, at an interaction strength $\sigma a_s = 0.03$. Each panel corresponds to a specific value of angular momentum. The crosses are the diagonalization results, and the circles show the analytical occupation numbers for center of mass rotation, Eq. (4.3). In this range of angular momentum, we note that there is good agreement, i.e., the system is in center of mass rotation.

the occupancies in Fig. 4.8. This is in agreement with the schematic phase diagram in Fig. 4.5, which shows that for a given interaction strength, the center of mass phase is only stable for smaller rotational frequencies. (Note that since the $L(\Omega)$ curve is continuous, varying L is qualitatively similar to varying Ω).

The intermediate "mixed" states have a crescent-like density, in agreement with Ref. [94]. Pair correlation functions for these states are shown in Fig. 4.9, with increasing angular momentum to the right. We have chosen a value of $\sigma a_s = 0.014$, where the system occupies these "mixed" states for all angular momenta. Note how the higher rotation pushes the atoms further away from the trap center.

4.2 Two-Component System

Another interesting aspect of BEC in dilute alkali gases is the possibility to create mixtures. A two-component Bose gas, as introduced in Sec. 1.4, shows a number of different fascinating quantum states that are not seen in the single-component condensate. In a two-component condensate, the vortices

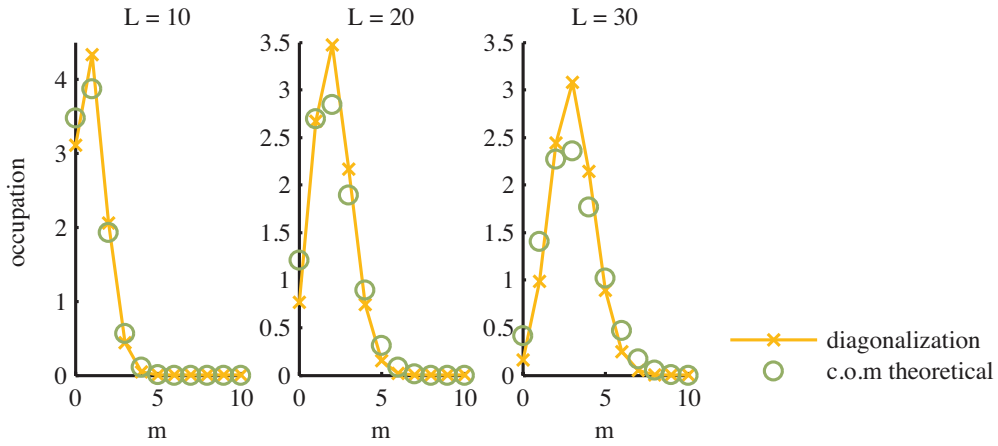

Figure 4.8: Occupation numbers for $N = 10$ atoms in a weakly anharmonic trap, at an interaction strength $\sigma a_s = 0.03$, at higher angular momenta than in Fig. 4.7. Again, crosses mark the diagonalization results, which here do not coincide with the center of mass occupancies, denoted with green circles. These figures do not show pure center of mass rotation, but "mixed" states.

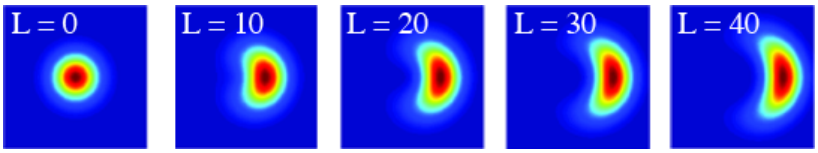

Figure 4.9: Pair correlations for 10 attractively interacting atoms in an anharmonic trap, at an intermediate interaction strength $\sigma a_s = -0.014$. This is the "mixed" state referred to in Fig. 4.5. The atoms are pushed outwards for increasing angular momentum, to the right in the figure. Again, each panel extends from $-3.5\, a_{\mathrm{osc}}$ to $3.5\, a_{\mathrm{osc}}$ and one particle is fixed at $x = 1.2\, a_{\mathrm{osc}}$.

that form are in general *coreless*. This means that there is a vortex in one of the components, but the core is not empty because it is filled up by the second component. The first vortex experiment, described in Sec. 2.2, was of this type. Later experiments have shown vortex lattices in a two-component condensate [97], where the cores of one component coincide with the density maxima of the other component. In some parameter regimes, the vortex lattice moreover changes from square to triangular, which has also been investigated theoretically [95, 96].

Many authors have investigated the structure and stability of the coreless vortices, see e.g. the review [21] and references therein. Most of these references consider the limit of strong interactions (Thomas-Fermi regime). A common approach is to consider the two-component system in a pseudospin representation and allow for spin-dependent interaction; i.e. the number of particles in each species is not conserved. Several interesting spin textures are found [98, 99]. A coreless vortex where one component rotates around the other (a "skyrmion" [100]) can occur when $N_A \neq N_B$. When instead $N_A = N_B$, there is a different structure appearing, sometimes called a "meron". In this case, each component forms an off-center vortex, along with an opposite, off-center density maximum; each component's density maximum coincides with the other's minimum. These two structures are similar to what we see as discussed below. There are also other, more complicated structures; see Ref. [21] for details.

We follow the definitions made in Sec. 1.4. For simplicity, we consider two species of particles having the same mass M and assume all interaction strengths to be equal, $U_{AA} = U_{BB} = U_{AB}$. This is not as unrealistic as it might first seem; in e.g. ^{87}Rb two hyperfine spin states can be trapped which have $a_{AA} : a_{AB} : a_{BB} = 1.03 : 1 : 0.97$, while for ^{23}Na we can have $1 : 1 : 0.96$ [21]. Furthermore, our investigations show that small deviations from these conditions only weakly modify the results presented here. We will also consistently choose $N_A \leq N_B$.

All diagonalization calculations in this section were performed in the lowest Landau level; i.e. they are valid (at least) for weak interactions $nU_0 \ll \hbar\omega$. Note that in LLL, for the non-rotating ground state $L = 0$ no phase separation between the two components is possible; each component occupies the Gaussian wavefunction ϕ_0 as defined in Eq. (2.16). Also, since the total energy in a harmonic trap depends on the interaction energy as $E_{\text{tot}} \propto N + L + U_0 E_{\text{int}}$ in LLL, the results are independent of the exact value of the interaction strength, in the limit of weak interaction.

The angular momentum of the system as a function of rotational frequency

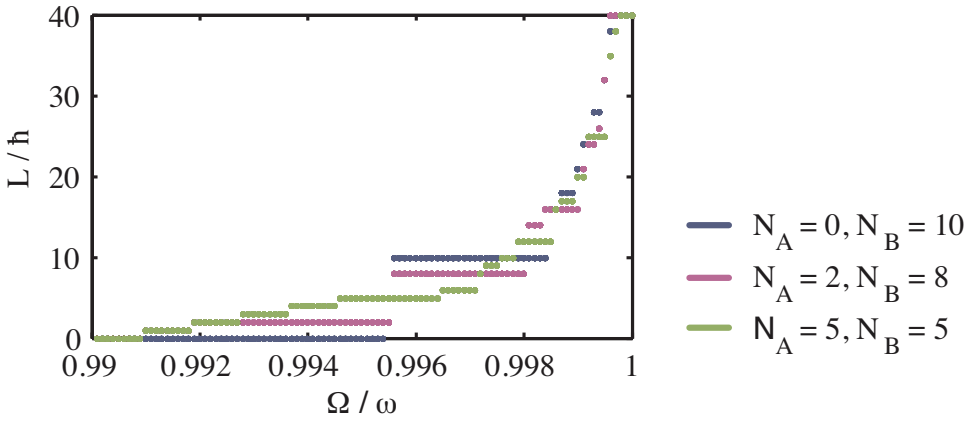

Figure 4.10: Angular momentum as a function of rotational frequency for systems with a total of 10 atoms. The blue curve is the single-component case, purple is for $N_A = 2$, $N_B = 8$, and the green points are for $N_A = N_B = 5$ particles. Note that the discrete jump that occurs at $L = N$ for the single-component system, is completely gone when $N_A = N_B$.

Ω/ω is shown in Fig. 4.10 for three different compositions of particle numbers N_A and N_B, but with constant total particle number $N = N_A + N_B$. The blue curve is the single-component case, i.e. the same as the blue curve in Fig. 4.2. The purple curve, where $N_A < N_B$, no longer has a stable state at $L = N$. Instead, there are two plateaus at $L = N_A$ and $L = N_B$. These are coreless vortices and are similar to unit vortices but in one component at the time: one component is rotating with unit angular momentum per particle of that species, and the other component is non-rotating at the center of the trap, filling up the vortex core. The green curve, where $N_A = N_B$, is continuous, apart from the discreteness induced by the finite particle number (in this case $N = 10$).

In Fig. 4.11 we show pair correlation profiles for a system of $N_A = N_B = 5$ particles, with one component in each row, and increasing angular momentum to the right. The angular momenta are those corresponding to the first steps in Fig. 4.10. The rotation causes the two species of bosons to separate in space into one density maximum for each component around $L = N_A = N_B$. This is similar to the "meron" discussed in Ref. [21]; however in that work the number of particles in each component was not fixed. These figures can also be interpreted as vortices: in each component, a vortex enters the system

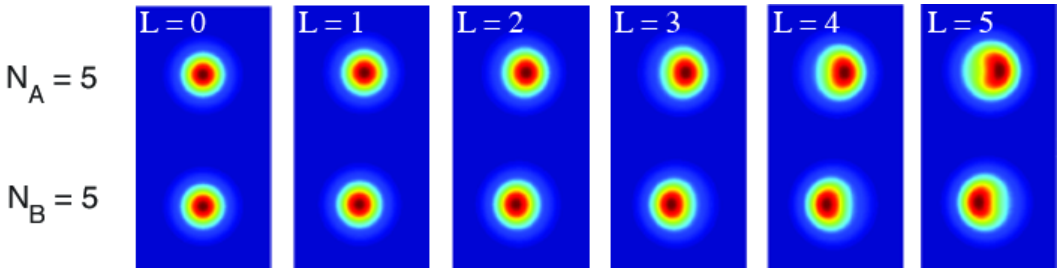

Figure 4.11: Pair correlation plots for a weakly interacting system of $N_A = N_B = 5$ particles in a harmonic trap, for increasing angular momenta to the right; one component displayed in each row. Note how the two species overlap at $L = 0$, but that the rotation induces a phase separation. A particle of species A is fixed at $x = 1.2\,a_{\mathrm{osc}}$, and each panel extends from $-3.5 \leq x/a_{\mathrm{osc}} \leq 3.5$.

from opposite sides (from the left in the upper panel, and from the right in the lower). This is also confirmed by the occupation numbers.

At higher angular momenta $L \gtrsim N_A + N_B$, shown in Fig. 4.12, the two components separate into states where each species has two density maxima. This corresponds to a second vortex entering each component, which can also be seen from the occupation numbers which contain mainly the contribution of states with $m = 0$, $m = 2$ and $m = 4$, for each component.

At even higher angular momenta, it is less clear how to interpret the pair correlation probabilities. The occupation numbers show that very many single-particle states contribute to the condensate wavefunction.

In Fig. 4.13 we show pair correlation profiles for a two-component system with unequal populations, $N_A = 2$ and $N_B = 8$; the angular momentum increases to the right. The angular momenta shown are those of the energetically stable states, or plateaus in Fig. 4.13. We see two examples of coreless vortices at $L = 2$ and $L = 8$. These are the "unit" vortices in this system and it is obvious they must be coreless: at $L = N_A = 2$, component A takes up all angular momentum and forms a vortex with one unit of angular momentum per particle, while component B is in its non-rotating ground state. The corresponding but opposite thing happens at $L = 8$, when component B is rotating around the smaller component.

At even higher angular momenta, we note that the larger component B can form a *doubly* quantized vortex at $L = 16 = 2 \cdot N_B$ (as also confirmed by occupation numbers). This state is energetically stable, even though the

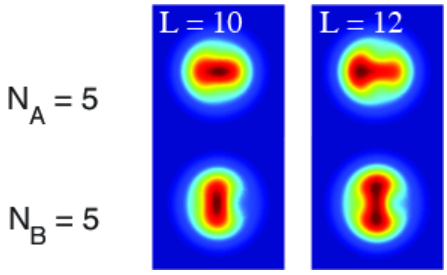

Figure 4.12: Pair correlation plots for a weakly interacting system of $N_A = N_B = 5$ particles in a harmonic trap, for two different angular momenta $L = 10$ and $L = 12$; one component displayed in each row. Here the two species separate such that they each have two maxima, coinciding with the other species' minima. Parameters as in Fig. 4.11.

external trapping is purely harmonic. Instead, it forms as a result of the interspecies interaction: as mentioned in Sec. 1.4, the density of one component acts as an effective potential on the other in the two-component GP equation (1.18). Since the smaller component A in the lower row is non-rotating, its density profile is Gaussian, and it exerts an effectively anharmonic potential on the rotating component. This explains, in a self-consistent way, how multiply quantized vortices can be energetically stable in this system.

States with several singly quantized vortices are still present in this system; they occur at e.g. $L = 14$ in the larger component. The last panel in Fig. 4.13 shows the angular momentum $L = 24 = 3 \cdot N_B$; however from the pair correlation it is not obvious how to characterize this state. Interpreted together with the occupation numbers it has features of both a triply quantized vortex and three singly quantized vortices.

In Paper III we also reported results for a two-component system found from GP calculations. With a single condensate wavefunction, there is an overall phase and vortices are detected as a position where the density has a minimum and the phase changes by 2π around that point. The GP calculations were performed with stronger as well as weaker interaction, and showed how vortices enter the condensate. For $L \geq N_{\max}$, where $N_{\max} = \max(N_A, N_B)$, the largest part of the angular momentum is carried by the larger component, just as in the diagonalization results. As the rotational frequency is increased beyond the unit vortex frequency, one more vortex enters from the outside and merges with the first to form a doubly quantized vortex at the center. Increasing Ω, the two vortices split into two singly charged vortices, as a third

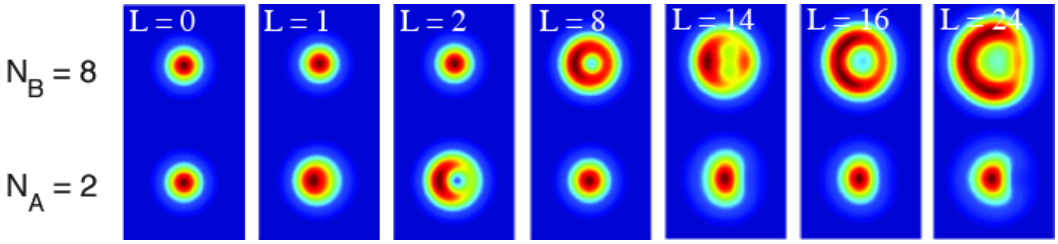

Figure 4.13: Pair correlation plots for a weakly interacting system of $N_A = 2$ and $N_B = 8$ particles in a harmonic trap, for increasing angular momenta to the right, with component A in the lower row and component B in the upper. Coreless "unit" vortices are found at $L = 2$ and $L = 8$. Both singly ($L = 2, 8, 14$) and multiply ($L = 16$) quantized vortices are found to be stable in this system. Note that for $L \geq N_B$, the larger component (B) takes up almost all the angular momentum. Again, one particle of species B is fixed at $x = 1.2\, a_{\mathrm{osc}}$, and each panel extends from $-3.5 \leq x/a_{\mathrm{osc}} \leq 3.5$.

vortex again enters from the outside. The three merge to form a triply quantized vortex, and the process starts again. However this pattern must change at some point, since the process is sustained by the non-rotation of the smaller component. At high enough frequencies, also the smaller component will take up a significant fraction of the angular momentum, and eventually a vortex lattice in both components is expected to occur [95, 96].

In the few-body system, we do not expect a vortex lattice at high angular momenta. However we do have evidence that the smaller component starts to take up angular momentum. At e.g. $L = 40$ the larger component has density maxima in two concentric rings, with the density of the smaller component peaking in the dip between those rings. This is most clearly seen by plotting the density of the two components along e.g. the x axis as done in Fig. 4.14. At these higher angular momenta, many states are near degenerate so the state shown is not necessarily the lowest-energy state for any rotational frequency Ω; however its neighboring states are very similar in structure.

The dispersion relation in the harmonically trapped two-component system turns out to be remarkably simple for particular ranges of angular momenta. As mentioned, it was known from before [59, 47] that in the case of a single-component Bose gas in a harmonic trap, the dispersion relation $E(L)$ is linear for $2 \leq L \leq N$. The diagonalization of a two-component Bose gas shows that this result can be generalized. Considering only interaction energy (since the one-body energy is simply $E_{\mathrm{sp}}/\hbar\omega = N + L$), with $N_{\mathrm{min}} = \min(N_A, N_B)$,

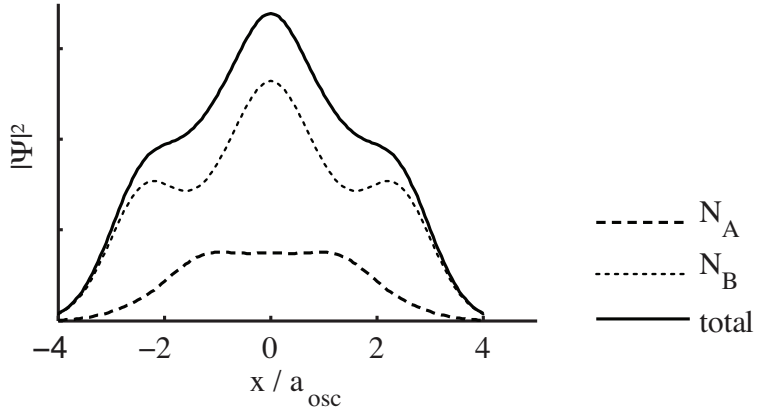

Figure 4.14: The density plotted along the line $y = 0$ for a system of $N_A = 2$ and $N_B = 8$ bosons at angular momentum $L = 40$. We note that the larger component (dotted curve) has two density maxima and that the density maximum of the smaller component (dashed line) coincides with a local minimum of the larger one. The full-drawn line shows the total density.

we find that in the two-component system $E(L)$ has a linear dependence on L in the region $N_{\min} \leq L \leq N_{\max}$. If we measure the energy in units of the interaction energy for two particles in the oscillator ground state, $v_0 = U_0 \int d\mathbf{r} \, |\phi_0|^4 = \sqrt{2/\pi}\hbar\omega a_s/a_z$, then the energy is given by

$$E(L)/v_0 = \frac{1}{2}N(N-1) - \frac{1}{4}N_{\min}N - \frac{1}{4}NL + \frac{1}{4}N_{\min}(N_{\min}-1). \qquad (4.4)$$

This was found to be true up to machine precision, and for any composition of the particle numbers N, $N_{\min}$, and $N_{\max}$ that we were able to examine. This linear dispersion relation is responsible for the discrete jump in Fig. 4.10 between the states with $L = N_{\min}$ and $L = N_{\max}$. In Paper III we investigated this for stronger interactions, to see whether this linearity would get a positive or negative curvature beyond the weakly interacting limit. Solving the GP equation for interaction strengths up to $\gamma = (N-1)v_0/\hbar\omega = 50$ revealed that the curvature is always positive, which excludes the possibility of persistent currents.

There is also an analytic expression for the interaction energy in the region $0 \leq L \leq N_{\min}$. Here, the energy $E(L)$ is parabolic:

$$E(L)/v_0 = \frac{1}{2}N(N-1) - \frac{1}{2}NL + \frac{1}{4}L(L-1). \qquad (4.5)$$

In fact, the structure of the wavefunction for this region is surprisingly simple: only states with $m = 0$ and $m = 1$ contribute. All other occupancies are exactly zero (within machine precision). This allows us to derive analytical expressions for the occupancies. For each component, the number of atoms in the $m = 1$ state is given by

$$\begin{aligned} (N_A)_{m=1} &= L\frac{N_B - L + 1}{N - 2L + 2}, \\ (N_B)_{m=1} &= L\frac{N_A - L + 1}{N - 2L + 2}; \end{aligned} \tag{4.6}$$

the corresponding expressions for the $m = 0$ states are found by subtraction since N_A and N_B are fixed.

The fact that only the states $m = 0$ and $m = 1$ contribute for $0 \leq L \leq N_{\min}$ can be motivated as follows. When the gas first starts to rotate, only the smaller component takes up angular momentum. The other component remains in its Gaussian ground state, and as already argued it exerts an effectively anharmonic potential on the rotating component. Thus the "effective single-particle energies" for the rotating component will be quadratic in m, which makes high m states unfavorable. Still it is remarkable that the occupancies of states with $m \geq 2$ are *exactly* zero in the weakly-interacting limit. In contrast, for a single-component condensate in the anharmonic trap, they have occupancies on the order $1/N$ as compared to the dominant $m = 0$ and $m = 1$ in the diagonalization calculations.

Again the consequences at stronger interactions are further investigated in Paper III, where a GP calculation for interaction strengths $(N - 1)U_0 \leq 50$ showed that indeed for $0 \leq L \leq N_{\min}$, the condensate wavefunction contains only the states with $m = 0$ and $m = 1$. Also, it was found that for the stronger interaction the dispersion relation was approximately parabolic for $N_{\min} \leq L \leq N_{\max}$, in approximate agreement with Eq. (4.5) valid for weak interactions.

In conclusion, diagonalization and GP calculations give a number of consistent results for the two-component Bose gas in a harmonic trap.

Chapter 5

Persistent Currents in a Bose Gas

Metastability of superflow was introduced in Sec. 2.5, where a single-component system was considered. Inspired by results from our previous studies, described in Chapt. 4, we now generalize and investigate a two-component Bose gas in an annular trap.

We begin with the simplest multiply connected geometry: a ring. The system can be considered quasi one-dimensional if wavefunctions are fixed in all but the azimuthal direction. The condensate is unconfined in the angular direction and periodic boundary conditions apply. If R is the radius of the ring, and S its cross sectional area, we can assume single-particle wavefunctions

$$\phi_m(\rho, \varphi, z) = \frac{e^{im\varphi}}{\sqrt{2\pi}} \frac{1}{\sqrt{RS}}, \tag{5.1}$$

which are zero everywhere except on the cross section of the ring. These wavefunctions are again of the form Eq. (2.10) and have angular momentum $L_z = \hbar m$. However, a condensate wavefunction $\Psi = \sqrt{N}\phi_m$ does not represent a vortex in a strict sense since the density minimum is forced by the trapping potential - indeed also the non-rotating state $m = 0$ has a density minimum at the center of the trap.

With the ansatz of constant functions in all but the azimuthal direction, the Hamiltonian for a two-component system (masses assumed to be equal)

reduces to

$$H = -\frac{\hbar^2}{2MR^2}\left(\sum_{i=1}^{N_A}\frac{\partial^2}{\partial\varphi_{A,i}^2}+\sum_{i=1}^{N_B}\frac{\partial^2}{\partial\varphi_{B,i}^2}\right)+\frac{U_{AA}}{2RS}\sum_{i\neq j=1}^{N_A}\delta\left(\varphi_{A,i}-\varphi_{A,j}\right) + \frac{U_{BB}}{2RS}\sum_{i\neq j=1}^{N_B}\delta\left(\varphi_{B,i}-\varphi_{B,j}\right)+\frac{U_{AB}}{RS}\sum_{i=1}^{N_A}\sum_{j=1}^{N_B}\delta\left(\varphi_{A,i}-\varphi_{B,j}\right). \quad (5.2)$$

We now introduce product wavefunctions $\Phi_A = \prod_i \phi_A(\mathbf{r}_i)$, and similarly for Φ_B, following the prescription in Sec. 1.2. The Gross-Pitaevskii energy functional is

$$E\left[\phi_A,\phi_B\right] = -N_A\frac{\hbar^2}{2MR^2}\int\phi_A^*\frac{\partial^2\phi_A}{\partial\varphi^2}d^3r - N_B\frac{\hbar^2}{2MR^2}\int\phi_B^*\frac{\partial^2\phi_B}{\partial\varphi^2}d^3r + \frac{U_{AA}}{2}N_A(N_A-1)\int\left|\phi_A\right|^4 d^3r+\frac{U_{BB}}{2}N_B(N_B-1)\int\left|\phi_B\right|^4 d^3r + U_{AB}N_AN_B\int\left|\phi_A\right|^2\left|\phi_B\right|^2 d^3r. \quad (5.3)$$

For equal interaction strengths $U_{AA} = U_{BB} = U_{AB} = U_0$, at zero angular momentum, this energy is minimized by constant functions $\phi_A = \phi_B = 1/\sqrt{2\pi RS}$. The ground state energy $\mathcal{E}_0$ is

$$\mathcal{E}_0/\epsilon = \frac{\tilde{U}}{4\pi}N(N-1), \quad (5.4)$$

where $\epsilon = \hbar^2/(2MR^2)$ and $\tilde{U} = U_0/(RS\epsilon)$.

Conveniently (using the contact interaction Eq. (1.7) as usual), the interaction energy between two particles is constant, independent of their particular states ϕ_m,

$$E_{\text{int}} = \left\langle\phi_k\phi_l|\hat{H}_{\text{int}}|\phi_m\phi_n\right\rangle = \frac{U}{2\pi RS}\delta_{k+l,m+n}. \quad (5.5)$$

As in Chapt. 4, we will measure angular momentum in units of $\hbar$ unless otherwise explicitly mentioned.

5.1 Dispersion Relation

As we reported in Paper IV, Bloch's results [77] on the dispersion relation for a single-component gas as described in Sec. 2.5 can be generalized to a

two-component system. Assume we have derived the dispersion relation for $0 \leq l \leq 1$, and found that the order parameters are given as

$$\Psi_A = \sum_m c_m \phi_m, \;\; \Psi_B = \sum_m d_m \phi_m, \tag{5.6}$$

with ϕ_m given in Eq. (5.1). We then know the order parameters also at higher angular momenta, as we now explain. For a given angular momentum l_0, $0 \leq l_0 \leq 1$, increasing to $l_n = l_0 + n$ amounts to exciting the center of mass. This implies Eqs. (5.6) must be multiplied by the factor $e^{in\sum \varphi_i}$; the prefactor to the relative wavefunction χ in Eq. (2.23). Writing this factor as a condensate wavefunction and performing the multiplication, we find that for l_n the condensate wavefunction must be given by

$$\Psi_A = \sum_m c_m \phi_{m+n}, \;\; \Psi_B = \sum_m d_m \phi_{m+n}. \tag{5.7}$$

The interaction energy of this state must be the same as that of the original state, since affecting the center of mass does not change the relative positions of the particles. The kinetic energy of the basis states ϕ_m scales as m^2 and if the expectation value of the angular momentum of the state Eq. (5.6) is l_0, then the new kinetic energy is $(l_0 + n)^2 = l_0^2 + 2l_0 n + n^2$, i.e., the kinetic energy has been increased by the amount $2l_0 n + n^2$. If we denote the energy per particle at $n \leq l_n \leq n + 1$ as $E_n(l_n)/N$, then we can write

$$\frac{E_n(l_n)}{N} - l_n^2 = \frac{E_0(l_0)}{N} - l_0^2. \tag{5.8}$$

Since this reasoning applies to any l_0 for which $0 \leq l_0 \leq 1$, and for any l_n, $n \leq l_n \leq n + 1$, there must be a function $e(l)$, which is periodic such that $e(l_0 + n) = e(l_0)$. So we find that the dispersion relation can be written as

$$\frac{E_n(l)}{N} = l^2 + e(l) = (l_0 + n)^2 + e(l_0), \tag{5.9}$$

which contains an envelope part l^2 plus a periodic function $e(l)$, just as in the single-component case.

We can also show that the function $e(l_0)$ is symmetric around $l_0 = 1/2$. If we consider the states

$$\Psi_A^R = \sum_m c_m \phi_{1-m}, \;\; \Psi_B^R = \sum_m d_m \phi_{1-m}, \tag{5.10}$$

the angular momentum is $l' = 1 - l$, and the kinetic energy is $\propto 1 - 2l + l^2$. Thus the energy difference as compared to the energy of the state Eq. (5.6) is $1 - 2l = l' - l$. But we can also calculate the energy difference from Eq. (5.9), which gives $\Delta E/N = l' - l + e(l') - e(l)$, which all in all gives $e(1 - l) = e(l)$. Thus, the function $e(l)$ is symmetric around the point $l = 1/2$. Our numerical calculations are in agreement with these observations even for finite-size systems.

Now, let us introduce the population ratios

$$x_A = \frac{N_A}{N}, \;\; x_B = \frac{N_B}{N}, \tag{5.11}$$

and we assume for definiteness that $x_A \leq x_B$. Consider condensate wavefunctions of the form

$$\Psi_A = \sqrt{x_A N}\,(c_0\phi_0 + c_1\phi_1)\,, \;\; \Psi_B = \sqrt{x_B N}\,(d_0\phi_0 + d_1\phi_1)\,. \tag{5.12}$$

The coefficients c_0, c_1, d_0 and d_1 are subject to the normalization constraints $|c_0|^2 + |c_1|^2 = 1$, $|d_0|^2 + |d_1|^2 = 1$, and we consider a fixed angular momentum $l = |c_1|^2 + |d_1|^2$. Now, the GP energy Eq. (5.3) of the state Eq. (5.12) can be evaluated and minimized, which gives

$$E/\epsilon N = l + \frac{\tilde{g}}{2\pi}\left\{\frac{1}{2} + \left(x_A\,|c_0|\,|c_1| - x_B\,|d_0|\,|d_1|\right)^2\right\}, \tag{5.13}$$

where $\tilde{g} = (N-1)\tilde{U}$ in analogy to previous definitions. For $0 \leq l \leq x_A$ and $x_B \leq l \leq 1$, the two terms in the parenthesis can be set to equal each other, and including more states could not lower the energy any further. Thus, the energy is linear in l, and only the states with $m = 0$ and $m = 1$ are occupied in this range of angular momenta. For the occupancies, we find that

$$\begin{aligned} c_1^2 &= \frac{l(x_B - l)}{x_A(1 - 2l)}, \\ d_1^2 &= \frac{l(x_A - l)}{x_B(1 - 2l)}, \end{aligned} \tag{5.14}$$

and from these c_0^2 and d_0^2 are easily found from the normalization condition. Note that these are, apart from terms of order unity, in agreement with Eqs. (4.6), found for the two-component Bose gas in a harmonic trap.

Numerical diagonalization of the Hamiltonian Eq. (5.2) gives results consistent with these mean-field considerations. We confirm that for $0 \leq L \leq N_A$

and $N_B \leq L \leq N$ (assuming $N_A \leq N_B$) only states with $m = 0$ and $m = 1$ are macroscopically occupied, and their occupancies are given by Eqs. (4.6). The energy is found to be exactly linear in the subspace of basis states $m = 0$ and $m = 1$, and approximate if more states are allowed to participate (which occurs in the diagonalization calculations for stronger interactions). Interestingly, analytical expressions for the full excitation spectrum of the system, can be found by numerical diagonalization in the subspace with $m = 0$ and $m = 1$.

The ground state energy at $L = 0$ is $\mathcal{E}_0/\epsilon = \tilde{U}N(N-1)/4\pi$, in agreement with Eq. (5.3). For $0 \leq L \leq N_A$, the energy spectrum is given exactly by

$$E_q(L)/\epsilon = \mathcal{E}_0 + L + \frac{\tilde{U}}{2\pi}\left(-L + q^2 + (N+1-2L)q\right), \tag{5.15}$$

where $q = 0$ gives the yrast state, $q = 1$ gives the first excited state at that angular momentum, and so on. This expression was found numerically, and the lowest-energy states $E_0(L)/\epsilon = \mathcal{E}_0 + (1 - \tilde{U}/4\pi)L$ agree with the mean-field result Eq. (5.13) apart from finite size corrections. An expression similar to Eq. (5.15) holds for $N_B \leq L \leq N$. The values of q, i.e. the number of excited states, is limited in this subspace by the number of particles in the smaller component, N_A and the total angular momentum L.

The diagonalization with only $m = 0$ and $m = 1$ states also revealed that for $N_A \leq L \leq N_B$, the spectrum is given by

$$E_q(L)/\epsilon = \mathcal{E}_0 + L + \frac{\tilde{U}}{2\pi}\left(-L^2 + NL - N_A(N_B+1) + q^2 + (N_B - N_A + 1)\,q\right) \tag{5.16}$$

This result is remarkable but less important than in the other regions of angular momenta, since in this region other states than $m = 0$ and $m = 1$ can lower the energy even in the limit of weak interactions. The occupancies in this region are linear in L,

$$c_1^2 = \frac{N_A}{N_A - N_B - 2}L - \frac{N_A(N_B-1)}{N_A - N_B - 2}, \tag{5.17}$$

and the other occupancies can be straightforwardly deducted using the conditions of normalization and definite angular momentum. In Fig. 5.1 we plot the energy spectrum for 20 particles in this subspace. As we see, in some regions the excited states can be described by both Eqs. (5.15) and (5.16); the yellow and purple curves correspond to these with $q = 4$. The green line is the yrast line for $0 \leq L \leq N_A$ which is achieved by setting $q = 0$ in Eq. (5.15); this result is expected to be valid also in a realistic system (larger basis).

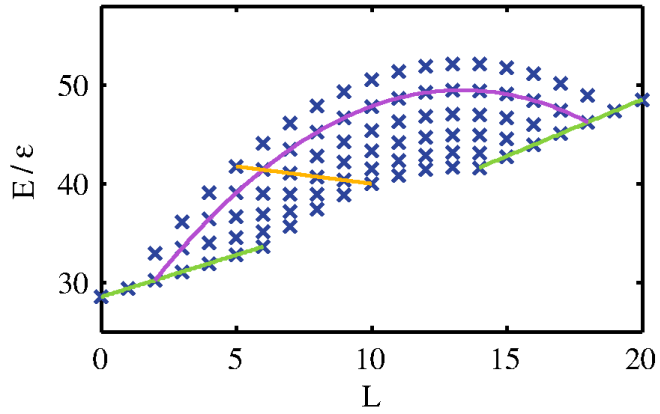

Figure 5.1: Dispersion relation in the subspace of basis states with $m = 0$ and $m = 1$ for a system with $N_A = 4$, $N_B = 16$ particles. The crosses are results from a full diagonalization of the Hamiltonian. The green line is the yrast line expected to be valid also in a "real" system (larger basis). The purple curve is calculated from Eq. (5.16) with $q = 4$. The yellow line shows Eq. (5.15), again with $q = 4$.

As a curiosity the simple expressions for the spectrum also gives us analytically the eigenvalues of a particular tri-diagonal matrix of arbitrary dimension. We write the eigenstates of the Hamiltonian as

$$|n\rangle = \left|0^n\ 1^{N_A-n}\right\rangle_A \left|0^{N_B-n}\ 1^n\right\rangle_B . \tag{5.18}$$

This state has angular momentum $L = N_A$ and in matrix formulation, the Hamiltonian Eq. (5.2) in this basis is a tri-diagonal matrix. We consider only interaction energy and set $\tilde{U} = 1$. If we name the matrix elements $f_{n,m}$, $n, m \geq 0$, then all are zero except

$$\begin{aligned} f_{n,n-1} &= n\sqrt{(L-n+1)(N-L-n+1)}, \\ f_{n,n} &= \frac{N}{2}(N-1) + n(N-2n), \\ f_{n,n+1} &= (n+1)\sqrt{(L-n)(N-L-n)}. \end{aligned} \tag{5.19}$$

with $n = 0, ..., L$. The expression within parenthesis of Eq. (5.15) trivially gives the eigenvalues of this matrix.

5.2 Persistent Currents

We now focus on metastability of persistent currents in a repulsively interacting Bose gas. As a reminder from Sec. 2.5: metastable persistent currents can appear when there is an energy barrier between the rotating state and the non-rotating absolute ground state. This barrier is caused by the interactions; if these are too weak, no metastable superflow can result.

A toy model calculation gives a minimum interaction strength g_{min} where superflow is possible. Assume a (single-component) condensate wavefunction including only states with $m = 0$ and $m = 1$:

$$\Psi = \sqrt{\frac{N}{2\pi RS}} \left(\sqrt{1-l} + \sqrt{l} e^{i(\varphi+\lambda)} \right). \tag{5.20}$$

This wavefunction has the angular momentum l, and λ is a parameter. Evaluating the GP energy functional Eq. (5.3), we find

$$E/\epsilon N = l + \frac{\tilde{g}}{2\pi} \left(\frac{1}{2} + l - l^2 \right). \tag{5.21}$$

The slope at $l = 1$, where the metastability can appear, becomes zero for $\tilde{g}_{\mathrm{min}} = 2\pi$; beyond this a local minimum develops and persistent currents can become possible. A similar procedure gives the minimum value g_{min} for persistent currents with higher angular momenta. However, we can in fact find the critical value exactly by including also the state $m = 2$; then we find $\tilde{g}_{\mathrm{min}} = 3\pi$.

In the two-component system, the dispersion relation is linearly increasing with l for $x_B \leq l \leq 1$ and no local minimum is possible at $l = 1$. Instead it can develop at $l = x_B$ and the condition is found to be

$$\tilde{g}_{\mathrm{min}} = \frac{3\pi}{(4x_B - 3)}. \tag{5.22}$$

A short outline of how to arrive at this condition is the following; it is similar to the single-component situation. At $l = x_B$ the B component essentially occupies the ϕ_1 state (see Eq. (5.1)) and the A component is in the non-rotating state ϕ_0. If we consider an angular momentum slightly below x_B, e.g. $l = x_B - \varepsilon$ with ε small, it is reasonable to assume order parameters of the form $\Psi_A \propto c_{-1}\phi_{-1} + c_0\phi_0 + c_1\phi_1$ and $\Psi_B \propto d_0\phi_0 + d_1\phi_1 + d_2\phi_2$. The coefficients $|c_{-1}|^2 \sim |c_1|^2 \sim \varepsilon$ and $|d_1|^2 \sim |d_2|^2 \sim \varepsilon$, so when evaluating the energy functional Eq. (5.3) terms of order $\sim \varepsilon^2$ can be ignored. Minimizing

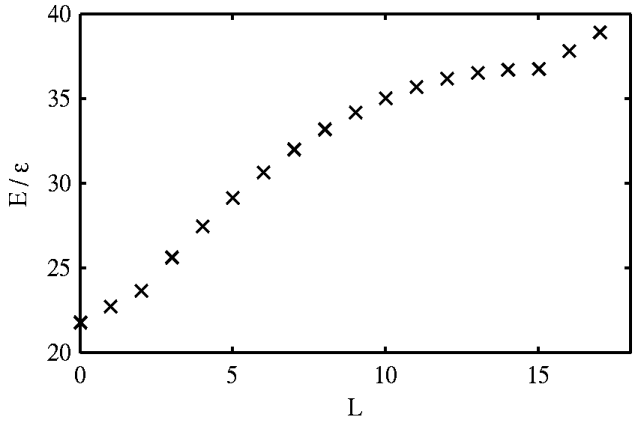

Figure 5.2: Dispersion relation for $N_A = 2$ and $N_B = 15$ particles ($x_B \approx 0.88$) at $\tilde{g} \approx 18$, which according to Eq. (5.22) is the minimum interaction strength where persistent currents could occur. This diagonalization calculation agrees with the analytical calculation: the dispersion relation is indeed flat at $L = 15$, and for stronger interactions, a local minimum develops.

under the usual constraints one can then calculate the slope of the dispersion relation and find $g_{\min}$. For details, see Paper IV.

The diagonalization calculations for the single-component case, $x_B = 1$, agree with the value of Eq. (5.22) to good accuracy. It is difficult, however, to make a systematic comparison for a two-component condensate due to the finite size of the system. Equation (5.22) diverges at $x_B = 3/4$ and in order for the diagonalization to be reliable, the interaction strength must not be too large i.e., a large value of x_B would be preferable. On the other hand, since $x_B = N_B/N$ and the number of particles has to be integer, a large x_B implies a large total particle number, which again makes diagonalization more difficult. However, we have performed calculations for some particular situations and results are consistent with Eq. (5.22). An example of a diagonalization calculation is shown in Fig. 5.2, where we have plotted the dispersion relation for $N_A = 2$, $N_B = 15$ particles at $\tilde{g} \approx 18$, which according to Eq. (5.22) is the interaction strength beyond which persistent currents can appear. We note that the diagonalization result agrees with this equation: the dispersion relation has a flat curvature at $L = 15$. For larger interaction strengths, we have confirmed that a minimum develops.

5.3 Two-Dimensional Annulus

A natural extension to the quasi one-dimensional ring is to consider an annulus with a finite width and a realistic wavefunction in this direction (as opposed to the step function considered earlier). There are several possible choices for a potential with these properties. The anharmonic potential in Eq. (2.19) with opposite signs of the quadratic and quartic terms gives rise to a "mexican hat" shape potential and has been used in e.g. Ref. [101]. In the experiment [82] a Gaussian potential was superimposed on the harmonic trapping, and this has also been theoretically investigated [102]. We report here results using a displaced harmonic potential

$$V(\rho) = \frac{1}{2} M\omega^2 \left(\rho - R_0\right)^2 . \tag{5.23}$$

This is a convenient choice since several results from the one-dimensional case scale with the variables ω and the radius of the "ring" R_0. We have also made sample investigations of a harmonic trapping with a superimposed Gaussian, and results are qualitatively similar.

The single-particle wavefunctions are of the form

$$\phi_m(\rho, \varphi) = f_m(\rho) \frac{e^{im\varphi}}{\sqrt{2\pi}}, \tag{5.24}$$

where we find the radial wavefunction $f_m(\rho)$ numerically. It is clear that for large ω, i.e. tight radial confinement, the radial part of the wavefunction will be very similar for different values of m. This means that even if we allow for motion in this direction, the system cannot make use of this degree of freedom and will behave as a one-dimensional system. However results must not quantitatively agree with those from the previous section since there the wavefunction in the radial direction was simply a step function.

Using the potential Eq. (5.23) we look for persistent currents in both single-component and two-component systems, employing mean-field calculations as well as diagonalization. In the diagonalization calculation, we find the interaction strength $g_{\min}$ where persistent currents first become possible, by investigating when the dispersion relation develops a local minimum. In the GP calculation, we use the method of imaginary time propagation as before [25]. This method, which transforms the GP equation to a diffusion-like equation, will drive the system along the dispersion line until it finds a minimum. We choose an initial wavefunction that has the angular momentum of the persistent current we are looking for; then, if the dispersion relation has a local

minimum, the final state of the propagation will still have angular momentum. If there is no local minimum, the final state will be the non-rotating ground state.

By varying ω or R_0, we can investigate how the minimal interaction strength necessary for persistent currents depends on the dimensionality of the system. For large confinement frequency ω, the confinement is very tight and the system behaves essentially as in the one-dimensional case. Nevertheless it has an extension in the radial direction $\sim a_{\rm osc} = \sqrt{\hbar/M\omega}$. As usual we assume the wavefunction fixed in the z direction, with a condensate size $\sim a_z$. We can rewrite the condition Eq. (5.22) using $\tilde{U} = U_0/(RS\epsilon)$, with $S \sim a_{\rm osc}a_z$ and $\epsilon = \hbar^2/(2MR^2)$, and find how $g_{\rm min}$ should scale with the parameters R_0 and ω. This gives

$$g_{\rm min} = \frac{3\pi}{2}\frac{\hbar^{5/2}a_z}{M^{3/2}}\frac{1}{R_0\sqrt{\omega}}, \tag{5.25}$$

with $x_B = 1$. This scaling behavior, valid when $R_0 \gg a_{\rm osc}$, has been verified numerically, by both diagonalization and GP calculations. An example is shown in Fig. 5.3. We have plotted the value of $g_{\rm min}$, as calculated from diagonalization, as a function of $1/R_0$, for constant $\omega = 1$. Clearly, for large R_0, $g_{\rm min}$ is linear in $1/R_0$, in agreement with Eq. (5.25). However, as the system becomes really two-dimensional, $g_{\rm min}$ starts to increase faster. This is reasonable, since we have added one degree of freedom to the system which it can use to lower its energy. Thus, stronger interaction is needed for the system to support persistent currents in two dimensions. We restrict the calculation to $R_0 \geq 2$, since for smaller values the density is no longer annular but has a significant contribution also at the trap center.

The case where instead ω is varied to show the dependence of $g_{\rm min}$ on the dimensionality, is shown in Paper V. There also the comparison with GP is reported, which is in good agreement. Again, when the system is approaching one-dimensionality, the scaling behavior of Eq. (5.25) is retained, and for an annulus with a finite width, $g_{\rm min}$ is increased as compared to the one-dimensional case.

We also study the dispersion relation that results from numerical diagonalization. The results that were found in the one-dimensional system remain approximately valid as the system becomes more two-dimensional. In the two-component system, the energy is approximately linear in L for $0 \leq L \leq N_A$ and $N_B \leq L \leq N$, and the dispersion relation is approximately composed of a periodic function plus a parabolic envelope.

For diagonalization of the two-component system in the annular trap, we run into the same complications as in the one-dimensional system: with fi-

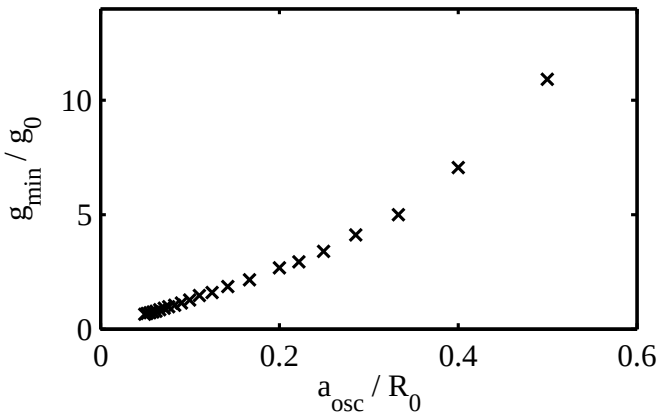

Figure 5.3: The critical interaction strength $g_{\min}$ where persistent currents become possible, as a function of $1/R_0$, where R_0 is the radius of the two-dimensional ring, see Eq. (5.23). The oscillator frequency is kept constant at $\omega = 1$. For small values of $1/R_0$, the system is essentially one-dimensional, and the function is a straight line in agreement with the 1D limit Eq. (5.25). However, at larger values of $1/R_0$, $g_{\min}$ increases faster as the system becomes more two-dimensional.

nite particle numbers, it takes large total particle numbers to achieve small fractions $x_A = N_A/N$. If this fraction is large, the interaction strength $g_{\min}$ which we are looking for is also large, which increases the necessary basis size in the diagonalization calculation. A diagonalization performed in a too small basis gives a value of $g_{\min}$ which is too low. This is because the state where the persistent current can take place, at $L = N_B$, requires fewer single-particle states to be well described than the states at slightly smaller angular momenta, $L \lesssim N_B$. Thus, if these latter states are not well described, their energy is too high which creates a false local minimum at $L = N_B$.

Even though we cannot freely vary x_A, we can make a sample calculation. For e.g. $N_A = 2$ and $N_B = 15$ particles, in an annular trap with $R_0 = 4$ and $\omega = 1$, it is possible to create a persistent current with one unit of circulation. The dispersion relation is shown in Fig. 5.4, which also shows the dispersion for the single-component system with $N = 17$. At this particular interaction strength $g/g_0 = 30$, the single-component dispersion relation has two local minima, and thus allows for persistent currents with one or two units of circulation. For the two-component system, the higher minimum has vanished.

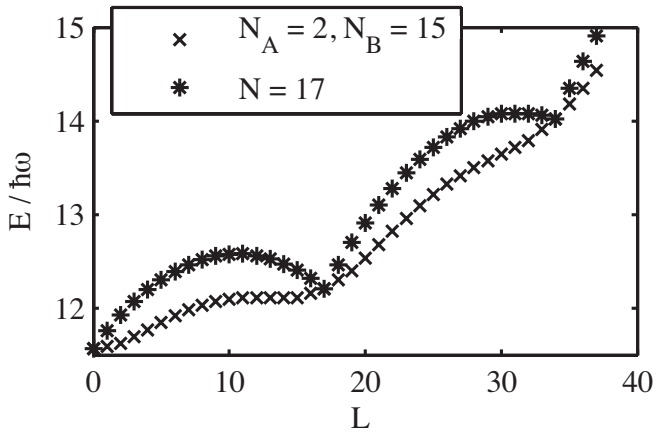

Figure 5.4: Disperson relation for $N_A = 2$ and $N_B = 15$ particles (crosses), and $N = 17$ particles (stars). The interaction strength is $g/g_0 = 30$. Note that the single-component system has two local minima, at $L = N$ and $L = 2N$, whereas in the system with a small admixture of a second component ($x_B \approx 0.88$), persistent currents with higher circulation are not possible.

In one dimension, we found that persistent currents with higher circulation disappeared as a second component was introduced. Remarkably, our Gross-Pitaevskii calculations show that with a finite radial width of the condensate and a small enough admixture of a second component, they are in fact still possible. This is an interesting finding. We have already shown (Sec. 4.2 and Paper III) that for a two-component condensate in a harmonic trap (fully two-dimensional), persistent currents are not possible. Starting from such a system, persistent currents are unstable, then they can appear as the trap is made annular, only to disappear again if the trap is made strictly one-dimensional.

Chapter 6

Conclusions and Outlook

Bose-Einstein condensation is a fascinating state of matter, which exhibits many counter-intuitive phenomena. The focus of this thesis has been the behavior of the zero-temperature Bose gas under rotation and two effects related to superfluidity: quantized vortices and meta-stable persistent currents. It was shown how diagonalization of the Hamiltonian can be applied to study mixtures of rotating Bose gases, which has given answers beyond the mean-field approximation and increased our understanding of these systems from a microscopic perspective.

Our studies can be divided into three sub-systems: a single-component gas in an anharmonic potential, a two-component gas in a harmonic potential, and finally single- and two-component gases in annular potentials. All three sub-systems have in common that the (effective) single-particle energies are quadratic in the single-particle angular momentum m, which implies that for weak enough interaction and low enough angular momenta, the condensate wavefunction is built up of states with only $m = 0$ and $m = 1$. In fact, in the two-component condensate in a harmonic trap, all other occupancies are *exactly* zero in the limit of weak interactions.

This remarkably simple structure of the condensate wavefunction has allowed us to derive a number of analytical results. For the two-component condensate in these three kinds of traps, there are analytical expressions for the occupancies in a range of small angular momenta. Further, for two components in either a two-dimensional harmonic trap, or a one-dimensional ring potential, also the dispersion relation can be written analytically, in a range of low angular momenta and for weak interaction. These expressions are exact in the weakly interacting limit. This is a rare case where there are exact

results for a quantum-mechanical many-body system which, through the use of Feshbach resonances [103], should also be realizable experimentally.

In a single-component condensate in a harmonic trap, multiply quantized vortices are known to always be unstable towards splitting into several singly quantized vortices. We have shown that this is not necessarily true in a two-component condensate. Multiply quantized vortices are in this system stable through being *coreless*, i.e., one component forms a vortex state while the other fills up the vortex core. The non-rotating component exerts an effectively anharmonic potential on the rotating species, and thus it is the repulsive interspecies interaction which generates this stabilizing mechanism.

Turning to annular traps, we have investigated the conditions under which the dispersion relation can have a local minimum, thus enabling metastable persistent currents. It was known from before that this can happen at strong enough interactions in a one-dimensional ring; we have generalized this to two-component systems both in rings and also two-dimensional annular traps. It is found that opening up the width of the annulus, thus making the system two-dimensional, increases the necessary interaction strength for persistent currents to occur. Generally for both one-dimensional rings and two-dimensional annuli, also the admixture of a second component increases the value of the critical interaction strength where persistent currents first appear.

Interestingly, we find that persistent currents with more than one unit of circulation are not stable in a two-component system in a one-dimensional ring. As the ring is modified to an annulus, they can appear for some interaction strength, but then if the annulus is modified to a harmonic trap, again these currents are destabilized. In the experiment of Ref. [82], a supercurrent with two units of circulation was created in a single-component system. The experimenters could modify their trapping potential from a harmonic oscillator to a toroid. They found that in the torus potential, the current with higher circulation was stable, but in the harmonic potential, it was not. It would be very interesting to test our prediction for the behavior of two-component systems in such a set-up, particularly if also the one-dimensional limit could be reached - in this limit again the current with higher circulation should vanish in a two-component condensate.

There are several straightforward extensions to these studies. Regarding the harmonically trapped two-component system, it seems likely that one could find an analytical expression for the exact many-body wavefunction of the yrast states at low angular momenta, similarly to that discussed in Refs. [60, 63, 62]. By varying the parameters which we so far kept fixed, or modifying the potentials in various ways (easily done within the diagonal-

ization scheme), one can map out the behavior of the Bose gas in a large parameter range, which reveals how one can in detail engineer the state of a BEC.

However, there is a multitude of other systems for which diagonalization of the Hamiltonian could be (and is being) applied. Even though the system size in some sense must be small (small particle numbers, restricted number of dimensions etc.), conclusions can be drawn that are relevant also for larger systems. Furthermore, recent advances in imaging techniques using fluorescence [104, 105, 106], have made it possible to access individual atoms trapped in optical lattices. Generally, the number of particles per lattices site in these experiments is of order unity or less. However, in the future it might be possible to trap a small number of atoms in each well of an optical lattice and detect these with high resolution. Diagonalization could possibly produce exact results to be compared with such an experiment. This would be an interesting opportunity to compare a theory essentially without approximations, with an experiment essentially without impurities.

Bibliography

[1] P. Kapitza, Nature **141**, 74 (1938)

[2] J. F. Allen and A. D. Misener, Nature **141**, 75 (1938)

[3] F. London, Nature **141**, 644 (1938)

[4] M.H. Anderson, J.R. Ensher, M.R. Matthews, C.E. Wieman, and E.A. Cornell, Science **269**, 198 (1995)

[5] K. B. Davis, M.-O. Mewes, M. R. Andrews, N. J. van Druten, D. S. Durfee, D. M. Kurn, and W. Ketterle, Phys. Rev. Lett. **75**, 3969 (1995)

[6] E. A. Cornell and C. E. Wieman, Rev. Mod. Phys. **74**, 875 (2002)

[7] W. Ketterle, Rev. Mod. Phys. **74**, 1131 (2002)

[8] A. D. Cronin, J. Schmiedmayer, and D. E. Pritchard, Rev. Mod. Phys. **81**, 1051–1129 (2009)

[9] O. Morsch and M. Oberthaler, Rev. Mod. Phys. **78**, 179 (2006)

[10] Y. Castin, Z. Hadzibabic, S. Stock, J. Dalibard, and S. Stringari, Phys. Rev. Lett. **96**, 040405 (2006)

[11] J. Dunningham, K. Burnett and W. D. Phillips, Phil. Trans. R. Soc. A **363**, 2165 (2005)

[12] B. T. Seaman, M. Krämer, D. Z. Anderson, and M. J. Holland, Phys. Rev. A **75**, 023615 (2007)

[13] R.A. Pepino, J. Cooper, D.Z. Anderson, and M.J. Holland, Phys. Rev. Lett. **103**, 140405 (2009).

[14] S. Inouye, M. R. Andrews, J. Stenger, H.-J. Miesner, D. M. Stamper-Kurn and W. Ketterle, Nature **392**, 151 (1998)

[15] C. Chin, R. Grimm, P. Julienne and E. Tiesinga, Rev. Mod. Phys. **82**, 1225 (2010)

[16] C. J. Pethick and H. Smith, *Bose-Einstein Condensation in Dilute Gases*, Cambridge University Press 2004

[17] L. Pitaevskii and S. Stringari, *Bose-Einstein Condensation*, Clarendon Press, Oxford 2003

[18] F. Dalfovo, S. Giorgini, L. P. Pitaevskii, and S. Stringari, Rev. Mod. Phys. **71**, 463 (1999)

[19] A. J. Leggett, Rev. Mod. Phys. **73**, 307 (2001)

[20] A. L. Fetter, Rev. Mod. Phys. **81**, 647 (2009)

[21] K. Kasamatsu, M. Tsubota, and M. Ueda, Int. J. of Mod. Phys. B, **19**, 1835 (2005)

[22] I. Bloch, J. Dalibard, and W. Zwerger, Rev. Mod. Phys. **80**, 885 (2008)

[23] H. Saarikoski, S. M. Reimann, A. Harju, and M. Manninen, arXiv:1006.1884v1, Rev. Mod. Phys. in print

[24] J. Dalibard, *Collisional dynamics of ultra-cold atomic gases*, Proceedings of the International School of Physics Enrico Fermi, Varenna 1998

[25] S. A. Chin and E. Krotscheck, Phys. Rev. E **72**, 036705 (2005)

[26] G. Modugno, M. Modugno, F. Riboli, G. Roati and M. Inguscio, Phys. Rev. Lett. **89**, 190404 (2002)

[27] D. S. Hall, M. R. Matthews, J. R. Ensher, C. E. Wieman, and E. A. Cornell, Phys. Rev. Lett. **81**, 1539 (1998)

[28] J. Stenger, S. Inouye, D. M. Stamper-Kurn, H.-J. Miesner, A. P. Chikkatur and W. Ketterle, Nature **396**, 345 (1998)

[29] Z. Hadzibabic, C. A. Dieckmann, S. Gupta, M. W. Zwierlein, A. Görlitz, and W. Ketterle, Phys. Rev. Lett. **88**, 160401 (2002)

[30] T.-L. Ho and V. B. Shenoy, Phys. Rev. Lett. **77**, 3276 (1996)

[31] B. D. Esry, Chris H. Greene, James P. Burke, Jr., and John L. Bohn, Phys. Rev. Lett. **78**, 3594 (1997)

[32] H. Pu and N. P. Bigelow, Phys. Rev. Lett. **80**, 1130 (1998)

[33] E. Timmermans, Phys. Rev. Lett. **81**, 5718 (1998)

[34] S. L. Cornish, N. R. Claussen, J. L. Roberts, E. A. Cornell, and C. E. Wieman, Phys. Rev. Lett. **85**, 1795 (2000)

[35] S. Viefers, J. Phys.: Condens. Matter **20**, 123202 (2008)

[36] N. R. Cooper, Advances in Physics **57**, 539 (2008)

[37] M. Möttönen, V. Pietilä, and S. M. M. Virtanen, Phys. Rev. Lett. **99**, 250406 (2007)

[38] E. A. L. Henn, J. A. Seman, E. R. F. Ramos, M. Caracanhas, P. Castilho, E. P. Olímpio, G. Roati, D. V. Magalhães, K. M. F. Magalhães, and V. S. Bagnato, Phys. Rev. A **79**, 043618 (2009)

[39] M. Kobayashi and M. Tsubota, Phys. Rev. Lett. **94**, 065302 (2005)

[40] M. S. Paoletti, Michael E. Fisher, K. R. Sreenivasan, and D. P. Lathrop, Phys. Rev. Lett. **101**, 154501 (2008)

[41] A. C. White, C. F. Barenghi, N. P. Proukakis, A. J. Youd, and D. H. Wacks, Phys. Rev. Lett. **104**, 075301 (2010)

[42] P. L. Halkyard, M. P. A. Jones, and S. A. Gardiner, Phys. Rev. A **81**, 061602(R) (2010)

[43] M. Abad, M. Guilleumas, R. Mayol, and M. Pi, D. M. Jezek, Phys. Rev. A **81**, 043619 (2010)

[44] T. W. Neely, E. C. Samson, A. S. Bradley, M. J. Davis, and B. P. Anderson, Phys. Rev. Lett. **104**, 160401 (2010)

[45] Y. Castin, and R. Dum, Eur. Phys. J. D **7**, 399 (1999)

[46] D. A. Butts and D. S. Rokhsar, Nature (London) **397**, 327 (1999)

[47] G. M. Kavoulakis, B. Mottelson, and C. J. Pethick, Phys. Rev. A **62**, 063605 (2000)

[48] Y. Shin, M. Saba, M. Vengalattore, T. A. Pasquini, C. Sanner, A. E. Leanhardt, M. Prentiss, D. E. Pritchard, and W. Ketterle, Phys. Rev. Lett. **93**, 160406 (2004)

[49] G. Baym and C. J. Pethick, Phys. Rev. Lett. **76**, 6 (1996)

[50] E. Lundh, C. J. Pethick, and H. Smith, Phys. Rev. A **55**, 2126 (1997)

[51] A. A. Svidzinsky and A. L. Fetter, Phys. Rev. A **62**, 063617 (2000)

[52] M. R. Matthews, B. P. Anderson, P. C. Haljan, D. S. Hall, C. E. Wieman, and E. A. Cornell, Phys. Rev. Lett. **83**, 2498 (1999)

[53] J. E. Williams and M. J. Holland, Nature **401**, 568 (1999)

[54] K. W. Madison, F. Chevy, W. Wohlleben, and J. Dalibard, Phys. Rev. Lett. **84**, 806 (2000)

[55] S. Sinha and Y. Castin, Phys. Rev. Lett. **87**, 190402 (2001)

[56] J. R. Abo-Shaeer, C. Raman, J. M. Vogels, and W. Ketterle, Science **292**, 476 (2001)

[57] B. Mottelson, Phys. Rev. Lett **83**, 2695 (1999)

[58] J. R. Grover, Phys. Rev. **157**, 832 (1967)

[59] G. F. Bertsch and T. Papenbrock, Phys. Rev. Lett. **83**, 5412 (1999)

[60] T. Papenbrock and G. F. Bertsch, Phys. Rev. A **63**, 023616 (2001)

[61] T. Papenbrock and G. F. Bertsch, J. Phys. A: Math. Gen. **34**, 603 (2001)

[62] A. D. Jackson and G. M. Kavoulakis, Phys. Rev. Lett. **85**, 2854 (2000)

[63] R. A. Smith and N. K. Wilkin, Phys. Rev. A **62**, 061602 (2000)

[64] S. Viefers and M. Taillefumier, J. Phys. B: At. Mol. Opt. Phys. **43**, 155302 (2010)

[65] A. L. Fetter, PRA **64**, 063608 (2001)

[66] E. Lundh, Phys. Rev. A **65**, 043604 (2002)

[67] I. Coddington, P. C. Haljan, P. Engels, V. Schweikhard, S. Tung and E. A. Cornell, Phys. Rev. A **70**, 063607 (2004)

[68] V. Schweikhard, I. Coddington, P. Engels, V. P. Mogendorff, and E. A. Cornell, Phys. Rev. Lett. **92**, 040404 (2004)

[69] V. Bretin, S. Stock, Y. Seurin, and J. Dalibard, Phys. Rev. Lett. **92**, 050403 (2004)

[70] A. Aftalion and P. Mason, Phys. Rev. A **81**, 023607 (2010)

[71] K. Kasamatsu, M. Tsubota, and M. Ueda, Phys. Rev. A **66**, 053606 (2002)

[72] A. E. Leanhardt, A. Görlitz, A. P. Chikkatur, D. Kielpinski, Y. Shin, D. E. Pritchard, and W. Ketterle, Phys. Rev. Lett. **89**, 190403 (2002)

[73] P. Engels, I. Coddington, P. C. Haljan, V. Schweikhard, and E. A. Cornell, Phys. Rev. Lett. **90**, 170405 (2003)

[74] G. B. Hess and W. M. Fairbank, Phys. Rev. Lett. **19**, 216 (1967)

[75] A. J. Leggett, Rev. Mod. Phys. **71**, S318 (1999)

[76] E. J. Mueller, Phys. Rev. A **66**, 063603 (2002)

[77] F. Bloch, Phys. Rev. A **7**, 2187 (1973)

[78] L. Salasnich, A. Parola, and L. Reatto, Phys. Rev. A **59**, 2990 (1999)

[79] M. Benakli, S. Raghavan, A. Smerzi, S. Fantoni and S. R. Shenoy, Europhys. Lett. **46**, 275 (1999)

[80] Yu. Kagan, N. V. Prokof'ev, and B. V. Svistunov, Phys. Rev. A **61**, 045601 (2000)

[81] M. Ögren and G. M. Kavoulakis, J. Low Temp. Phys. **149**, 176 (2007)

[82] C. Ryu, M. F. Andersen, P. Cladé, Vasant Natarajan, K. Helmerson, and W. D. Phillips, Phys. Rev. Lett. **99**, 260401 (2007)

[83] M. Ueda and A. J. Leggett, Phys. Rev. Lett. **83**, 1489 (1999)

[84] R. Kanamoto, H. Saito, and M. Ueda, Phys. Rev. A **68**, 043619 (2003)

[85] G. M. Kavoulakis, Phys. Rev. A 69, 023613 (2004)

[86] A. D. Jackson, G. M. Kavoulakis, B. Mottelson, and S. M. Reimann, Phys. Rev. Lett. **86**, 945 (2001)

[87] D.C. Sorensen, R.B. Lehoucq, C. Yang, and K. Maschhoff, ARPACK Users' Guide, www.caam.rice.edu/software/ARPACK

[88] A. D. Jackson, G. M. Kavoulakis, and E. Lundh, Phys. Rev. A 69, 053619 (2004)

[89] A. D. Jackson, G. M. Kavoulakis, Phys. Rev. A **70**, 023601 (2004)

[90] N. K. Wilkin, J. M. F. Gunn, and R. A. Smith, Phys. Rev. Lett. **80**, 2265 (1998)

[91] G. M. Kavoulakis, A. D. Jackson, and Gordon Baym, Phys. Rev. A **70**, 043603 (2004)

[92] T. K. Ghosh, Phys. Rev. A **69**, 043606 (2004)

[93] E. Lundh, A. Collin, and K.-A. Suominen, Phys. Rev. Lett. 92, 070401 (2004)

[94] A. Collin, E. Lundh, and K.-A. Suominen, Phys. Rev. A **71**, 023613 (2005)

[95] E. J. Mueller and T.-L. Ho, Phys. Rev. Lett. **88**, 180403 (2002)

[96] K. Kasamatsu, M. Tsubota, and M. Ueda, Phys. Rev. Lett. **91**, 150406 (2003)

[97] V. Schweikhard, I. Coddington, P. Engels, S. Tung, and E. A. Cornell, Phys. Rev. Lett. **93**, 210403 (2004)

[98] H. T. C. Stoof, E. Vliegen, and U. Al Khawaja, Phys. Rev. Lett. **87**, 120407 (2001)

[99] J.-P. Martikainen, A. Collin, and K.-A. Suominen, Phys. Rev. Lett. **88**, 090404 (2002)

[100] U. Al Khawaja and H. T. C. Stoof, Nature **411**, 918 (2001)

[101] A. Aftalion and I. Danaila, Phys. Rev. A **69**, 033608 (2004)

[102] J. Tempere, J. T. Devreese and E. R. I. Abraham, Phys. Rev. A **64**, 023603 (2001)

[103] G. Roati, M. Zaccanti, C. D'Errico, J. Catani, M. Modugno, A. Simoni, M. Inguscio, and G. Modugno, Phys. Rev. Lett. **99**, 010403 (2007)

[104] K. D. Nelson, X. Li and D. S. Weiss, Nature Physics **3**, 556 (2007)

[105] W. S. Bakr, J. I. Gillen, A. Peng, S. Fölling, and M. Greiner, Nature **462**, 74 (2009)

[106] J. F. Sherson, C. Weitenberg, M. Endres, M. Cheneau, I. Bloch, and S. Kuhr, Nature 09378 (2010)

Part II

The Papers

Chapter 7

Brief Summaries of the Papers

All papers present studies related to the rotational properties of dilute Bose gases at zero temperature. In general, I have been responsible for the diagonalization calculations. This method has the advantage of being "exact" in the limit of weak interaction strength (depending on the choice of basis), but due to numerical constraints, we are limited to small particle numbers on the order of 10. In an actual experimental condensate, the particle number is very large, $\sim 10^4 - 10^6$. Thus, to give a good description of the experimental system, we usually compare our calculations to mean-field calculations using the Gross-Pitaevskii approach. This has the disadvantage that it does not incorporate correlations, but on the other hand it does not show finite-size effects. These two methods complement each other, which gives a more reliable description of the properties of the system.

Paper I: Rotating Bose-Einstein Condensates Confined in an Anharmonic Potential

S. Bargi, G. M. Kavoulakis, and S. M. Reimann,
Phys. Rev. A **73**, 033613 (2006)

The harmonic oscillator trap is a special case due to its equally-spaced energy spectrum, which produces a large degree of degeneracy in a many-particle system. This has several consequences; it is e.g. not possible to rotate the system at a frequency higher than the trap frequency, and if a doubly quantized vortex is produced, it is energetically unstable and will break up into two singly quantized vortices. Furthermore, in attractively interacting condensates in

harmonic traps, vortices are never stable and the system will accommodate angular momentum through center of mass rotation.

Here we instead investigate a slightly anharmonic trap, to break this degeneracy. We find that this gives rise to energetically stable multiply quantized vortices in both repulsively and attractively interacting condensates. In the attractive case we also find evidence for center of mass rotation, which occurs at stronger attractive interaction.

The importance of our study is that it goes beyond the mean-field approximation of the Gross-Pitaevskii equation, which does not take correlations into account. Thus its validity, particularly in the case of attractive interactions, requires confirmation. However, our results are consistent with previous Gross-Pitaevskii results, which thus can be considered reliable.

I did all the calculations and produced all figures, and participated in writing the text. The analysis of the data was done in collaboration between all three authors.

Paper II: Mixtures of Bose Gases under Rotation

S. Bargi, J. Christensson, G. M. Kavoulakis, and S. M. Reimann
Phys. Rev. Lett. **98**, 130403 (2007)

Bose-Einstein condensation in a two-component system is a non-trivial generalization, and we investigate the behavior of such a gas in a harmonic trap under rotation. We find that the system, under certain conditions, forms coreless vortices when it is rotated; i.e., while one component forms a vortex, the other remains non-rotating and fills up its core. This happens even when the two components have equal masses and scattering lengths, as long as the number of particles is different in the two. We find a connection to Paper I by showing how the non-rotating component exerts an effectively anharmonic potential on the rotating component.

In a single-component condensate in a harmonic trap, it is well known that the dispersion relation for angular momenta $L \leq N$, where N is the particle number, is given by a straight line. We generalize this result to a two-component condensate, and give analytical expressions. We also find analytical expressions for the occupation numbers in a range of angular momentum, which is possible due to the fact that only two single-particle states contribute to the order parameter in this range.

I produced all the numerical calculations and found the analytical expressions for the dispersion relation and occupation numbers. I contributed to the theoretical analysis of these results, except for the Bogoliubov analysis. I

produced all figures and participated in writing the text.

Paper III: Rotational Properties of a Mixture of Two Bose Gases

J. Christensson, S. Bargi, K. Kärkkäinen, Y. Yu, G. M. Kavoulakis, M. Manninen and S. M. Reimann
New J. Phys **10,** 033029 (2008)

In this paper, the work on rotating two-component condensates is continued, and the results of Papers I and II are further connected. We find that multiply quantized vortices can be energetically stable under certain circumstances, due to the interspecies interaction: one component is non-rotating at the center of the trap, and its Gaussian density profile acts as an anharmonic disturbance on the other component. We find these results both using diagonalization, and Gross-Pitaevskii calculations. Furthermore, we find that persistent currents are not possible in this system.

The diagonalization calculations were independently produced by myself and J. Christensson. I participated in the analysis of our results, and in editing the text and figures.

Paper IV: Mixtures of Bose Gases Confined in a Ring Potential

J. Smyrnakis, S. Bargi, G. M. Kavoulakis, M. Magiropoulos, K. Kärkkäinen, and S. M. Reimann
Phys. Rev. Lett **103**, 100404 (2009)

In this paper we investigate a number of properties of a two-component Bose gas trapped in a ring potential. We give the conditions under which phase separation occurs, and derive general features of the dispersion relation.

Rotational states that are separated from the non-rotating ground state by an energy barrier give rise to *persistent currents*, i.e. currents which in effect do not decay, since their life time is exponential in the height of the barrier. In the present system, such a barrier can arise due to the repulsive interactions between the atoms. Thus, if the interactions are strong enough, metastable persistent currents can occur. We calculate the interaction strength necessary for this phenomenon to appear in a two-component Bose gas as a function of the relative population of the two species. To this end, we make some analytical considerations and complete these with a diagonalization calculation. We

also show that in the two-component system, persistent currents with higher circulation are not stable. Finally, we give an analytical expression for the full excitation spectrum of the system in a certain range of angular momenta.

I produced the diagonalization results reported in "Beyond the mean-field approximation" and found the analytical expression for the excitation spectrum, and I produced Fig. 2.

Paper V: Persistent Currents in Bose Gases Confined in Annular Traps

S. Bargi, F. Malet, G. M. Kavoulakis and S. M. Reimann
Manuscript in preparation to be submitted to Phys. Rev. A.

Our previous study (Paper IV) on a two-component Bose gas in a ring potential allowed for motion in only one direction; along the ring. Experimental set-ups cannot (at this date) go to this limit, but produce traps that are effectively two-dimensional. Thus, it is very relevant to study the two-dimensional ring-like trap, which is what we have done in this paper.

We find that persistent currents can still be energetically stable in two dimensions, but at a stronger interaction strength as compared to the 1D case. We calculate this minimum interaction strength in a single-component system as a function of the "dimensionality" of the trap both using the mean-field Gross-Pitaevskii equation as well as diagonalization of the Hamiltonian. We also investigate persistent currents in a two-dimensional two-component system, and calculate the minimum interaction strength where they occur, as a function of the relative population. Due to numeric limitations, this is only done within the mean-field approach, and the diagonalization is used to confirm the results at certain parameter values.

I produced all diagonalization results, participated in the analysis of all results, and did the main part of writing the text.

I
Rotating Bose-Einstein Condensates Confined in an Anharmonic Potential

Paper I

Rotating Bose-Einstein condensates confined in an anharmonic potential

S. Bargi, G. M. Kavoulakis, and S. M. Reimann
Mathematical Physics, LTH, Lund University, P.O. Box 118, SE-22100, Lund, Sweden
(Received 20 December 2005; published 16 March 2006)

We consider bosonic atoms that rotate in an anharmonic trapping potential. Using numerical diagonalization of the Hamiltonian, we get evidence for various phases of the gas for different values of the coupling between the atoms and of the rotational frequency of the trap. These include vortex excitation of single and multiple quantization, the phase of center-of-mass excitation, and the unstable phase.

DOI: 10.1103/PhysRevA.73.033613 PACS number(s): 03.75.Hh, 05.30.Jp, 67.40.Db

I. INTRODUCTION

The behavior of confined, Bose-Einstein-condensed atoms under rotation has been studied extensively in recent years, both experimentally [1–5] as well as theoretically. One factor which is very crucial in these studies is the form of the confinement. In most of the experiments performed on cold gases of atoms, the trapping potential is harmonic. It is interesting, however, that the harmonic trapping is special in many respects, as we show below. For this reason recent theoretical studies [6–22], as well as the experiment of Ref. [23], have considered traps with other functional forms, in which the trapping potential grows more rapidly than quadratically at distances far away from the center of the cloud. Such trapping potentials introduce many novel phases.

Motivated by this observation, we examine the lowest state of a Bose-Einstein condensate in a rotating anharmonic trap. Up to now, all theoretical studies that have been performed on this problem were based upon the mean-field approximation. However, especially in the case of effective attractive interactions between the atoms, the use of the mean-field approximation is questionable. For example, in a harmonic potential, the many-body state for attractive interactions has correlations [24,25] that are not captured by the mean-field many-body state which is assumed to have a product form. Furthermore, in any anharmonic potential (including the one considered in this study) the center-of-mass coordinate does not decouple from the relative coordinates (as in the case of harmonic trapping) and this also makes the use of the mean-field approximation questionable. In our study we present "exact" results—for small numbers of atoms—from numerical diagonalization of the Hamiltonian, which goes beyond the mean-field approximation.

Experimentally it is possible to tune both the frequency of rotation of the trap, as well as the strength of the interatomic interaction. Motivated by these facts, we consider here a fixed trapping potential and examine the various phases and the corresponding phase diagram as function of the rotational frequency and of the coupling.

In what follows we present our model in Sec. II. In Sec. III we discuss the general structure of the phase diagram. In Sec. IV we describe the details of the numerical diagonalization. In Secs. V and VI we present and analyze our results for effective repulsive and attractive interatomic interactions, respectively. Finally, in Sec. VII we summarize our main results.

II. MODEL

The Hamiltonian that we consider consists of the single-particle part $h(\mathbf{r}_i)$ and the interaction $V(\mathbf{r}_i-\mathbf{r}_j)$, which is taken to be of the form of a contact potential $V(\mathbf{r}_i-\mathbf{r}_j)=U_0\delta(\mathbf{r}_i-\mathbf{r}_j)$,

$$H=\sum_{i=1}^{N} h(\mathbf{r}_i)+\frac{1}{2}\sum_{i\neq j=1}^{N} V(\mathbf{r}_i-\mathbf{r}_j). \tag{1}$$

Here N is the number of atoms and $U_0=4\pi\hbar^2 a/M$, where a is the scattering length for elastic atom-atom collisions, and M is the atom mass. The single-particle part of the Hamiltonian has the usual form

$$h(\mathbf{r})=-\frac{\hbar^2}{2M}\nabla^2+V_{\mathrm{trap}}(\mathbf{r}), \tag{2}$$

where the trap is assumed to be symmetric around the z axis. This is also taken to be the axis of rotation. In cylindrical coordinates ρ, ϕ, and z,

$$V_{\mathrm{trap}}(\mathbf{r})=\frac{1}{2}M\omega^2\rho^2\left(1+\lambda\frac{\rho^2}{a_0^2}\right)+V(z). \tag{3}$$

Here ω is the trap frequency of the harmonic part of V_{trap}, λ is a dimensionless constant which is the coefficient of the anharmonic term in V_{trap} (taken to be much smaller than unity in this study, as is also the case in the experiment of Ref. [23]), and $a_0=\sqrt{\hbar/M\omega}$ is the oscillator length. Along the z axis we assume that the trapping potential $V(z)$ is sufficiently strong that the typical separation between single-particle energy levels is much larger than the typical interaction energy. This assumption implies that the motion along the z axis is frozen out and our problem is essentially two dimensional.

III. GENERAL STRUCTURE OF THE PHASE DIAGRAM

As mentioned in the Introduction, motivated by the experimental situation, we here examine the phase diagram as a function of the rotational frequency Ω of the trap and of the strength of the interaction. It is natural to measure Ω in units of ω and the strength of the interaction $\sim nU_0$, where n is the atomic density, in units of the oscillator energy $\hbar\omega$. The corresponding dimensionless ratio $nU_0/\hbar\omega$ is $\sim\sigma a$, where $\sigma=N/Z$ is the density per unit length. Here Z is the width of the atomic cloud along the z axis.

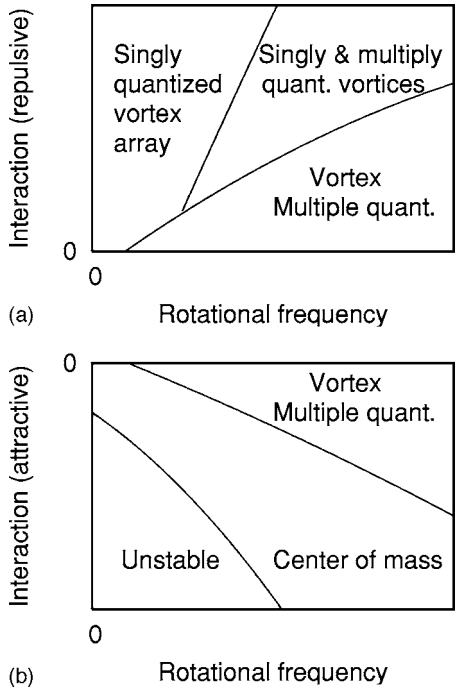

FIG. 1. Schematic phase diagram which shows the various phases as the rotational frequency and the coupling are varied.

It is instructive to first consider the general structure of the phase diagram [10,15,16]. This consists of several distinct phases. Let us start with repulsive interactions $a>0$. For a fixed Ω, as σa increases, the total energy eventually becomes dominated by the interaction energy, which is minimized via the formation of singly quantized vortex states. This is similar to vortex formation in liquid helium, or in harmonically trapped gases.

On the other hand, for a constant interaction strength, as the rotational frequency increases—and the single-particle part is the dominant part of the Hamiltonian—the total energy of the gas is minimized via formation of multiply quantized vortices. This is most easily seen if one thinks of the effective potential felt by the atoms, which consists of $V_{\rm trap}$ minus the centrifugal potential,

$$V_{\rm eff}(\mathbf{r}) = V_{\rm trap}(\mathbf{r}) - \frac{1}{2}M\Omega^2\rho^2$$

$$= \frac{1}{2}M(\omega^2-\Omega^2)\rho^2 + \frac{\lambda}{2}M\omega^2\frac{\rho^4}{a_0^2} + V(z). \qquad (4)$$

For the form of $V_{\rm trap}$ we have considered, $V_{\rm eff}$ takes the form of a Mexican-hat shape for $\Omega>\omega$, and thus the atoms prefer to reside along the bottom of this potential. This is precisely the density distribution that corresponds to multiply quantized vortex states. From Eq. (4) it is also clear that for harmonic trapping $\lambda=0$, Ω cannot exceed ω, since the atoms will fly apart. For any other potential that grows more rapidly than ρ^2 at large distances, the effective potential is bounded, independently of Ω. Finally, when both σa and Ω/ω are sufficiently large, there is a third, mixed phase consisting of a multiply quantized vortex state at the center of the cloud, surrounded by singly quantized vortices. This configuration in a sense compromises between the single-particle energy and the interaction energy.

Turning to the case of effective attractive interactions $a<0$, for small enough $\sigma|a|$, the phase diagram is, crudely speaking, symmetric with respect to σa. The lowest state of the gas is determined by the single-particle part of the Hamiltonian, and thus the corresponding state still consists of multiply quantized vortex states. For higher values of $\sigma|a|$, these states are again unstable against the formation of a combination of multiply quantized and singly quantized vortices, as in the mixed phase described for positive σa. The only difference is that the single-particle density distribution resembles that of a localized "blob" rotating around the minimum of the effective potential $V_{\rm eff}$ [17]. For even higher values of $\sigma|a|$, the phase that minimizes the energy is that of the center-of-mass excitation first seen in harmonically trapped atoms [24,25]. In this phase the angular momentum is carried by the center of mass. The single-particle density distribution resembles that of the "mixed" phase (i.e., a localized blob), although the structure of the many-body wave function is very different. Finally, for sufficiently large values of $\sigma|a|$ the gas collapses [26–28]. Figure 1 shows a schematic phase diagram.

IV. NUMERICAL DIAGONALIZATION OF THE HAMILTONIAN

As mentioned earlier, in the present study we perform numerical diagonalization of the Hamiltonian for a given atom number N and angular momentum $L\hbar$. To achieve this, we first solve the single-particle eigenvalue problem numerically,

$$h\phi_{n_r,m} = E_{n_r,m}\phi_{n_r,m}, \qquad (5)$$

using the Numerov method. The eigenfunctions and eigenenergies are characterized by two quantum numbers, the number of radial nodes n_r, and the number of quanta of angular momentum m. Making the simplified assumption of weak interactions $\sigma|a|\ll 1$, we perform our calculation within the approximation of the lowest Landau level, $n_r=0$ and $m\geqslant 0$. States with $n_r\neq 0$ or negative m are higher in energy by a term of order $\hbar\omega$. This assumption allows us to consider relatively large values of N and L. More generally in order for our calculation to converge, the number of Landau levels that have to be considered has to be at least as large as $\sigma|a|$. Finally, one should remember that while for repulsive interactions σa can have any value, for attractive interactions, $\sigma|a|\lesssim 1$, as otherwise the system collapses. Therefore, the lowest-Landau-level approximation is more restrictive for repulsive interactions, yet it gives a rather good description of the various phases, even in this case.

Having found the single-particle eigenstates, we then set up the Fock states, which are the eigenstates of the number operator $\hat{N}$ and of the total angular momentum $\hat{L}$, respectively. As a final step we set up the corresponding Hamiltonian matrix between the various Fock states, which we diagonalize numerically. The diagonal matrix elements consist both of the single-particle part, as well as the interaction.

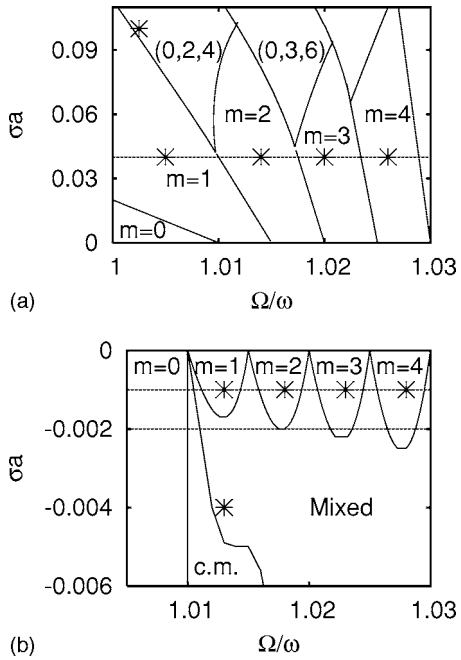

FIG. 2. The phase diagram calculated within the mean-field approximation for $\lambda=0.005$ from Refs. [15–17]. The "c.m." phase is the center-of-mass phase. The stars and the three dashed horizontal lines represent all of the values of σa and Ω/ω that have been examined and analyzed in the present study, except for those of Fig. 10, which are below the bottom of the lower graph.

The only nonzero off-diagonal matrix elements result from the interaction. The output of the Hamiltonian gives us not only the lowest state, but the whole energy spectrum. Since our calculation is performed for fixed angular momentum, in order to work with a fixed Ω we consider the energy in the rotating frame, which is given by the usual transformation

$$H' = H - L\Omega. \tag{6}$$

Having found the many-body eigenstates and eigenvalues for some range of L, then for a fixed Ω we identify the eigenstate with the lowest eigenenergy according to Eq. (6). The many-body eigenfunction that corresponds to the lowest eigenenergy—which is expressed in terms of the Fock states—is then analyzed in terms of the occupancy of the single-particle states. The calculation of the occupancies is a trivial operation and, remarkably, each of the phases described in the previous section is characterized by a distinct distribution. This fact provides indisputable evidence for the phases we expect to get from the arguments of the previous section and from the predictions of the mean field (Figs. 1 and 2).

V. RESULTS: REPULSIVE INTERACTIONS

We turn now to the analysis of our results, starting with the case of repulsive interactions. As we argued earlier, for sufficiently weak interactions we expect the phase of multiple quantization to have the lowest energy. For convenience we compare our results with those of the phase diagram of Ref. [15]. We thus choose $\lambda=0.005$ [29], and evaluate the

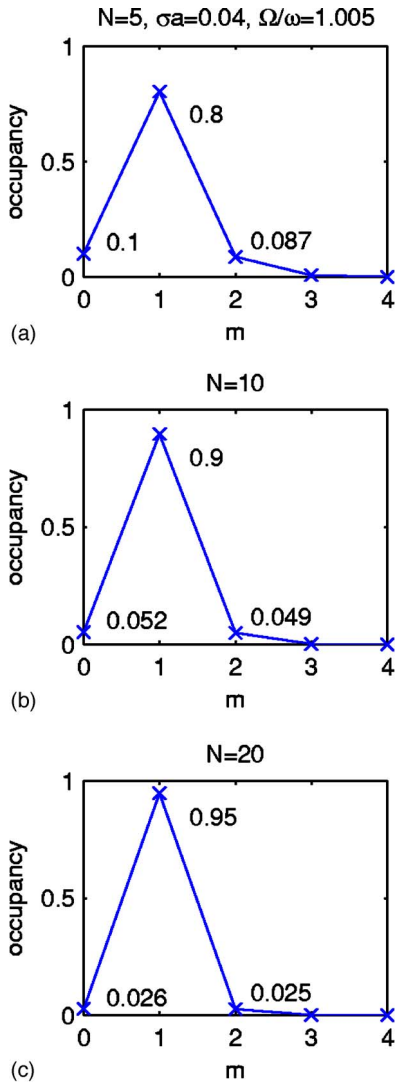

FIG. 3. (Color online) The occupancy of the single-particle states of angular momentum m for $\lambda=0.005$, $\sigma a=0.04$, $\Omega/\omega=1.005$, and for $N=5$ (a), 10 (b), and $N=20$ (c). These graphs demonstrate that the occupancy of all states with $m\neq 1$ is, to leading order, $1/N$. The occupancy of the $m=1$ state is unity minus corrections of order $1/N$ to leading order. In the mean-field approximation this phase corresponds to a single vortex state.

occupancy of the single-particle states for $\sigma a=0.04$, $\Omega/\omega=1.005$, for $N=5$, 10, and 20 atoms, as shown in Fig. 3. This graph demonstrates clearly that as N increases, the occupancy of the $m=1$ state approaches unity, while the occupancy of all other states tends to zero (scaling as $1/N$ to leading order). In the mean-field description the order parameter ψ is simply

$$\psi = \phi_{0,1}, \tag{7}$$

which represents a single vortex state located at the center of the cloud.

In Fig. 4 we calculate the occupancies of the single-particle states for $\lambda=0.005$ and $\sigma a=0.04$ and for four values of $\Omega/\omega=1.005$, 1.014, 1.020, and 1.026. This graph confirms that indeed the system (in its lowest state) undergoes discon-

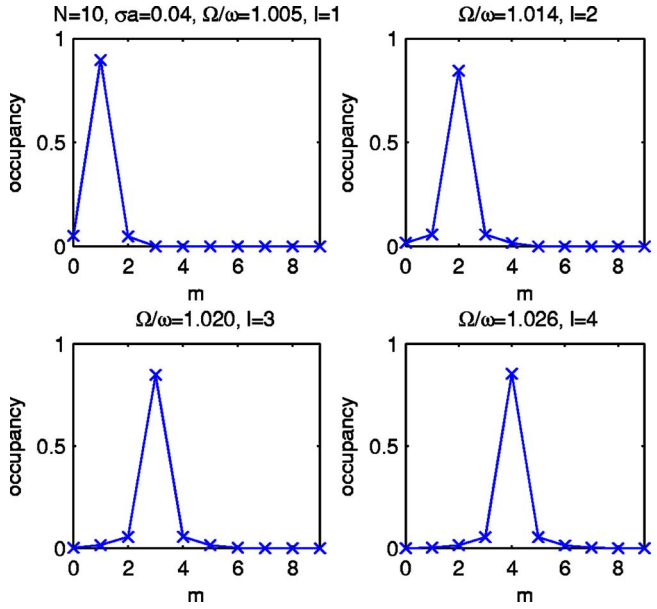

FIG. 4. (Color online) The occupancy of the single-particle states of angular momentum m for $\lambda=0.005$, $\sigma a=0.04$, $N=10$ atoms, and $\Omega/\omega=1.005$ (top left), 1.014 (top right), 1.020 (bottom left), and 1.026 (bottom right). The angular momentum of the gas changes discontinuously between successive values of m as Ω increases. These phases correspond to multiply quantized vortex states.

tinuous transitions between states of multiple quantization of successive values of m. Figure 5 shows the corresponding angular momentum per particle $l=L/N$ in the lowest state of the gas versus Ω/ω, for a fixed value of $\sigma a=0.04$. This graph consists of discontinuous jumps in l as Ω increases. The asterisks in this graph show the result of the mean-field calculation [16], which compares well with our result for small Ω. For larger Ω the agreement becomes worse. This is because the contribution of the anharmonic term to the energy was calculated perturbatively in λ in Ref. [16]. This correction increases quadratically with m, and for larger values of this quantum number, the perturbative result deviates from the exact.

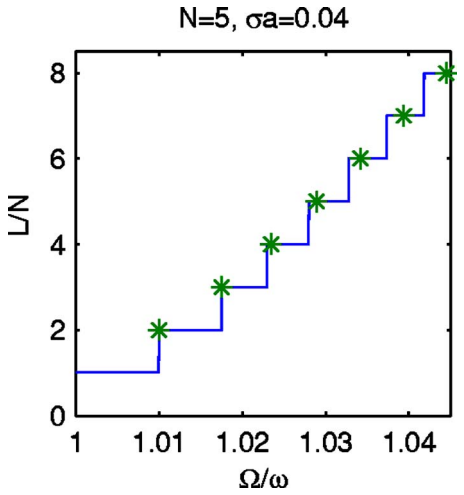

FIG. 5. (Color online) The total angular momentum of the gas in its lowest-energy state as a function of Ω/ω, for fixed $\lambda=0.005$, $\sigma a=0.04$, and $N=5$. The stars denote the result of a perturbative, mean-field calculation from Ref. [16].

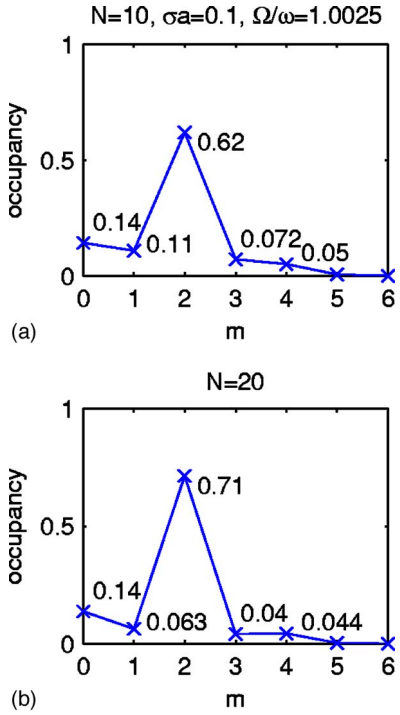

FIG. 6. (Color online) The occupancy of the single-particle states of angular momentum m for $\lambda=0.005$, $\sigma a=0.1$, $\Omega/\omega=1.0025$ and $N=10$ (a) and 20 (b). Here $L/N=1.8$. These graphs demonstrate that the dominant states are the ones with $m=0$, 2, and 4, in agreement with the mean-field calculations of Refs. [15,16]. In the mean-field approximation this corresponds to a "mixed" phase discussed in the text.

For repulsive interactions, as σa increases, mean-field theory predicts that the system undergoes a continuous transition from some multiply quantized vortex state of angular momentum m_0 to a "mixed" state which, to leading order, is a linear superposition of three states with angular momentum m_1, m_0, and m_2, with $m_1+m_2=2m_0$. Thus the order parameter has the form

$$\psi = c_{m_1}\phi_{0,m_1} + c_{m_0}\phi_{0,m_0} + c_{m_2}\phi_{0,m_2}, \tag{8}$$

where the coefficients are complex numbers. We have confirmed that our method gives a similar transition, as shown in Fig. 6. In this figure we plot the occupancy of the single-particle states for $\sigma a=0.1$, $\Omega/\omega=1.0025$, and $\lambda=0.005$, for $N=10$ and 20. From these two graphs we see that the states with $m_1=0$, $m_0=2$, $m_2=4$ are the dominant ones for large N. This is again in agreement with the prediction of mean-field theory. Finally, the angular momentum per particle $l=L/N$ is 1.8 in this state.

VI. RESULTS: ATTRACTIVE INTERACTIONS

For an effective attractive interaction between the atoms the corresponding phase diagram is even richer. We have obtained evidence for all the phases that are expected, namely, the multiply quantized vortex states, the mixed

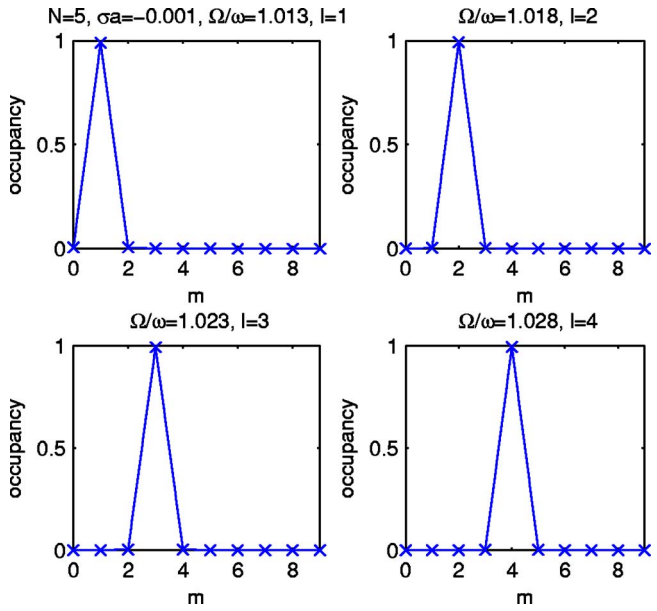

FIG. 7. (Color online) The occupancy of the single-particle states of angular momentum m for $\lambda=0.005$, $\sigma a=-0.001$, $N=5$ atoms, and $\Omega/\omega=1.013$ (top left), 1.018 (top right), 1.023 (bottom left), and 1.028 (bottom right). In the mean-field approximation this phase corresponds to multiply quantized vortex states.

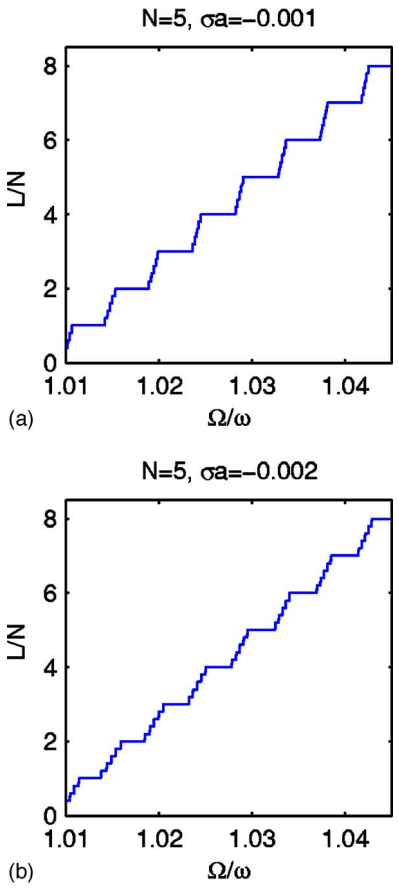

FIG. 8. (Color online) The angular momentum per particle in the state of lowest energy as a function of Ω/ω, for $\lambda=0.005$, $N=5$, and $\sigma a=-0.001$ (a) and -0.002 (b). The plateaus correspond to multiply quantized vortex states, which become more narrow as $\sigma|a|$ increases (as also shown in Fig. 2), in agreement with the mean-field approximation [17]. The small wiggles in the curves between the plateaus are an artifact of the discreteness of L that we have considered.

phase that consists of singly and multiply quantized vortices, the one involving center-of-mass excitation, and finally the unstable one.

Figure 7 shows the occupancies of the single-particle states in the lowest state of the gas for a fixed $\lambda=0.005$ and $\sigma a=-0.001$, and for four values of $\Omega/\omega=1.013$, 1.018, 1.023, and 1.028. As in Fig. 4, as Ω increases, we see that states of multiple quantization $\phi_{0,m}$ with successive values of m become macroscopically occupied. In Fig. 8 we plot the angular momentum per particle $l=L/N$ versus Ω/ω for $\sigma a=-0.001$ and -0.002. Here there is a difference as compared to repulsive interactions, which is also consistent with the prediction of mean-field theory. In order for the gas to get from some state of multiple quantization m_0 to m_0+1 (corresponding to the plateaus in Fig. 8), it has to go through some "mixed state," and thus these transitions are continuous. Furthermore, the width (in Ω/ω) of the plateaus decreases with increasing $\sigma|a|$. This effect is clearly seen between the two graphs in Fig. 8.

To get evidence for the mixed phase, we increase $\sigma|a|$, $\sigma a=-0.004$, and plot the occupancies of the single-particle states in Fig. 9 for a fixed $\Omega/\omega=1.013$, and $N=5$, 10, and 20. Here L/N is 1.0. The dominant single-particle states are the ones with $m=0$, 1, and 2, with a very small admixture of $m=3$. Again, this is in agreement with mean-field theory, which predicts that close to the phase boundary, any multiply quantized vortex state of strength m_0 is unstable against a state with three components of angular momentum m_0-1, m_0, and m_0+1,

$$\psi = c_{m_0-1}\phi_{0,m_0-1} + c_{m_0}\phi_{0,m_0} + c_{m_0+1}\phi_{0,m_0+1}. \tag{9}$$

In such a linear superposition of single-particle states, the corresponding single-particle density distribution may (and it actually does) look very much like that of a localized blob [17], although this is a phase involving vortex excitation.

The phase of the center-of-mass excitation expected in this problem [17] was also clearly seen in our calculation for even more negative values of σa. This phase was first discovered in harmonic traps [24,25]. Remarkably, the many-body wave function can be written analytically and has a very different structure as compared to the product form assumed within the mean-field approximation. This fact makes the validity of the mean-field approximation questionable for attractive interactions.

The occupancy of the single-particle states can also be expressed analytically. In Ref. [24] it has been shown that the occupancy $|c_m|^2$ of a single-particle state with angular momentum m in a many-body state with center-of-mass excitation of L units of angular momentum and N atoms is

$$|c_m(L,N)|^2 = \frac{(N-1)^{L-m}L!}{N^L(L-m)!m!}. \tag{10}$$

The crosses in Fig. 10 show the occupancy of the single-particle states calculated numerically for $\sigma a=-0.05$, λ

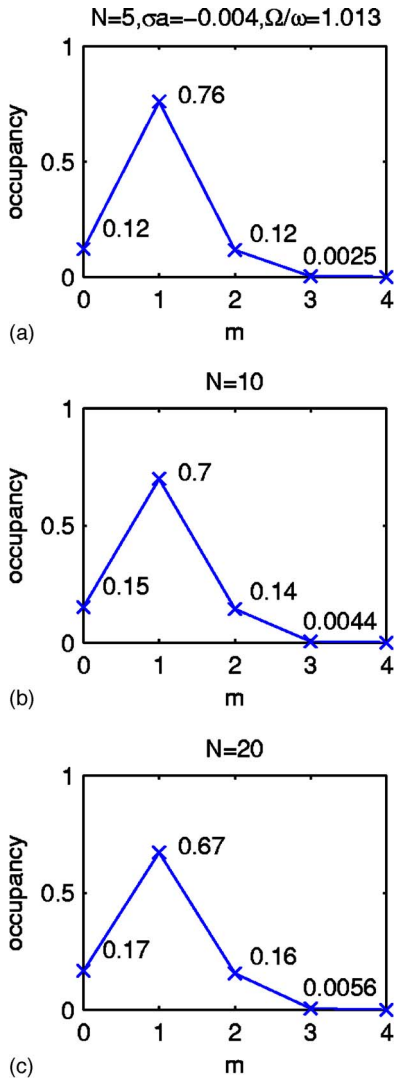

FIG. 9. (Color online) The occupancy of the single-particle states of angular momentum m for $\lambda=0.005$, $\sigma a=-0.004$, $\Omega/\omega=1.013$, and for $N=5$ (a), 10 (b), and 20 (c). Here $L/N=1.0$. These graphs demonstrate that the dominant states are the ones with $m=0$, 1, and 2, with a small admixture of the state with $m=3$, in agreement with Ref. [17]. In the mean-field approximation, this corresponds to the mixed phase discussed in the text.

$=0.005$, $N=10$, and six values of $\Omega/\omega=1.012$, 1.014, 1.016, 1.018, 1.022, and 1.026. The circles represent $|c_m|^2$ of Eq. (10). We confirmed that the difference between the occupancies calculated within our study and the prediction of Eq. (10) decreases with increasing N and increasing $\sigma|a|$ (as long as the gas is stable). These data again provide clear evidence for the phase of center-of-mass excitation.

It should also be mentioned that the phase boundary between the mixed phase and the one of center-of-mass excitation lies much lower than the one calculated variationally in Ref. [17]. The reason is that the phase boundary of Ref. [17] (for these two specific phases) is just an upper bound, and the present calculation is consistent with this fact.

Finally, the unstable phase [26–28] also shows up in our model. This is seen in the present calculation via the sign of

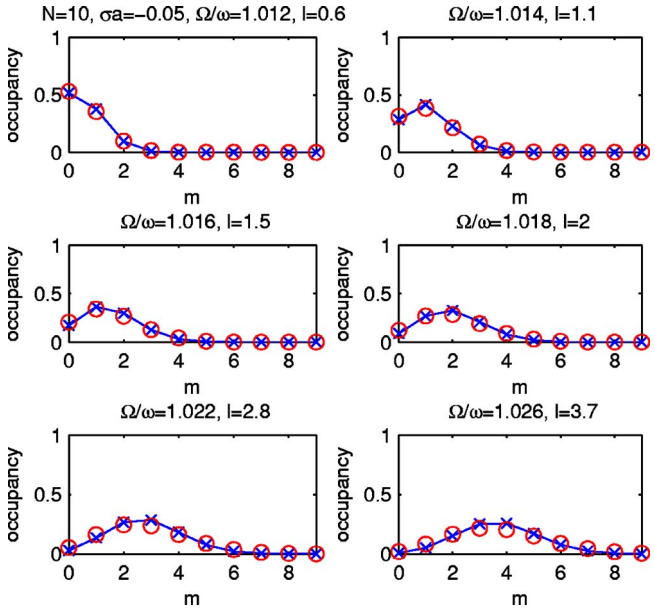

FIG. 10. (Color online) The crosses show the occupancy of the single-particle states of angular momentum m for $\lambda=0.005$, $\sigma a=-0.05$, $N=5$ atoms, and $\Omega/\omega=1.012$ (top left), 1.014 (top right), 1.016 (middle left), 1.018 (middle right), 1.022 (bottom left), and 1.026 (bottom right). This phase has a very large overlap with that of the center-of-mass excitation. The circles show the results calculated from Eq. (10).

the chemical potential which becomes negative for a value of $\sigma a\approx -1$. This result is inconsistent with the assumption of weak interactions, $\sigma|a|\ll 1$, as the approximation of lowest Landau level breaks down. To get a quantitatively accurate description of this instability one would have to include higher Landau levels.

VII. SUMMARY

To summarize, in the present study we considered bosonic atoms that rotate in an anharmonic trap. We attacked this problem with the method of numerical diagonalization of the Hamiltonian, which goes beyond the mean-field approximation but also forced us to consider small numbers of atoms. Apart from the assumption of weak interatomic interactions, our results are exact. We got evidence for all the phases that are expected, namely, vortex excitation of multiple quantization, single quantization, and mixed, center-of-mass motion, and finally the unstable phase. The locations of the phase boundaries were consistent with those calculated within the mean-field approximation.

ACKNOWLEDGMENTS

We thank Yongle Yu for his assistance on the numerical calculations. This work was partly financed by the European Community project ULTRA-1D (Grant No. NMP4-CT-2003-505457), the Swedish Research Council, and the Swedish Foundation for Strategic Research.

[1] M. R. Matthews, B. P. Anderson, P. C. Haljan, D. S. Hall, C. E. Wieman, and E. A. Cornell, Phys. Rev. Lett. **83**, 2498 (1999).
[2] K. W. Madison, F. Chevy, W. Wohlleben, and J. Dalibard, Phys. Rev. Lett. **84**, 806 (2000); F. Chevy, K. W. Madison, and J. Dalibard, *ibid.* **85**, 2223 (2000); K. W. Madison, F. Chevy, V. Bretin, and J. Dalibard, *ibid.* **86**, 4443 (2001).
[3] J. R. Abo-Shaeer, C. Raman, J. M. Vogels, and W. Ketterle, Science **292**, 476 (2001).
[4] P. C. Haljan, I. Coddington, P. Engels, and E. A. Cornell, Phys. Rev. Lett. **87**, 210403 (2001); P. Engels, I. Coddington, P. C. Haljan, and E. A. Cornell, *ibid.* **89**, 100403 (2002).
[5] P. Engels, I. Coddington, P. C. Haljan, V. Schweikhard, and E. A. Cornell, Phys. Rev. Lett. **90**, 170405 (2003).
[6] A. L. Fetter, Phys. Rev. A **64**, 063608 (2001).
[7] E. Lundh, Phys. Rev. A **65**, 043604 (2002).
[8] K. Kasamatsu, M. Tsubota, and M. Ueda, Phys. Rev. A **66**, 053606 (2002).
[9] U. R. Fischer and G. Baym, Phys. Rev. Lett. **90**, 140402 (2003).
[10] G. M. Kavoulakis and G. Baym, New J. Phys. **5**, 51.1 (2003).
[11] T. P. Simula, A. A. Penckwitt, and R. J. Ballagh, Phys. Rev. Lett. **92**, 060401 (2004).
[12] E. Lundh, A. Collin, and K.-A. Suominen, Phys. Rev. Lett. **92**, 070401 (2004).
[13] A. Aftalion and I. Danaila, Phys. Rev. A **69**, 033608 (2004).
[14] T. K. Ghosh, Phys. Rev. A **69**, 043606 (2004).
[15] A. D. Jackson, G. M. Kavoulakis, and E. Lundh, Phys. Rev. A **69**, 053619 (2004).
[16] A. D. Jackson and G. M. Kavoulakis, Phys. Rev. A **70**, 023601 (2004).
[17] G. M. Kavoulakis, A. D. Jackson, and G. Baym, Phys. Rev. A **70**, 043603 (2004).
[18] A. Collin, E. Lundh, and K.-A. Suominen, Phys. Rev. A **71**, 023613 (2005).
[19] M. Cozzini, A. L. Fetter, B. Jackson, and S. Stringari, Phys. Rev. Lett. **94**, 100402 (2005).
[20] H. Fu and E. Zaremba, Phys. Rev. A **73**, 013614 (2006).
[21] N. Papanicolaou, S. Komineas, and N. R. Cooper, Phys. Rev. A **72**, 053609 (2005).
[22] A. Collin, Phys. Rev. A **73**, 013611 (2006).
[23] V. Bretin, S. Stock, Y. Seurin, and J. Dalibard, Phys. Rev. Lett. **92**, 050403 (2004).
[24] N. K. Wilkin, J. M. F. Gunn, and R. A. Smith, Phys. Rev. Lett. **80**, 2265 (1998).
[25] B. Mottelson, Phys. Rev. Lett. **83**, 2695 (1999).
[26] G. Baym and C. J. Pethick, Phys. Rev. Lett. **76**, 6 (1996).
[27] M. Ueda and A. J. Leggett, Phys. Rev. Lett. **80**, 1576 (1998).
[28] E. J. Mueller and G. Baym, Phys. Rev. A **62**, 053605 (2000).
[29] In Ref. [15] the value of λ that was used was 0.05; however, here we use $\lambda=0.005$. To compare the present results with those of this reference, the axes of the phase diagram of Ref. [15] have been rescaled. This rescaling is allowed because of the universality of the phase diagram in the limit of small λ, as shown in this reference.

II
Mixtures of Bose Gases under Rotation

Paper II

Mixtures of Bose Gases under Rotation

S. Bargi, J. Christensson, G. M. Kavoulakis, and S. M. Reimann
Mathematical Physics, Lund Institute of Technology, P.O. Box 118, SE-22100 Lund, Sweden
(Received 31 January 2007; published 29 March 2007)

We examine the rotational properties of a mixture of two Bose gases. Considering the limit of weak interactions between the atoms, we investigate the behavior of the system under a fixed angular momentum. We demonstrate a number of exact results in this many-body system.

DOI: 10.1103/PhysRevLett.98.130403 PACS numbers: 05.30.Jp, 03.75.Lm, 67.40.−w

One of the many interesting aspects of the field of cold atoms is that one may create mixtures of different species. The equilibrium density distribution of the atoms is an interesting problem by itself, since the different components may coexist, or separate, depending on the value of the coupling constants between the atoms of the same and of the different species. If this system rotates, the problem becomes even more interesting. In this case, the state of lowest energy may involve rotation of either one of the components, or rotation of all the components. Actually, the first vortex state in cold gases of atoms was observed experimentally in a two-component system [1], following the theoretical suggestion of Ref. [2]. More recently, vortices have also been created and observed in spinor Bose-Einstein condensates [3,4]. Theoretically, there have been several studies of this problem [5–7], mostly in the case where the number of vortices is relatively large. Kasamatsu, Tsubota, and Ueda have also given a review of the work that has been done on this problem [8].

In this Letter, we consider a rotating two-component Bose gas in the limit of weak interactions and slow rotation, where the number of vortices is of order unity. Surprisingly, a number of exact analytical results exist for the energy of this system. The corresponding many-body wave function also has a relatively simple structure.

We assume equal masses M for the two components, and a harmonic trapping potential $V_t = M(\omega^2\rho^2 + \omega_z^2 z^2)/2$, with $\rho^2 = x^2 + y^2$. The trapping frequency ω_z along the axis of rotation is assumed to be much higher than ω. In addition, we consider weak atom-atom interactions, much smaller than the oscillator energy $\hbar\omega$, and work within the subspace of states of the lowest-Landau level. The motion of the atoms is thus frozen along the axis of rotation and our problem becomes quasi-two-dimensional [9]. The relevant eigenstates are $\Phi_m(\rho,\theta)\varphi_0(z)$, where $\Phi_m(\rho,\theta)$ are the lowest-Landau-level eigenfunctions of the two-dimensional oscillator with angular momentum $m\hbar$, and $\varphi_0(z)$ is the lowest harmonic oscillator eigenstate along the z axis.

The assumption of weak interactions also excludes the possibility of phase separation in the absence of rotation [10], since the atoms of both species reside in the lowest state $\Phi_{0,0}(\mathbf{r}) = \Phi_0(\rho,\theta)\varphi_0(z)$, while the depletion of the condensate due to the interaction may be treated perturbatively.

We label the two (distinguishable) components of the gas as A and B. In what follows the atom-atom interaction is assumed to be a contact potential of equal scattering lengths for collisions between the same species and the different ones, $a_{AA} = a_{BB} = a_{AB} = a$. The interaction energy is measured in units of $\upsilon_0 = U_0 \int |\Phi_{0,0}(\mathbf{r})|^4 d^3r = (2/\pi)^{1/2}\hbar\omega a/a_z$, where $U_0 = 4\pi\hbar^2 a/M$, and $a_0 = (\hbar/M\omega)^{1/2}$, $a_z = (\hbar/M\omega_z)^{1/2}$ are the oscillator lengths on the plane of rotation and perpendicular to it.

If N_A and N_B denote the number of atoms in each component, we examine the behavior of this system for a fixed amount of L units of angular momentum, with $0 \le L \le N_{\max}$, where $N_{\max} = \max(N_A, N_B)$. We use both numerical diagonalization of the many-body Hamiltonian for small systems, as well as the mean-field approximation. Remarkably, as we explain in detail below, there is a number of exact results in this range of angular momenta.

More specifically, when $0 \le L \le N_{\min}$, where $N_{\min} = \min(N_A, N_B)$, using exact diagonalization of the many-body Hamiltonian, we find that the interaction energy of the lowest-energy state has a parabolic dependence on L in this range,

$$\mathcal{E}_0(L)/\upsilon_0 = \tfrac{1}{2}N(N-1) - \tfrac{1}{2}NL + \tfrac{1}{4}L(L-1), \quad (1)$$

with $N = N_A + N_B$. In addition, the lowest-energy state consists only of the single-particle states of the harmonic oscillator with $m = 0$ and $m = 1$. The occupancy of the $m = 1$ state of each component is given by

$$(N_A)_{m=1} = L\frac{N_B - L + 1}{N - 2L + 2}, \quad (2)$$

$$(N_B)_{m=1} = L\frac{N_A - L + 1}{N - 2L + 2}, \quad (3)$$

while $(N_A)_{m=0} = N_A - (N_A)_{m=1}$ and $(N_B)_{m=0} = N_B - (N_B)_{m=1}$.

As L becomes larger than $N_{\min}$, there is a phase transition. For $N_{\min} \le L \le N_{\max}$, the single-particle states that constitute the many-body state are no longer only the ones with $m = 0$ and $m = 1$ (as in the case $0 \le L \le N_{\min}$), and, in addition, the interaction energy varies linearly with L,

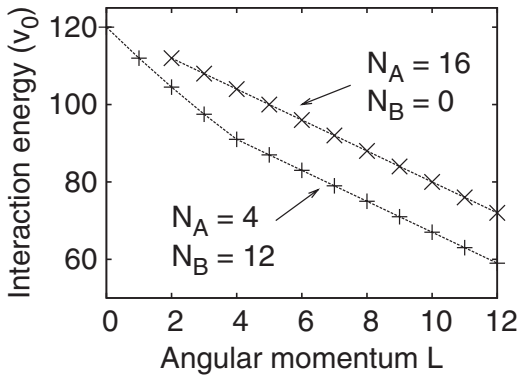

FIG. 1. The interaction energy that results from numerical diagonalization of the Hamiltonian, with $N_A = 4$ and $N_B = 12$ (lower curve, marked by "+"), as well as $N_A = 16$, and $N_B = 0$ (higher curve, marked by "×"), as a function of the angular momentum L, for $0 \le L \le 12$.

$$\mathcal{E}_0(L)/v_0 = \tfrac{1}{2}N(N-1) - \tfrac{1}{4}N_{\min}N - \tfrac{1}{4}NL + \tfrac{1}{4}N_{\min}(N_{\min}-1). \quad (4)$$

The lower curve in Fig. 1 shows the interaction energy of a system with $N_A = 4$ and $N_B = 12$, for $0 \le L \le 12$. For $0 \le L \le 4$ the energy is parabolic, and for $4 \le L \le 12$, it is linear. These are exact results, within numerical accuracy. The higher curve is the interaction energy of a single-component system of $N = 16$ atoms. It is known that in this case, the interaction energy is exactly linear for $2 \le L \le N = 16$ [11]. This line is parallel to the line which gives the interaction energy of the system with $N_A = 4$ and $N_B = 12$ for $N_A = 4 \le L \le N_B = 12$. Figure 2 shows the occupancy of the single-particle states that result from the numerical diagonalization of the Hamiltonian.

The physical picture that emerges from these calculations is intriguing: as L increases, a vortex state enters the component with the smaller population from infinity and ends up at the center of the trap when $L = N_{\min}$. In addition, another vortex state enters the component with the larger population from the opposite side of the trap, reaching a minimum distance from the center of the trap for $L \approx N_A/2$ (this estimate is valid if $1 \ll N_A \ll N_B$), and then returns to infinity when $L = N_{\min}$. This minimum distance is $\approx 2(N_B/N_A)a_0$. For $N_{\min} \le L \le N_{\max}$, the vortex in the cloud with the smaller population (that is located at the center of the trap when $L = N_{\min}$) moves outwards, ending up at infinity when $L = N_{\max}$, while a vortex in the other component moves inwards again, ending up at the center of the trap when $L = N_{\max}$. Figure 3 shows clearly these effects via the conditional probability distributions, for $N_A = 4$, and $N_B = 12$. We note that in the range $0 < L < N_A = 4$, the (distant) vortex in the large component (lower row, species B) is too far away from the center of the cloud to be visible, because of the exponential drop of the density. The plots in Fig. 3 (and Fig. 5) are not very sensitive to the total number of atoms $N = N_A + N_B$, and resemble the behavior of the system in the thermodynamic limit of large N.

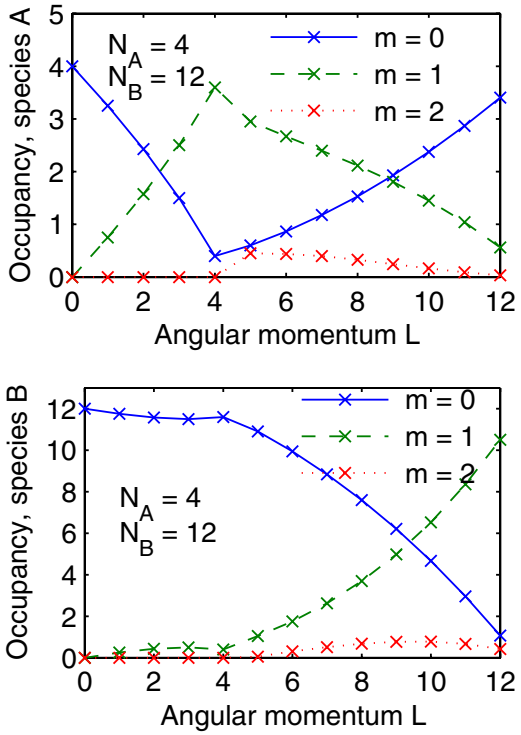

FIG. 2 (color online). The occupancy of the single-particle states with $m = 0$, 1 and 2, as function of the angular momentum L, for $0 \le L \le 12$, that results from numerical diagonalization of the Hamiltonian, with $N_A = 4$ and $N_B = 12$. The upper panel refers to species A, and the lower one to species B.

In the case of equal populations, $N_A = N_B$, the parabolic expression for the interaction energy, Eq. (1), holds all the way between $0 \le L \le N_A = N_B$. Figure 4 shows the interaction energy and Fig. 5 the occupancies of the single-particle states, which vary linearly with L. The corresponding physical picture is quite different in this case, as shown in Fig. 6. The system is now symmetric with respect to the two components, and a vortex state enters each of the components (from opposite sides). These vortices reach a minimum distance from the center of the trap equal to a_0, when $L = N_A = N_B$.

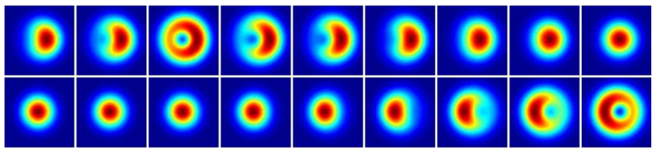

FIG. 3 (color online). The conditional probability distribution, with $N_A = 4$ (higher row), and $N_B = 12$ (lower row). Each graph extends between $-2.4a_0$ and $2.4a_0$. The reference point is located at $(x, y) = (a_0, 0)$ in the higher graph. The angular momentum L increases from left to right, $L = 2, 3, 4(= N_A), 5, 6, 8, 10, 11$, and $12(= N_B)$.

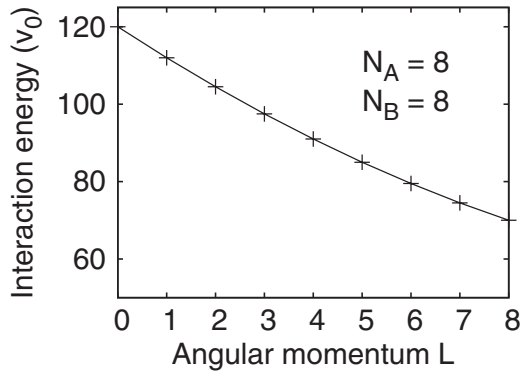

FIG. 4. The interaction energy that results from numerical diagonalization of the Hamiltonian, with $N_A = N_B = 8$, as function of the angular momentum L, for $0 \le L \le 8$.

The simplicity of the system that we have studied allows one to get some relatively simple analytical results, which we present below. As we saw earlier, when $L = N_A$ or $L = N_B$, there is a unit vortex state in species A or B, while the other species is in the lowest oscillator state with $m = 0$. Since (at least to leading order and next to leading order) only the states with $m = 0$ and $m = 1$ are occupied, the Fock states are of the general form (if, for example, $L = N_B$)

$$|n\rangle = |0^{N_A-n}, 1^n\rangle \bigotimes |0^n, 1^{N_B-n}\rangle. \tag{5}$$

Expressing the eigenstates of the interaction V as $|\Phi\rangle = \sum_n (-1)^n f_n |n\rangle$, the eigenvalue equation takes the form

$$V_{n,n} f_n - V_{n,n-1} f_{n-1} - V_{n,n+1} f_{n+1} = \mathcal{E} f_n, \tag{6}$$

where $V_{n,m}$ are the matrix elements of the interaction between the above states. Remarkably, if $N_A = N_B = N/2$, then

$$V_{n,n} - V_{n,n-1} - V_{n,n+1} = 5N(N-2)v_0/16, \tag{7}$$

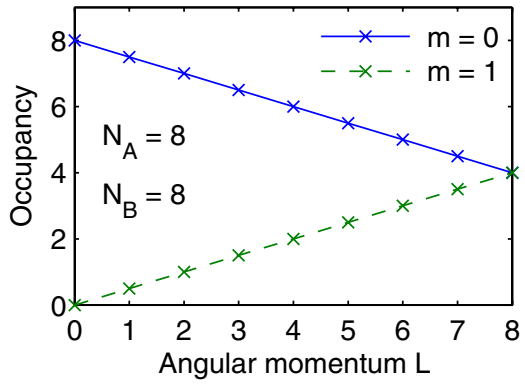

FIG. 5 (color online). The occupancy of the single-particle states with $m = 0$ and $m = 1$, as function of the angular momentum $0 \le L \le 8$, that results from numerical diagonalization of the Hamiltonian, with $N_A = N_B = 8$.

which implies that in this case, the lowest eigenenergy is $\mathcal{E}_0 = 5N(N-2)v_0/16$, in agreement with Eq. (1). The corresponding eigenfunction is simply $|\Phi_0\rangle = \sum_n (-1)^n |n\rangle$.

In the case $N_A \neq N_B$, with, e.g., $L = N_B$, n is of order unity, and therefore the interaction may be written as

$$V/v_0 = \tfrac{1}{2}N_A(N_A-1) + \tfrac{1}{4}N_B(N_B-1) + \tfrac{1}{2}N_A N_B + \tfrac{1}{2}(N_A+N_B)\hat{b}_0^\dagger \hat{b}_0 + \tfrac{1}{2}\sqrt{N_A N_B}(\hat{b}_0 \hat{a}_1^\dagger + \hat{b}_0^\dagger \hat{a}_1), \tag{8}$$

where $\hat{a}_m (\hat{a}_m^\dagger)$ and $\hat{b}_m (\hat{b}_m^\dagger)$ are annihilation (creation) operators of the species A and B with angular momentum $m\hbar$. The above expression for V can be diagonalized with a Bogoliubov transformation,

$$V/v_0 = \tfrac{1}{4}|N_A - N_B|(2\hat{\alpha}^\dagger \hat{\alpha} + 1) + \tfrac{1}{4}N_A(2N_A - 3) + \tfrac{1}{4}N_B(N_B - 2) + \tfrac{1}{2}N_A N_B, \tag{9}$$

where $\hat{\alpha}^\dagger \hat{\alpha}$ is a number operator. When $N_A = N_B = N/2$, the lowest eigenenergy is $5N(N-2)/16$, in agreement with Eq. (1). When $N_A \neq N_B$, the lowest eigenenergy is

$$\mathcal{E}_0/v_0 = \tfrac{1}{4}|N_A - N_B| + \tfrac{1}{4}N_A(2N_A - 3) + \tfrac{1}{4}N_B(N_B - 2) + \tfrac{1}{2}N_A N_B. \tag{10}$$

The above expression agrees exactly with Eq. (1) when $N_A < N_B = L$, and to leading order in N when $N_A > N_B = L$.

In addition, according to Eq. (9), the excitation energies are equally spaced, separated by $|N_A - N_B|v_0/2 + \mathcal{O}(v_0)$. Therefore, one very important difference between the case $N_A = N_B$ and $N_A \neq N_B$ is that in the first case there are low-lying excited states, with an energy separation of order v_0, while in the second [where in general $N_A - N_B \sim \mathcal{O}(N)$], the low-lying excited states are separated from the lowest state by an energy of order Nv_0.

Let us now turn to the mean-field description of this system, for $0 \le L \le N_{\min}$. We consider the following order parameters for the two species (restricting ourselves to the states with $m = 0$ and $m = 1$ only),

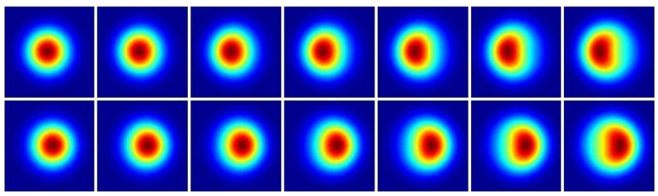

FIG. 6 (color online). The conditional probability distribution, with $N_A = N_B = 8$. The two rows refer to the two different species. Each graph extends between $-2.4a_0$ and $2.4a_0$. The reference point is located at $(x, y) = (a_0, 0)$ in the lower graph. The angular momentum L increases from left to right, $L = 2, 3, \ldots, 8$.

$$\Psi_A = (c_0\Phi_0 + c_1\Phi_1)\varphi_0(z),$$
$$\Psi_B = (d_0\Phi_0 + d_1\Phi_1)\varphi_0(z), \quad (11)$$

where c_0, c_1, d_0, d_1 are variational parameters. Given the order parameters, the many-body state is $\Psi_{\rm MF} = \prod_{i=1}^{N_A}\Psi_A(\mathbf{r}_i)\prod_{j=1}^{N_B}\Psi_B(\mathbf{r}_j)$. The normalization for each species implies that $|c_0|^2 + |c_1|^2 = 1$, and $|d_0|^2 + |d_1|^2 = 1$, while the condition for the angular momentum gives $N_A|c_1|^2 + N_B|d_1|^2 = L$. The interaction energy is

$$\mathcal{E}_{\rm MF} = \tfrac{1}{2}N_A(N_A-1)U_0\int|\Psi_A|^4d^3r + \tfrac{1}{2}N_B(N_B-1)U_0 \times\int|\Psi_B|^4d^3r + N_AN_BU_0\int|\Psi_A|^2|\Psi_B|^2d^3r, \quad (12)$$

which can be expressed easily in terms of the variational parameters c_0, c_1, d_0 and d_1, with use of Eqs. (11). When $N_A = N_B$, then $|c_0|^2 = |d_0|^2$, and also $|c_1|^2 = |d_1|^2$, which implies that $|c_1|^2 = |d_1|^2 = L/N = l$. Therefore, one finds that $\mathcal{E}_{\rm MF}/N^2 = (2 - 2l + l^2)\upsilon_0/4$, in agreement (to leading order in N) with the result of exact diagonalization, Eq. (1). When $N_A \neq N_B$, minimization of the energy with respect to one (free) of the four variational parameters (the other three are then fixed by the three constraints) gives a result that agrees to leading order in N with that of numerical diagonalization.

The fact that for $0 \leq L \leq N_{\rm min}$ the lowest many-body state consists of only the $m = 0$ and $m = 1$ single-particle states is remarkable. To get some insight into this result, we consider the two coupled Gross-Pitaevskii equations, which describe the order parameters Ψ_A and Ψ_B. If μ_A and μ_B is the chemical potential of each component, then

$$\left(-\frac{\hbar^2\nabla^2}{2M} + V_t + U_0|\Psi_B|^2\right)\Psi_A + U_0|\Psi_A|^2\Psi_A = \mu_A\Psi_A,$$
$$\left(-\frac{\hbar^2\nabla^2}{2M} + V_t + U_0|\Psi_A|^2\right)\Psi_B + U_0|\Psi_B|^2\Psi_B = \mu_B\Psi_B. \quad (13)$$

For a large population imbalance, where, for example, $1 \ll N_A \ll N_B$, for $0 \leq L \leq N_{\rm min} = N_A$, most of the angular momentum is carried by the species A (with the smaller population). As mentioned earlier, in the range $0 \leq L \leq N_{\rm min}$, although there is also a vortex state in species B, this is far away from the center of the cloud. As a result, the order parameter of species B is essentially the Gaussian state, with the corresponding density being $|\Psi_B(\rho, z)|^2 \approx n_B(0,0)e^{-\rho^2/a_0^2 - z^2/a_z^2}$, where $n_B(0,0)$ is the density of species B at the center of the trap, i.e., at $\rho = 0$ and $z = 0$.

This component acts as an external potential on species A. Thus, the total "effective" potential acting on species A is (expanding the function $e^{-\rho^2/a_0^2}$),

$$V_{\rm eff}(\rho, 0) \approx \frac{M}{2}\omega^2\rho^2 + U_0n_B(0,0)\left(1 - \frac{\rho^2}{a_0^2} + \frac{\rho^4}{2a_0^4}\right), \quad (14)$$

for distances close to the center of the cloud. One may argue that in this self-consistent analysis, the quadratic term in the expansion changes the effective trap frequency, while the quartic term acts as an anharmonic potential. We argue that this anharmonic term is responsible for the fact that only the states with $m = 0$ and $m = 1$ are occupied [12]. Actually, this is more or less how the group of J. Dalibard investigated the problem of multiple quantization of vortex states [13]. In that case, it was an external laser beam that created an external, repulsive Gaussian potential, as opposed to the present problem, where this potential results from the interaction between the different components.

We acknowledge financial support from the European Community project ULTRA-1D (No. NMP4-CT-2003-505457), the Swedish Research Council, and the Swedish Foundation for Strategic Research.

[1] M. R. Matthews, B. P. Anderson, P. C. Haljan, D. S. Hall, C. E. Wieman, and E. A. Cornell, Phys. Rev. Lett. **83**, 2498 (1999).
[2] J. E. Williams and M. J. Holland, Nature (London) **401**, 568 (1999).
[3] A. E. Leanhardt, Y. Shin, D. Kielpinski, D. E. Pritchard, and W. Ketterle, Phys. Rev. Lett. **90**, 140403 (2003).
[4] V. Schweikhard, I. Coddington, P. Engels, S. Tung, and E. A. Cornell, Phys. Rev. Lett. **93**, 210403 (2004).
[5] E. J. Mueller and T.-L. Ho, Phys. Rev. Lett. **88**, 180403 (2002).
[6] K. Kasamatsu, M. Tsubota, and M. Ueda Phys. Rev. Lett. **91**, 150406 (2003).
[7] K. Kasamatsu, M. Tsubota, and M. Ueda Phys. Rev. A **71**, 043611 (2005).
[8] K. Kasamatsu, M. Tsubota, and M. Ueda, Int. J. Mod. Phys. B **19**, 1835 (2005).
[9] B. Mottelson, Phys. Rev. Lett. **83**, 2695 (1999).
[10] C. J. Pethick and H. Smith, *Bose-Einstein Condensation in Dilute Gases* (Cambridge University Press, Cambridge, England, 2002).
[11] See, e.g., G. F. Bertsch and T. Papenbrock, Phys. Rev. Lett. **83**, 5412 (1999), and references therein.
[12] See, e.g., A. L. Fetter, Phys. Rev. A **64**, 063608 (2001); E. Lundh, Phys. Rev. A **65**, 043604 (2002), and references therein.
[13] V. Bretin, S. Stock, Y. Seurin, and J. Dalibard, Phys. Rev. Lett. **92**, 050403 (2004).

III
Rotational Properties of a Mixtures of Two Bose Gases

Paper III

New Journal of Physics
The open-access journal for physics

Rotational properties of a mixture of two Bose gases

J Christensson[1], S Bargi[1], K Kärkkäinen[1], Y Yu[1,2], G M Kavoulakis[1,3], M Manninen[4] and S M Reimann[1]

[1] Mathematical Physics, Lund Institute of Technology, PO Box 118, SE-22100 Lund, Sweden
[2] Wuhan Institute of Physics and Mathematics, CAS, Wuhan 430071, People's Republic of China
[3] Technological Education Institute of Crete, PO Box 1939, GR-71004 Heraklion, Greece
[4] Nanoscience Center, Department of Physics, FIN-40014 University of Jyväskylä, Finland
E-mail: georgios.kavoulakis@matfys.lth.se

New Journal of Physics **10** (2008) 033029 (8pp)
Received 20 November 2007
Published 18 March 2008
Online at http://www.njp.org/
doi:10.1088/1367-2630/10/3/033029

Abstract. A rotating, two-component Bose–Einstein condensate is shown to exhibit vortices of multiple quantization, which are possible due to the interatomic interactions between the two species. Also, persistent currents are absent in this system. Finally, the order parameter has a very simple structure for a range of angular momenta.

When a superfluid is set into rotation, it demonstrates many fascinating phenomena, such as quantized vortex states and persistent flow [1]. The studies of rotational properties of superfluids originated some decades ago, mostly in connection with liquid helium, nuclei and neutron stars. More recently, similar properties have also been studied extensively in cold gases of trapped atoms.

Quantum gases of atoms provide an ideal system for studying multi-component superfluids. At first sight, the rotational properties of a multi-component gas may look like a trivial generalization of the case of a single component. However, as long as the different components interact and exchange angular momentum, the extra degrees of freedom associated with the motion of each species is not at all a trivial effect. On the contrary, this coupled system may demonstrate some very different phenomena, see e.g. [2]–[4]. Several experimental and theoretical studies have been performed on this problem, see e.g. [5]–[12] and the review article [13].

In this study, the rotational properties of a superfluid that consists of two distinguishable components are examined. Three main conclusions result from our study.

Firstly, under appropriate conditions, one may achieve vortex states of multiple quantization. It is important to note that these states result from the interaction between the different species, and not from the functional form of the external confinement. It is well known from older studies of single-component gases that any external potential that increases more rapidly than quadratically gives rise to vortex states of multiple quantization, for sufficiently weak interactions ([14] and references therein); in contrast, in a harmonic potential, the vortex states are always singly quantized. In the present study, vortex states of multiple quantization result purely because of the interaction between the different components, even in a harmonic external potential. Therefore, our study may serve as an alternative way to achieve such states [15]. It is interesting that in a somewhat different class of solutions found and discussed in [11], the stable vortex core forms part of a stable particle-like soliton.

Secondly, our simulations indicate that multi-component gases do not support persistent currents, in agreement with older studies of homogeneous superfluids [3, 4]. Essentially, the energy barrier that separates the (metastable) state with circulation/flow from the non-rotating state is absent in this case, as the numerical results, as well as the intuitive arguments presented below, suggest. This result has been associated with the $SU(2)$ symmetry of the system that we consider here [16]. While all the studies mentioned above are based on the mean-field approximation, some of our results are based on numerical diagonalization of the many-body Hamiltonian and go beyond the mean-field approximation.

Finally, we investigate the structure of the lowest state of the gas, in the range of the total angular momentum L between zero and $N_{\min} = \min(N_A, N_B)$, where N_A and N_B are the populations of the two species labeled A and B. In this range of L, only the single-particle states with $m = 0$ and 1 are macroscopically occupied, as derived in [17] within the approximation of the lowest Landau level of weak interactions. Remarkably, our numerical simulations within the mean-field approximation, which go well beyond the limit of weak interactions, show that this result is more general.

For simplicity we assume equal masses for the atoms of the two components, $M_A = M_B = M$. Also, we model the elastic collisions between the atoms by a contact potential, with equal scattering lengths for collisions between the same species and different species, $a_{AA} = a_{BB} = a_{AB} = a$ (except in figure 4). Our results are not sensitive to the above equality and hold even if $a_{AA} \approx a_{BB} \approx a_{AB}$, as in rubidium, for example[5]. For the atom populations we assume $N_A \neq N_B$, but $N_A/N_B \lesssim 1$ (without loss of generality). The trapping potential is assumed to be harmonic, $V_{ext}(\mathbf{r}) = M(\omega^2\rho^2 + \omega_z^2 z^2)/2$. Our Hamiltonian is thus

$$\hat{H} = \sum_{i=1}^{N_A+N_B} -\frac{\hbar^2\nabla_i^2}{2M} + V_{ext}(\mathbf{r}_i) + \frac{U_0}{2}\sum_{i\neq j=1}^{N_A+N_B}\delta(\mathbf{r}_i - \mathbf{r}_j), \tag{1}$$

where $U_0 = 4\pi\hbar^2 a/M$. We consider rotation around the z-axis, and also assume that $\hbar\omega_z \gg \hbar\omega$, and $\hbar\omega_z \gg n_0 U_0$, where n_0 is the typical atom density. With these assumptions, our problem becomes effectively two-dimensional (2D), as the atoms reside in the lowest harmonic oscillator

[5] One should be careful with the question of phase separation between the two species, even in the absence of rotation. For zero or weak interactions, both components reside within the lowest Landau level of the harmonic oscillator and there is no phase separation. Even up to the highest value of the interaction strength that we have considered ($\gamma = 50$), we found no phase separation neither for $a_{AA} = a_{BB} = a_{AB}$ nor for $a_{AA} \approx a_{BB} \approx a_{AB}$.

state along the axis of rotation. Thus, there are only two quantum numbers that characterize the motion of the atoms, the number of radial nodes n, and the quantum number m associated with the angular momentum. The corresponding eigenstates of the harmonic oscillator in 2D are labeled $\Phi_{n,m}$.

Within the mean-field approximation, the energy of the gas in the rest frame is

$$E = \sum_{i=\mathrm{A,B}} \int \Psi_i^* \left(-\frac{\hbar^2 \nabla^2}{2M} + V_{\mathrm{ext}}(\mathbf{r}) \right) \Psi_i \, \mathrm{d}^3 r + \frac{U_0}{2} \int (|\Psi_\mathrm{A}|^4 + |\Psi_\mathrm{B}|^4 + 2|\Psi_\mathrm{A}|^2 |\Psi_\mathrm{B}|^2) \, \mathrm{d}^3 r, \tag{2}$$

where Ψ_A and Ψ_B are the order parameters of the two components. By considering variations in Ψ_A^* and Ψ_B^*, we get the two coupled Gross–Pitaevskii-like equations,

$$\begin{aligned} \left(-\frac{\hbar^2 \nabla^2}{2M} + V_{\mathrm{ext}} + U_0 |\Psi_\mathrm{B}|^2 \right) \Psi_\mathrm{A} + U_0 |\Psi_\mathrm{A}|^2 \Psi_\mathrm{A} &= \mu_\mathrm{A} \Psi_\mathrm{A}, \\ \left(-\frac{\hbar^2 \nabla^2}{2M} + V_{\mathrm{ext}} + U_0 |\Psi_\mathrm{A}|^2 \right) \Psi_\mathrm{B} + U_0 |\Psi_\mathrm{B}|^2 \Psi_\mathrm{B} &= \mu_\mathrm{B} \Psi_\mathrm{B}, \end{aligned} \tag{3}$$

where μ_A and μ_B are the chemical potentials of the two components. We use the method of relaxation [18] to minimize the energy of equation (2) in the rotating frame, $E' = E - L\Omega$, where Ω is its angular velocity. Within the method of relaxation one has to specify the initial state. In our simulations, we considered a linear combination of oscillator states or some previously obtained state (e.g. for a slightly different value of some external parameter, like the angular frequency of rotation). Some of the results were computed twice with two different initial states (naturally not all of them were computed twice since these calculations are time-consuming). In all those instances, the two states relaxed to the same final state.

For the diagonalization of the many-body Hamiltonian, we further assume weak interactions, $n_0 U_0 \ll \hbar\omega$, and work within the subspace of the states of the lowest Landau level, with $n = 0$. This condition is not necessary; however, it allows us to consider a relatively larger number of atoms and higher values of the angular momentum. We consider all the Fock states which are eigenstates of the number operators $\hat{N}_\mathrm{A}$, $\hat{N}_\mathrm{B}$ of each species, and of the operator of the total angular momentum $\hat{L}$, and diagonalize the resulting matrix.

Combination of the mean-field approximation and of numerical diagonalization of the many-body Hamiltonian allows us to examine both limits of weak as well as strong interactions. For obvious reasons we use the diagonalization in the limit of weak interactions, and the mean-field approximation (mostly) in the limit of strong interactions. The interaction energy is measured in units of $v_0 = U_0 \int |\Phi_{0,0}(x, y)|^4 |\phi_0(z)|^4 \, \mathrm{d}^3 r = (2/\pi)^{1/2} \hbar\omega a / a_z$, where $\phi_0(z)$ is the lowest state of the oscillator potential along the z-axis, and $a_z = (\hbar / M\omega_z)^{1/2}$ is the oscillator length along this axis. For convenience, we introduce the dimensionless constant $\gamma = N v_0 / \hbar\omega = \sqrt{2/\pi} N a / a_z$, with $N = N_\mathrm{A} + N_\mathrm{B}$ being the total number of atoms, which measures the strength of the interaction.

We first study the limit of weak coupling, $\gamma \ll 1$, and use numerical diagonalization. Considering $N_\mathrm{A} = 4$ and $N_\mathrm{B} = 16$ atoms, we use the conditional probability distributions to plot the density of the two components, for $L = 4$, 16, 28 and 32, as shown in figure 1. When $L = 4 = N_\mathrm{A}$, and $L = 16 = N_\mathrm{B}$, the component whose population is equal to L forms a vortex state at the center of the trap, while the other component does not rotate, residing in the core of the vortex. This is a so-called 'coreless' vortex state [5, 6, 19]. As L increases beyond

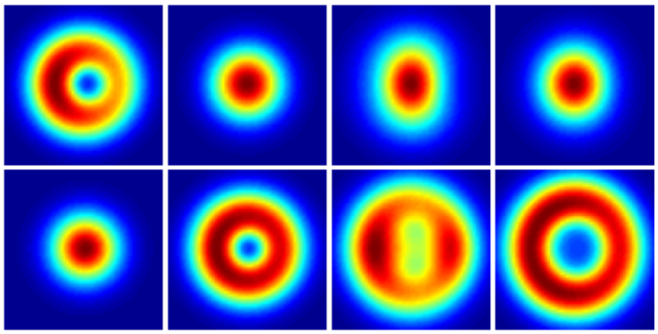

Figure 1. The conditional probability distribution of the two components, with $N_A = 4$ (higher row), and $N_B = 16$ (lower row). Each graph extends between $-2.4a_0$ and $2.4a_0$ in both directions. The reference point is located at $(x, y) = (1.25a_0, 0)$ in the lower graphs (B component), but the pictures are (at least qualitatively) insensitive to its position. The angular momentum L increases from left to right, $L = 4\ (= N_A)$, $16\ (= N_B)$, 28 and $32\ (= 2N_B)$.

$L = N_B = 16$, a second vortex enters component B, and for $L = 2N_B = 32$, this merges with the other vortex to form a doubly quantized vortex state. For this value of $L = 32$, the smaller component A does not carry any angular momentum (apart from corrections of the order of $1/N$). The fact that this is indeed a doubly quantized vortex state is confirmed by the occupancy of the single-particle states. By increasing N_A, N_B, and $L = 2N_B$ proportionally, we observe that the occupancy of the single-particle state with $m = 2$ of component B approaches unity, while the occupancy of all the other states are at most of order $1/N_B$. The same happens for the single-particle state with $m = 0$ of the non-rotating component A.

A similar situation emerges for the case of stronger coupling, $\gamma = 50$, where we have minimized the mean-field energy of equation (2) in the rotating frame (in the absence of rotation the two clouds do not phase separate). For example, we get convergent solutions, shown in figure 2, for $N_B/N_A = 2.777$ and (i): $L_A = N_A$, $L_B = 0$, for $\Omega/\omega = 0.35$ (top left), (ii) $L_A = 0$, $L_B = N_B$, for $\Omega/\omega = 0.45$ (top middle), (iii) $L_A = 0.755N_A$, $L_B = 1.171N_B$, for $\Omega/\omega = 0.555$ (top right), (iv) $L_A = 0$, $L_B = 2N_B$, for $\Omega/\omega = 0.60$ (bottom left), (v) $L_A = 0.876N_A$, $L_B = 2.057N_B$, for $\Omega/\omega = 0.69$ (bottom middle), and (vii) $L_A = 0$, $L_B = 3N_B$, for $\Omega/\omega = 0.73$ (bottom right). Here, L_A and L_B are the angular momenta of the two components, with $L = L_A + L_B$. Again, when $L = 2N_B$, and $L = 3N_B$, the phase plots show clearly a doubly quantized and a triply quantized vortex state in component B, and a non-rotating cloud in component A.

The picture that appears from these calculations is intriguing: as Ω increases, a multiply quantized vortex state of multiplicity κ splits into κ singly quantized ones, and at the same time, one more singly quantized vortex state enters the cloud from infinity. Eventually, all these vortices merge into a multiply quantized one of multiplicity equal to $\kappa + 1$. Figure 2 shows the above results for various values of Ω. Clearly this picture breaks down for larger values of Ω. The vortex states of multiple quantization in the one component are self-consistent solutions of the two coupled Gross–Pitaevskii equations, whose basic characteristic is that the other component does not rotate. For large enough Ω, both components carry a finite fraction of the total angular momentum and vortex states of multiple quantization are no longer energetically favorable. Eventually, both components form vortex lattices, see e.g. [9, 10].

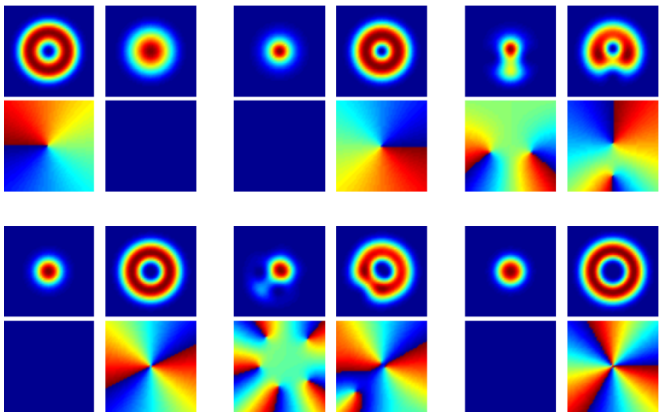

Figure 2. The density (higher graphs of each panel) and the phase (lower graphs of each panel) of the order parameters Ψ_A (left graphs of each panel) and Ψ_B (right graphs of each panel), with $N_B/N_A = 2.777$ and a coupling $\gamma = 50$. Each graph extends between -4.41 and $4.41a_0$ in both directions. The values of the angular momentum per atom and of Ω in each panel are given in the text.

The mechanical stability of states which involve the gradual entry of the vortices from the periphery of the cloud is novel. This behavior is absent in one-component systems, in both harmonic, and anharmonic trapping potentials. In one-component gases, only vortex phases of given rotational symmetry are mechanically stable ([21]; [22] and references therein). In the present problem, the mechanical stability of states with no rotational symmetry (shown in figure 2) is a consequence of the non-negative curvature of the dispersion relation (i.e. of the total energy) $\mathcal{E}(L)$. This observation also connects with the (absence of) metastable, persistent currents (i.e. the second main result of our study), which we present below.

In [17], we have given a simple argument for the presence of vortex states of multiple quantization within the mean-field approximation. At least when the ratio between N_A and N_B is of the order of unity (but $N_A \neq N_B$), there are self-consistent solutions of equations (3) of vortex states of multiple quantization. Within these solutions, the smaller component (say component A) does not rotate, providing an 'effective' external potential $V_{\mathrm{eff,B}}(\mathbf{r}) = V_{\mathrm{ext}}(\mathbf{r}) + U_0 n_A(\mathbf{r})$ for the other one (component B), which is anharmonic close to the center of the trap. This effectively anharmonic potential is responsible for the multiple quantization of the vortex states. Therefore, we conclude that for a relatively small population imbalance, the 'coreless vortices' are vortices of multiple quantization.

The second aspect of our study is the absence of metastable currents (in the laboratory frame, for $\Omega = 0$). A convenient and physically transparent way to think about persistent currents is that they correspond to metastable minima in the dispersion relation $\mathcal{E} = \mathcal{E}(L)$ [22]. A non-negative curvature of $\mathcal{E}(L)$ for all values of L implies the absence of metastability. For all the couplings we have examined, both within the numerical diagonalization and within the mean-field approximation, we have found a non-negative second derivative of the dispersion relation. Figure 3 shows L_A/N_A, L_B/N_B and L/N versus Ω, for $\gamma = 50$. These curves are calculated by minimizing the energy $\mathcal{E}(L)$ in the rotating frame for a fixed Ω and plotting the angular momentum per particle of the corresponding state for the given rotational frequency.

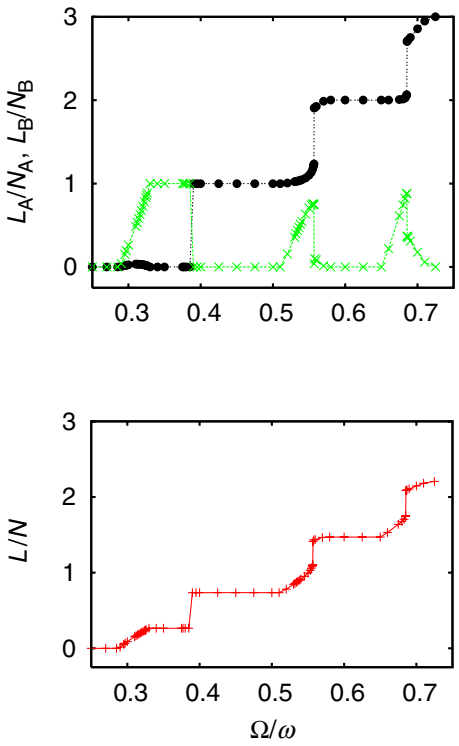

Figure 3. Upper graph: the angular momentum L_A/N_A (crosses) and L_B/N_B (dots), as a function of Ω. Lower graph: L/N as a function of Ω. All curves result from the minimization of the energy in the rotating frame, within the mean-field approximation, for $\gamma = 50$.

Again, our argument for the effective anharmonic potential is consistent with this positive curvature. Let us consider for simplicity $a_{AA} = a_{BB} = 0$ and $a_{AB} \neq 0$. Then, the problem of solving equations (3) becomes essentially a (coupled) eigenvalue problem. If $E_{0,m}$ are the (lowest) eigenvalues of the effective (anharmonic) potential felt by the rotating component for a given angular momentum $m\hbar$, then $\partial^2 E_{0,m}/\partial m^2$ is always positive. For example, if one considers a weakly anharmonic effective potential, $V_{\rm eff}(\rho) = M\omega^2\rho^2[1 + \lambda(\rho/a_0)^{2k}]/2$, where $k = 1, 2, \ldots$ is a positive integer, $a_0 = (\hbar/M\omega)^{1/2}$ is the oscillator length, and $0 < \lambda \ll 1$ is a small dimensionless constant, according to perturbation theory, $E_{0,m} = \hbar\omega[|m| + \lambda(|m| + 1) \ldots (|m| + k)/2]$, which clearly has a positive curvature.

One may gain some physical insight into the absence of persistent currents by understanding the difference between a gas with one and two components. In the case of a single component, for sufficiently strong (and repulsive) interactions, an energy barrier that separates the state with circulation from the vortex-free state may develop. In the simplest model where the atoms rotate in a toroidal trap, in order for them to get rid of the circulation, they have to form a node in their density, which costs interaction energy, and this creates the energy barrier [22, 23]. On the other hand, in the presence of a second component, this node may be filled with atoms of the other species, and therefore the system may get rid of the circulation with no energy expense. This physical picture is also supported by the density plots in figures 2 and 4.

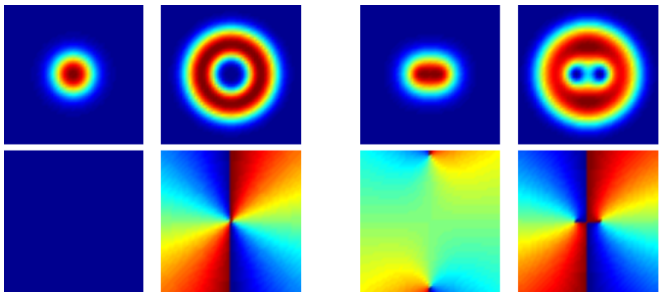

Figure 4. The density (upper graphs) and the phase (lower graphs) of the order parameters Ψ_A (left graphs of each panel) and Ψ_B (right graphs of each panel), with $N_B/N_A = 2.777$. Here, $\Omega/\omega = 0.6$ and $\gamma = 50$. In the left panel, $L_A = 0$ and $L_B/N_B = 2$. In the right panel, the scattering length a_{BB} is twice as large as in the left panel, $a_{BB} = 2a$. In this case, $L_A/N_A = 0.05$ and $L_B/N_B = 1.936$. All graphs extend between -4.41 and $4.41a_0$.

For example, in the case of coreless vortices, the core of the vortex is filled with the other (non-rotating) component [13]. More generally, the density minima of the one component coincide, roughly speaking, with the density maxima of the other component, resulting in a total density $n_{tot} = |\Psi_A|^2 + |\Psi_B|^2$ which does not have any local minima or nodes.

Our third result is based on the mean-field approximation. For $0 \leqslant L \leqslant N_{min}$, where $N_{min} = \min(N_A, N_B)$, the only components of the order parameters Ψ_A and Ψ_B are the single-particle states with $m = 0$ and $m = 1$, i.e.

$$\Psi_A = \sum_n c_{n,0}\Phi_{n,0} + c_{n,1}\Phi_{n,1},$$
$$\Psi_B = \sum_n d_{n,0}\Phi_{n,0} + d_{n,1}\Phi_{n,1}, \tag{4}$$

where $c_{n,0}$, $c_{n,1}$, $d_{n,0}$ and $d_{n,1}$ are functions of L and of the coupling. The numerical simulations that we perform within a range of couplings $\gamma \leqslant 50$ that extend well beyond the lowest-Landau level approximation reveal this very simple structure for the lowest state of both components. Also, the corresponding dispersion relation is numerically very close to a parabola, as in the case of weak interactions [17]. Again, one may attribute these facts to the effective potential that arises from the interaction between the two species [17].

In the studies that have examined a single-component gas in an external anharmonic potential, it has been shown that as the strength of the interaction increases, there is a phase transition from the phase of multiple quantization to the phase of single quantization [21]. In the present case the situation is more complex, since the effective anharmonic potential is generated by the interaction between the two species as a result of a self-consistent solution. Still, a similar phase transition takes place here when, for example, one keeps the scattering lengths a_{AA} and a_{AB} fixed and increases a_{BB} that corresponds to the rotating component. Figure 4 shows the density and the phase of both species, for $a_{AA} = a_{BB} = a_{AB} = a$ (left panel) and $a_{BB} = 2a_{AA} = 2a_{AB} = 2a$ (right panel). Component B undergoes a phase transition from a doubly quantized vortex state to two singly quantized vortices. This phase transition is continuous, second order as in the case of the single component that is confined in an anharmonic trapping potential [24].

To conclude, mixtures of bosons demonstrate numerous novel superfluid properties and provide a model system for studying them. Here, we have given a flavor of the richness of this problem. Many of the results presented in our study are worth investigating further when, for example, one changes the ratio of the populations, the coupling constant between the same and different species, or the masses.

Acknowledgments

We acknowledge financial support from the European Community project ULTRA-1D (NMP4-CT-2003-505457), the Swedish Research Council, the Swedish Foundation for Strategic Research and the NordForsk Nordic Network on 'Low-dimensional physics'. GMK thanks M Magiropoulos for useful discussions.

References

[1] Leggett A J 1999 *Rev. Mod. Phys.* **71** S318
[2] Mermin N D and Ho T-L 1976 *Phys. Rev. Lett.* **36** 594
[3] Bhattacharyya P, Ho T-L and Mermin N D 1977 *Phys. Rev. Lett.* **39** 1290
[4] Ho T-L 1982 *Phys. Rev. Lett.* **49** 1837
[5] Matthews M R, Anderson B P, Haljan P C, Hall D S, Wieman C E and Cornell E A 1999 *Phys. Rev. Lett.* **83** 2498
[6] Leanhardt A E, Shin Y, Kielpinski D, Pritchard D E and Ketterle W 2003 *Phys. Rev. Lett.* **90** 140403
[7] Schweikhard V, Coddington I, Engels P, Tung S and Cornell E A 2004 *Phys. Rev. Lett.* **93** 210403
[8] Williams J E and Holland M J 1999 *Nature* **401** 568
[9] Mueller E J and Ho T-L 2002 *Phys. Rev. Lett.* **88** 180403
[10] Kasamatsu K, Tsubota M and Ueda M 2003 *Phys. Rev. Lett.* **91** 150406
[11] Ruostekoski J 2004 *Phys. Rev.* A **70** 041601
[12] Kasamatsu K, Tsubota M and Ueda M 2005 *Phys. Rev.* A **71** 043611
[13] Kasamatsu K, Tsubota M and Ueda M 2005 *Int. J. Mod. Phys.* B **19** 1835
[14] Fetter A L 2001 *Phys. Rev.* A **64** 063608
Lundh E 2002 *Phys. Rev.* A **65** 043604
[15] Bretin V, Stock S, Seurin Y and Dalibard J 2004 *Phys. Rev. Lett.* **92** 050403
[16] Fetter A L and Svidzinsky A A 2001 *J. Phys.: Condens. Matter* **13** R135
[17] Bargi S, Christensson J, Kavoulakis G M and Reimann S M 2007 *Phys. Rev. Lett.* **98** 130403
[18] Chin S A and Krotscheck E 2005 *Phys. Rev.* E **72** 036705
[19] Blaauwgeers R, Eltsov V B, Krusius M, Ruohio J J, Schanen R and Volovik G E 2000 *Nature* **404** 471
[20] Butts D A and Rokhsar D S 1999 *Nature* **397** 327
[21] Kavoulakis G M and Baym G 2003 *New J. Phys.* **5** 51
[22] Leggett A J 2001 *Rev. Mod. Phys.* **73** 307
[23] Rokhsar D 1997 *Preprint* cond-mat/9709212
[24] Jackson A D, Kavoulakis G M and Lundh E 2004 *Phys. Rev.* A **69** 053619
Jackson A D and Kavoulakis G M 2004 *Phys. Rev.* A **70** 023601

IV
Mixtures of Bose Gases Confined in a Ring Potential

Paper IV

Mixtures of Bose Gases Confined in a Ring Potential

J. Smyrnakis,[1] S. Bargi,[2] G. M. Kavoulakis,[1] M. Magiropoulos,[1] K. Kärkkäinen,[2] and S. M. Reimann[2]

[1]*Technological Education Institute of Crete, P.O. Box 1939, GR-71004, Heraklion, Greece*

[2]*Mathematical Physics, Lund Institute of Technology, P.O. Box 118, SE-22100 Lund, Sweden*

(Received 18 May 2009; revised manuscript received 20 July 2009; published 2 September 2009)

The rotational properties of a mixture of two distinguishable Bose gases that are confined in a ring potential provide novel physical effects that we demonstrate in this study. Persistent currents are shown to be stable for a range of the population imbalance between the two components at low angular momentum. At higher values of the angular momentum, even small admixtures of a second species of atoms make the persistent currents highly fragile.

DOI: 10.1103/PhysRevLett.103.100404 PACS numbers: 67.60.Bc, 03.75.Lm, 03.75.Mn, 05.30.Jp

Introduction.—One of the most fascinating phenomena associated with superfluidity [1] is the stability of persistent currents. In some remarkable experiments that have been performed recently, Bose-Einstein condensed atoms were confined in annular traps [2,3], in which persistent currents could be created and observed [4]. In an earlier experiment, the resistant-free motion of an object through a Bose-Einstein condensate below some critical velocity was also observed [5].

Motivated by these recent advances, in the present study we consider a mixture of two (distinguishable) Bose gases at zero temperature [6,7], that are confined to one dimension with periodic boundary conditions, i.e., in a ring potential, deriving a series of exact and analytic results.

The main issue of our study concerns the rotational properties of this system and the stability of persistent currents. In higher dimensions it has been argued that mixtures of Bose gases do not support persistent currents, because there is no energy cost for the system to get rid of its circulation (i.e., the line integral of the velocity field around a closed loop that encircles the ring), as long as angular momentum can be transferred between the two species [8]. Here, we demonstrate that when the total angular momentum per atom varies between zero and unity, currents are stable for a certain range of the ratio of the populations of the two species. We calculate the critical strength of the coupling for a given value of this ratio, which we determine analytically and exactly. On the other hand, for higher values of the angular momentum per atom, persistent currents in one-component systems are very fragile, as even small admixtures of a second species of atoms destabilize the currents.

Model.—Assuming a ring potential (which corresponds to a very tight annular trap along the transverse direction [9]), the Hamiltonian of the system that we study for the two components that we label as A and B is $H = H_{AA} + H_{BB} + \tilde{U}_{AB}\sum_{i=1,j=1}^{N_A,N_B}\delta(\theta_i - \theta_j)$, where

$$H_{kk} = \sum_{i=1}^{N_k} -\frac{\hbar^2}{2M_kR^2}\frac{\partial^2}{\partial\theta_i^2} + \frac{1}{2}\tilde{U}_{kk}\sum_{i\neq j=1}^{N_k}\delta(\theta_i - \theta_j), \quad (1)$$

with $k = A, B$. Here M_k are the atom masses, while $\tilde{U}_{kk} = 4\pi\hbar^2 a_{kk}/(M_kRS)$ and $\tilde{U}_{AB} = 2\pi\hbar^2 a_{AB}/(M_{AB}RS)$ are the matrix elements for zero-energy elastic atom-atom collisions (all assumed to be positive), with $M_{AB} = M_AM_B/(M_A + M_B)$ being the reduced mass. Also, R is the radius of the annulus and S its cross section, with $R \gg \sqrt{S}$.

We start from the mean-field approximation, introducing the order parameters of the two components ϕ_A and ϕ_B; later we also go beyond the mean-field approximation, diagonalizing the Hamiltonian H numerically and analytically. The resulting (coupled) nonlinear Gross-Pitaevskii-like equations are

$$-\frac{\partial^2\phi_k}{\partial\theta^2} + N_kU_{kk}|\phi_k|^2\phi_k + N_lU_{kl}|\phi_l|^2\phi_k = \mu_k\phi_k, \quad (2)$$

where $\int|\phi_k|^2d\theta = 1$. Here μ_k are the chemical potentials divided by the kinetic energy $\varepsilon = \hbar^2/(2MR^2)$, where we have assumed for simplicity equal masses for the two species, $M_A = M_B = M$. Also, $U_{kl} = \tilde{U}_{kl}/\epsilon$, with $k, l = A, B$.

Energetic stability, dynamic stability, and phase separation.—Before we turn to the rotational properties, let us consider briefly the question of phase separation. In homogeneous systems it has been shown that the condition for energetic stability of the homogeneous solution is [10–12] $U_{AB}^2 - U_{AA}U_{BB} < 0$, and also $U_{AA} > 0$, $U_{BB} > 0$. One may generalize this result for the case of a finite system, taking into account the contribution of the kinetic energy. The details of this calculation will be reported elsewhere. Here we just mention that this more general condition is $\gamma_{AB}^2 - \gamma_{AA}\gamma_{BB} < 1/4 + (\gamma_{AA} + \gamma_{BB})/2$, where we have introduced the parameters $\gamma_{k,l} = U_{k,l}\sqrt{N_kN_l}/(2\pi)$ for convenience (these parameters give the ratio between the typical interaction energy and the typical kinetic energy). As one crosses the phase boundary, the two clouds develop sinusoidal variations in their density, with an amplitude that increases continuously from zero.

The dynamic stability of the system may be examined with use of the (two coupled) Bogoliubov–de Gennes equations. Again, the details of this calculation will be

reported elsewhere. The dispersion that one obtains from this analysis is $\omega^2 = m^4 + m^2(\gamma_{AA} + \gamma_{BB} \pm \sqrt{(\gamma_{AA} - \gamma_{BB})^2 + 4\gamma_{AB}^2})$. The requirement of a real ω implies the same condition as that for energetic stability.

Effect of the periodicity on the dispersion relation.—The one-dimensional motion that we have assumed in our calculation, in combination with the periodic boundary conditions have some important consequences on the dispersion relation, which are also present in the case of a single-component gas, as shown by Bloch [13]. The matrix elements that determine the interaction energy do not depend on the quantum numbers of the angular momentum m, and also the center of mass coordinate separates from the relative coordinates. As a result, solving the problem in the interval $0 \leq l \leq 1$, where $l = (L_A + L_B)/(N_A + N_B)$ is the angular momentum per particle, then exciting the center of mass motion, we may evaluate the spectrum at any other interval $n \leq l \leq n + 1$. More specifically, if $\phi_{A,0} = \sum_m c_m \Phi_m$ and $\phi_{B,0} = \sum_m d_m \Phi_m$ are the order parameters for $0 \leq l \leq 1$, then the order parameters for $n \leq l \leq n + 1$ are given by $\phi_{A,n} = \sum_m c_m \Phi_{m+n}$, and $\phi_{B,n} = \sum_m d_m \Phi_{m+n}$.

Denoting the energy per atom for $n \leq l \leq n + 1$ as $E_n(l)/N$, then $E_n(l)/N = E_0(l_0)/N + n^2 + 2nl_0$, where $0 \leq l_0 \leq 1$, and $l = l_0 + n$. Therefore, $E_n(l)/N - l^2 = E_0(l_0)/N - l_0^2$, which are both equal to a periodic function $e(l)$, i.e., $e(l_0 + n) = e(l_0)$. Thus, we write quite generally that

$$E_n(l)/N = l^2 + e(l) = (l_0 + n)^2 + e(l_0). \quad (3)$$

In other words, the energy of the system for $n \leq l \leq n + 1$ consists of an envelope part, i.e., the first term on the right, which arises because of the center of mass excitation, plus a periodic part $e(l)$.

Furthermore, the function $e(l_0)$ is symmetric around $l_0 = 1/2$ (an example of this symmetry is demonstrated below, where it is shown that E_0/N is linear for $0 \leq l \leq x_B = 1 - x_A$ and $x_A \leq l \leq 1$). To see this, let us consider the states $\phi_A^R = \sum_m c_m \Phi_{1-m}$, and $\phi_B^R = \sum_m d_m \Phi_{1-m}$, with an l' equal to $1 - l$, or $l + l' = 1$. It turns out that the difference in the energy per particle in the states ϕ_A^R, ϕ_B^R, and ϕ_A, ϕ_B is $\Delta E/N = l' - l$. However, according to Eq. (3), $\Delta E/N = l' - l + e(l') - e(l)$, and therefore $e(l') = e(l)$, which means that $e(l_0)$ is indeed symmetric around $l_0 = 1/2$.

Rotational properties.—Since, according to what was mentioned above, the dispersion relation is quasiperiodic, in order to study the rotational properties of the gas, we restrict ourselves to the interval $0 \leq l \leq 1$. We introduce the variables $x_A = N_A/(N_A + N_B)$ and $x_B = N_B/(N_A + N_B)$, and assume without loss of generality that $x_B < x_A$, with $x_A + x_B = 1$. In what follows we also assume equal scattering lengths, and therefore $U_{AA} = U_{BB} = U_{AB} = U$. The condition of equal scattering lengths is not far from reality, with rubidium atoms in different hyperfine states being an example. Interestingly, in this case there is a series of exact, analytic results. If this condition is weakly violated, the deviations from these results will be small.

According to the result mentioned earlier, for $U_{AA} = U_{BB} = U_{AB}$ the gas is in the homogeneous phase, and it is both dynamically, as well as energetically, stable. In this case, we find that for $0 \leq l \leq x_B$ and $x_A \leq l \leq 1$, only the states with Φ_0 and Φ_1 are (macroscopically) occupied. The interaction energy of the gas is equal to that of the nonrotating system, since the total density $n(\theta) = n_A(\theta) + n_B(\theta)$ is homogeneous. As a result, the total energy of the gas varies linearly with l. These are exact results within the mean-field approximation. On the other hand, for $x_B < l < x_A$ more states contribute to the order parameters, while the dispersion relation is not linear in this interval. More specifically, let us consider the states of some fixed expectation value of the angular momentum l, $\phi_{A,0} = c_0\Phi_0 + c_1\Phi_1$, and $\phi_{B,0} = d_0\Phi_0 + d_1\Phi_1$, with $x_A|c_1|^2 + x_B|d_1|^2 = l$, and also $|c_0|^2 + |c_1|^2 = 1$, $|d_0|^2 + |d_1|^2 = 1$. The above states have a maximum value of l equal to unity. Evaluating the total energy E_0 and minimizing it, it turns out that

$$E_0/N = l + \gamma[1/2 + (x_A|c_0||c_1| - x_B|d_0||d_1|)^2], \quad (4)$$

where $N = N_A + N_B$ is the total number of atoms and $\gamma = NU/(2\pi)$. For $0 \leq l \leq x_B$ and $x_A \leq l \leq 1$, the last two terms may be set equal to each other, which means that $E_0/N = l + \gamma/2$. Remarkably, any other single-particle state cannot lower the energy and its occupancy is exactly zero. The occupancies of the single-particle states with $m = 0$ and $m = 1$ are $c_0^2 = (x_A - l)(1 - l)/[x_A(1 - 2l)]$, and $c_1^2 = l(x_B - l)/[x_A(1 - 2l)]$; d_0^2 and d_1^2 are given by similar formulas, with x_A and x_B interchanged. The same expressions hold for a mixtures of two Bose gases that are confined in harmonic traps [14], but in this case the energy is parabolic and not linear in l.

Persistent currents.—Let us now examine the question of stability of persistent currents. In the case of only one component, for $\gamma > 3/2$, the system supports persistent currents at $l = 1$ [15,16]. As we saw earlier, if one starts with $x_A = 1$ and $x_B = 0$ and increases the population of the B component, the dispersion relation is exactly linear for $x_A \leq l \leq 1$. The question is thus whether the dispersion relation has a local minimum at $l = x_A$, where we know the order parameters exactly, i.e., $\phi_{A,0} = \Phi_1$, and $\phi_{B,0} = \Phi_0$. This fact allows us to examine the region just below $l = x_A$ (and the region just above $l = x_B$, if necessary).

More specifically, if $\epsilon = x_A - l$ is a small and positive quantity, one may argue that $c_0^2 \propto c_2^2 \propto \epsilon$, while $d_{-1}^2 \propto d_1^2 \propto \epsilon$. The asymmetry between the two species arises because $c_1 = 1$ and $d_0 = 1$ at $l = x_A$. As a result, for component A, $c_0c_1^2c_2 \propto c_1^2c_2^2$, which implies that $c_2 \propto c_0$, while for component B, $d_{-1}d_0^2d_1 \propto d_{-1}^2d_0^2$, and thus $d_{-1} \propto d_1$. All the other coefficients are of higher order in ϵ, and thus negligible as $l \to x_A^-$. Since the stability of the persistent currents is determined from the slope of the dispersion

relation, we may keep only the terms which are linear in ϵ. Under these assumptions we find that the energy per particle is, up to ϵ,

$$E_0/N - \gamma/2 \approx l + 2x_A c_2^2 + 2x_B d_{-1}^2 + \gamma[x_A(c_0 + c_2) + x_B(d_{-1} + d_1)]^2, \quad (5)$$

where we have expressed c_1 in terms of c_0 and c_2, and d_0 in terms of d_{-1} and d_1 through the normalization conditions. The above expression has to be minimized under the constraint of fixed angular momentum, $l = x_A(c_1^2 + 2c_2^2) + x_B(-d_{-1}^2 + d_1^2) = x_A - \epsilon$. We do this by minimizing the function $E_0/N + \lambda[x_A(c_1^2 + 2c_2^2) + x_B(-d_{-1}^2 + d_1^2)]$, where λ is a Lagrange multiplier. The resulting equation that connects λ, x_A, x_B, and γ is $\lambda(\lambda^2 - 4)[\lambda + 2(x_B - x_A)] = 2\gamma$. For any γ, the above equation has three solutions, two of which are physically relevant. The one appears for $0 \le \lambda \le 2(x_A - x_B) = 2(2x_A - 1)$, which is ≤ 2, and the other one for $\lambda \ge 2$. The first solution gives the critical value of γ, $\gamma_{\rm cr}$, which gives a zero slope of the spectrum E_0/N for $0 \le l \le 1$, at $l = x_A^-$ as function of x_A, namely,

$$\gamma_{\rm cr} = (3/2)/(4x_A - 3). \quad (6)$$

The above expression not only gives the exact value of $\gamma_{\rm cr}$ for $x_A = 1$ and $x_B = 0$ (which is $3/2$, as mentioned earlier), but also for any (allowed) value of x_A. Since the above function diverges for $x_A \to 3/4$, persistent currents are only possible for $3/4 < x_A \le 1$.

In the intervals of higher angular momentum, $n \le l \le n + 1$ with $n \ne 0$, the situation with stability is rather different. According to Eq. (3) the periodic part of the dispersion relation $e(l)$ repeats itself in each of these intervals with a slope that is equal to $(n + 1)^2 - n^2 = 2n + 1 = 3, 5, 7, \ldots$. For $n \ne 0$ one has to use the other solution for $\lambda > 2(x_A - x_B)$. For the case of only one component, $x_A = 1$ and $x_B = 0$, this solution implies that persistent currents are stable for the values $\gamma_{\rm cr} = (2n + 1)(2n + 3)/2$, at $l = n + 1$. While the above states support persistent currents, as soon as x_B becomes nonzero—even if $x_B \to 0$ but finite—the other solution that lies in the interval $0 \le \lambda \le 2(x_A - x_B)$ has a lower energy, and destabilizes the current. In other words, the currents are very fragile with respect to admixtures of a second species of atoms. As a result, the system cannot support persistent currents at any interval other than the first one with $n \ne 0$, for $x_B \ne 0$. Figure 1 shows $\gamma_{\rm cr}$ of Eq. (6), as well as the points corresponding to $\gamma_{\rm cr} = (2n + 1)(2n + 3)/2$ for $n = 1$, 2, and 3.

To gain some physical insight on the above results, we note that for $0 \le l \le 1$, since the system is in the state $\phi_A = \Phi_1$ and $\phi_B = \Phi_0$ at $l = x_A$, it may reduce its angular momentum by either transferring some atoms of species A from Φ_1 to Φ_0, or some atoms of species B from Φ_0 to Φ_{-1}. However, the second option is energetically expensive because the angular momentum of Φ_{-1} is opposite to the angular momentum of the system. In the second interval $1 \le l \le 2$ (and in any higher one) the system is in the state $\phi_A = \Phi_2$ and $\phi_B = \Phi_1$ when $l = 1 + x_A$. In this case, however, the most efficient way for the gas to reduce its angular momentum is to transfer atoms of species B from Φ_1 to Φ_0, and not to transfer atoms of species A from Φ_2 to Φ_1, as in the first interval. It is precisely this asymmetry between the first and any other interval that allows stable persistent currents in the first interval only, but not in any other.

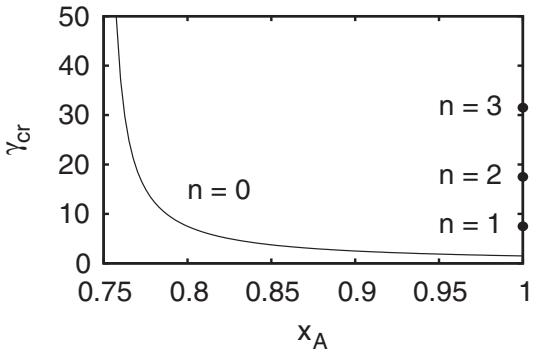

FIG. 1. The critical coupling $\gamma_{\rm cr}$ given by Eq. (6), in the interval $0 \le l \le 1$, as a function of x_A, for a ring potential. The points at $x_A = 1$ show $\gamma_{\rm cr}$ for the higher intervals of l, as explained in the text.

Beyond the mean-field approximation.—To go beyond the mean-field approximation, we have also performed numerical diagonalization of the Hamiltonian for fixed numbers of N_A, N_B, and L units of angular momentum. In the case of one component, we have confirmed the results derived within the mean-field approximation $\gamma_{\rm cr} = 3/2$ for $n = 0$, and $\gamma_{\rm cr} = 15/2$ for $n = 1$. What is even more interesting is the lowest eigenenergy of the Hamiltonian for $N_A = 17$, $N_B = 0$, as well as for $N_A = 15$, $N_B = 2$, in the range $0 \le L \le 38$, including all the single-particle states with $|m| \le 7$, for $U = \pi$, which is shown in Fig. 2 [the corresponding value of γ has to be calculated according to the formula $\gamma = (N - 1)U/(2\pi)$, which gives $\gamma = 8$]. Figure 2 indicates clearly the meta-

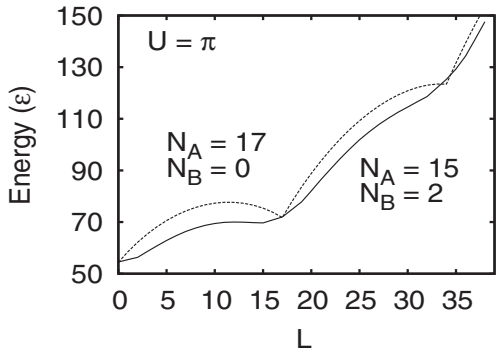

FIG. 2. The lowest eigenenergies of the Hamiltonian for $N_A = 17$, $N_B = 0$ (higher, dashed curve), as well as for $N_A = 15$, $N_B = 2$ (lower, solid curve), with $U = \pi$, in the range $0 \le L \le 38$, in the truncated space of single-particle states with $|m| \le 7$.

stability of the currents for $L = N_A$ and $L = 2N_A$ when there is only one component. With the addition of even a small second component, the local minimum around $L = 2N_A$ disappears, destroying the metastable current, while the minimum around $L = N_A$ still exists [$\gamma_{\rm cr} \approx 2.83$, according to Eq. (6)], in agreement with the mean-field approximation.

We have also found numerically that for $0 \leq L \leq N_B$ (and $N_A \leq L \leq N_A + N_B$), the (whole) excitation spectrum is given by the formula $E_q(L) = L + U/(2\pi)[q^2 + (N + 1 - 2L)q + N(N-1)/2 - L]$, where $q = 0, 1, 2, \ldots$ in the truncated space of single-particle states with $m = 0$ and 1 (the only ones which are macroscopically occupied in the limit of large N). The lowest energy per particle $E_0(L)/N = l + \gamma/2$ agrees with the result of mean field in the limit $N \to \infty$, $L \to \infty$ with $L/N = l$ (finite) and NU finite.

A more specific case of the above spectrum may even be derived analytically with use of the Bogoliubov transformation, for $L = N_B$ (or $L = N_A$), within the same truncated space of the single-particle states with $m = 0$ and 1. Within the Bogoliubov approximation, the Hamiltonian takes the form in this case

$$H = N_B + U/(2\pi)[N(N-1)/2 + (N/2)(a_1^\dagger a_1 + b_0^\dagger b_0) + \sqrt{N_A N_B}(a_1 b_0 + a_1^\dagger b_0^\dagger)], \quad (7)$$

where a_1 is the annihilation operator of a boson of species A with angular momentum $m = 1$, and b_0 is the annihilation operator of species B with $m = 0$. This Hamiltonian is diagonalized with a Bogoliubov transformation, which implies that the eigenvalues are (assuming, for example, that $N_A > N_B$)

$$\mathcal{E}_q(N_B) = N_B + \frac{U}{2\pi}\left[\frac{N}{2}(N-2) + (N_A - N_B)(2q+1)\right]. \quad (8)$$

We then find that the difference $E_q(L = N_B) - \mathcal{E}_q(L = N_B) = Uq(q+1) \propto 1/N$, and thus vanishes for large N.

Conclusions.—This study provides an interesting illustration of the physical origin of persistent currents and, more generally, of superfluidity. The extra degrees of freedom due to the second component, combined with the assumed one-dimensionality and the periodicity of the Hamiltonian, introduce novel physical effects, which have not been known in the physics of the ''traditional'' superfluids.

More specifically, (i) in one-component systems, sufficiently high values of the coupling give rise to persistent currents [1]. In the present case, unless the population of the second species is sufficiently small—in which case one goes back to the one-component case—the second species provides an energetically inexpensive way for the system to get rid of its circulation: the node that is necessary to form in the component that carries the circulation, in order for the circulation to escape from the ring, is filled by the second component, very much like the coreless vortices studied in higher dimensions. (ii) The reduced dimensionality introduces another remarkable effect: while metastability of persistent currents is absent in two-component systems in higher dimensions [8,14], here the assumed one-dimensional motion makes it possible for persistent currents to be stable, at least under specific conditions. (iii) The assumed periodicity in the Hamiltonian reflects itself on the dispersion relation, which is quasiperiodic, as in the one-component problem. On the other hand, while persistent currents corresponding to the first interval of the angular momentum of the quasiperiodic part of the spectrum are stable, for higher values of the angular momentum, persistent currents are highly fragile, even for a very small admixture of a second species. This result is also in sharp contrast to the one-component case.

The results presented in our study definitely deserve experimental investigation, in order for our predictions to be confirmed. One effect that deserves both theoretical, as well as experimental, attention is the deviation from the one-dimensional motion assumed here. One may argue that as this deviation increases, competing mechanisms change the behavior of the system, interpolating between one- and two- or three-dimensional motion, thus giving rise to rich physical effects.

Last but not least, in addition to the above more theoretical remarks, the large degree of tunability of the persistent currents that we have demonstrated here also makes these systems very appealing in terms of future technological applications.

We acknowledge financial support from the Swedish Research Council and the Swedish Foundation for Strategic Research.

[1] A. J. Leggett, Rev. Mod. Phys. **73**, 307 (2001).
[2] S. Gupta *et al.*, Phys. Rev. Lett. **95**, 143201 (2005).
[3] S. E. Olson *et al.*, Phys. Rev. A **76**, 061404(R) (2007).
[4] C. Ryu *et al.*, Phys. Rev. Lett. **99**, 260401 (2007).
[5] C. Raman *et al.*, Phys. Rev. Lett. **83**, 2502 (1999).
[6] E. J. Mueller and T. L. Ho, Phys. Rev. Lett. **88**, 180403 (2002).
[7] V. Schweikhard *et al.*, Phys. Rev. Lett. **93**, 210403 (2004).
[8] Tin-Lun Ho, Phys. Rev. Lett. **49**, 1837 (1982).
[9] Conditions of quasi-one-dimensional motion have already been achieved; see, e.g., A. Görlitz *et al.*, Phys. Rev. Lett. **87**, 130402 (2001).
[10] P. Ao and S. T. Chui, Phys. Rev. A **58**, 4836 (1998).
[11] E. Timmermans, Phys. Rev. Lett. **81**, 5718 (1998).
[12] C. J. Pethick and H. Smith, *Bose-Einstein Condensation in Dilute Gases* (Cambridge University Press, Cambridge, England, 2002).
[13] F. Bloch, Phys. Rev. A **7**, 2187 (1973).
[14] S. Bargi *et al.*, Phys. Rev. Lett. **98**, 130403 (2007).
[15] R. Kanamoto *et al.*, Phys. Rev. A **68**, 043619 (2003).
[16] G. M. Kavoulakis, Phys. Rev. A **69**, 023613 (2004).

V
Persistent Currents in Bose Gases Confined in Annular Traps

Paper V

Persistent currents in Bose gases confined in annular traps

S. Bargi[1], F. Malet[1], G. M. Kavoulakis[2], and S. M. Reimann[1]
[1] *Mathematical Physics, Lund Institute of Technology, P.O. Box 118, SE-22100 Lund, Sweden*
[2] *Technological Educational Institute of Crete, P.O. Box 1939, GR-71004, Heraklion, Greece*
(Dated: August 23, 2010)

We examine the problem of stability of persistent currents in a mixture of two Bose gases trapped in an annular potential. We evaluate the critical coupling for metastability in the transition from quasi-one to two-dimensional motion. We also evaluate the critical coupling for metastability in a mixture of two species as function of the population imbalance. The stability of the currents is shown to be sensitive to the deviation from one-dimensional motion.

PACS numbers: 05.30.Jp, 03.75.-b, 67.60.Bc

I. INTRODUCTION

Bose-Einstein condensates of dilute vapors of atoms offer a very promising testing ground for questions associated with superfluidity for a number of reasons. Firstly, these gases are dilute as opposed, for example, to the "traditional" superfluid liquid helium. Furthermore, the atomic gases can be manipulated in many different ways, including the shape of the confining potential, the strength and the sign of the effective interatomic interaction, the number of different species in multicomponent systems, etc.

While the term "superfluidity" covers a whole collection of many different phenomena [1], we focus in the present study on the metastability of superflow in annular traps [2–6]. Persistent flow has been observed recently in a Bose-Einstein condensate of sodium atoms confined in a toroidal trap [4]. In this experiment, an initial angular momentum of $\hbar$ per particle was transferred to the atoms and the rotational flow was observed to persist for up to ten seconds, limited only by the trap lifetime and other experimental imperfections. Persistent currents with two units of angular momentum were also observed in the same experiment.

Theoretical studies have examined the existence of metastable states in Bose-Einstein condensed gases trapped in single- [7–9] and double-ring-like [10–12] confining potentials. As shown in Ref. [8], mixtures of two components that are confined in a strictly one-dimensional single ring support persistent currents, but the interaction strength necessary for metastability increases with the admixture of the second component. For comparable populations of the two components, the critical value of the coupling becomes infinite. Finally, persistent currents with a value of the circulation higher than one unit were shown to be stable only in single-component systems.

In the present study we investigate the effect of the deviations from purely one-dimensional motion on the metastability of the currents. We also examine two-component Bose-Einstein condensates, and find that it is possible to have metastable superflow for sufficiently small admixtures of the second component. One of the novel results of our study is that in this latter case the deviation from one-dimensional motion gives rise to persistent currents with circulation higher than one unit, as opposed to the purely one-dimensional case.

The paper is organized as follows. We describe in Sec. II our model, and in Sec. III the two methods that we have employed to solve it, i.e., the mean-field approximation and numerical diagonalization of the Hamiltonian. In Sec. IV we present our results. More specifically, in Sec. IV.A we consider the single-component case and study the existence of metastable states in the transition from quasi-one-dimensional to two-dimensional motion. In Sec. IV.B we examine the effect of the admixture of a second component on the stability of the persistent currents, comparing the obtained results with the ones of strictly one-dimensional motion. Finally, we present our summary and conclusions in Sec. V.

II. MODEL

Let us consider two distinguishable species of bosonic atoms, labelled as A and B, with populations N_A and N_B respectively; without loss of generality we assume below that $N_B \leq N_A$. We also assume two-dimensional motion, which in an experiment corresponds to the case of very tight confinement in the perpendicular direction. In the plane of motion we model the annular trap by a displaced harmonic potential,

$$V(\rho) = \frac{1}{2} M\omega^2 (\rho - R_0)^2, \tag{1}$$

which is plotted in Fig. 1. Here ρ is the usual radial variable in cylindrical polar coordinates, R_0 is the radius of the annulus, ω is the trap frequency, and M is the atom mass, which we assume for simplicity to be equal for both species. We stress that the results presented below with the potential of Eq. (1) are – at least qualitatively – similar to the ones that we have obtained using a harmonic-plus-Gaussian trapping potential.

In order to investigate the effects due to the transition from quasi-one-dimensional to two-dimensional motion, we vary the confinement strength ω in the radial direction. For large ω, the confinement is strong enough to freeze out the motion in this direction, which makes the

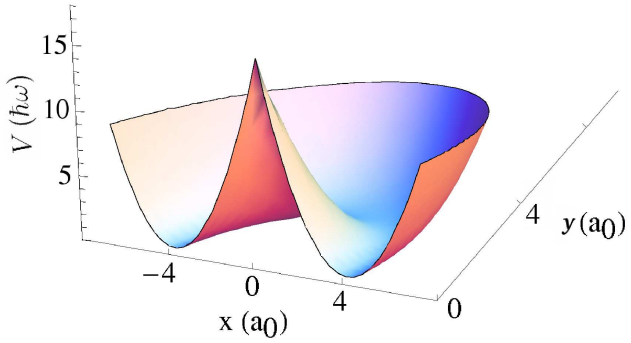

FIG. 1: (Color online) The confining potential V of Eq. (1) as a function of the cartesian coordinates (x, y), for $R_0/a_0 = 4$ and $\omega/\omega_0 = 1$.

system quasi-one-dimensional. As ω decreases, the confinement becomes weaker and, as a result, the motion becomes two-dimensional. In all the calculations presented below we fix the radius of the annulus to $R_0/a_0 = 4$, where $a_0 = \sqrt{\hbar/(M\omega_0)}$ is the ususal oscillator length corresponding to some fixed frequency ω_0.

The interatomic interactions are modelled via the usual effective contact potential, which is assumed to be repulsive. Therefore, the Hamiltonian H of the system is $H = H_{\rm sp} + H_{\rm int}$, where $H_{\rm sp}$ is the single-particle part

$$H_{\rm sp} = \sum_{i=1}^{N} \left(-\frac{\hbar^2}{2M}\nabla_i^2 + V(\mathbf{r}_i) \right), \qquad (2)$$

and $H_{\rm int}$ is the interaction part, given by

$$H_{\rm int} = \frac{u_{AA}}{2} \sum_{i\neq j=1}^{N_A} \delta(\mathbf{r}_i - \mathbf{r}_j) + \frac{u_{BB}}{2} \sum_{i\neq j=1}^{N_B} \delta(\mathbf{r}_i - \mathbf{r}_j) + u_{AB} \sum_{i,j=1}^{N_A,N_B} \delta(\mathbf{r}_i - \mathbf{r}_j). \qquad (3)$$

Here the parameters u_{kl} are proportional to the s-wave scattering lengths for zero-energy elastic atom-atom collisions. For simplicity, we take $u_{AA} = u_{BB} = u_{AB} \equiv u$, which is also experimentally relevant in several cases; furthermore, since the interaction is assumed repulsive, $u > 0$.

III. METHOD

We attack this problem using both the mean-field Gross-Pitaevskii approximation, as well as diagonalization of the many-body Hamiltonian.

Within the diagonalization approach, we fix the particle numbers N_A and N_B and the total angular momentum $L\hbar$, and use the Lanczos method [13] to obtain the eigenenergies and the corresponding eigenvectors. This can be done for a range of the values of L, yielding the dispersion relation $E(L)$, i.e., the smallest eigenvalue for some given L, allowing us to identify the possible local minima associated with the metastable states that give rise to persistent currents in the system.

The basis states that we choose in this approach are the eigenfunctions of the single-particle problem, which are of the form

$$\psi_{n,m}(\rho,\theta) = \frac{e^{im\theta}}{\sqrt{2\pi}} R_{n,m}(\rho). \qquad (4)$$

The quantum number n corresponds to the radial excitations, m is the quantum number associated with the angular momentum, which results from the rotational symmetry of our problem, and θ is the usual angular variable in cylindrical polar coordinates. The radial wavefunctions $R_{n,m}(\rho)$ are evaluated numerically. If $E_{n,m}$ are the corresponding eigenvalues, we work under the assumption that the typical value of the interaction energy $V_{\rm int}$ is weak enough, so that $V_{\rm int} \ll E_{1,0}$. Thus, we set $n = 0$ and the only quantum number that remains is m, whose highest value is chosen so that $V_{\rm int} \lesssim E_{0,m} \ll E_{1,0}$. Having evaluated the single-particle states, these are then combined in all possible ways to form a basis of the Fock states for the many-body problem for some fixed N_A, N_B, and L.

Turning to the mean-field approximation, within this approach the system is described via the two order parameters of the two components, ϕ_A and ϕ_B. From Eqs. (2) and (3) one obtains the two coupled Gross-Pitaevskii-like equations for these two order parameters

$$-\frac{\hbar^2\nabla^2}{2M}\phi_A + V(r)\phi_A + g_{AA}|\phi_A|^2\phi_A + g_{AB}|\phi_B|^2\phi_A = \mu_A\phi_A,$$
$$-\frac{\hbar^2\nabla^2}{2M}\phi_B + V(r)\phi_B + g_{BB}|\phi_B|^2\phi_B + g_{AB}|\phi_A|^2\phi_B = \mu_B\phi_B. \qquad (5)$$

In the above equations the two order parameters are normalized as $\int |\phi_A|^2 d^2\mathbf{r} = 1$, and $\int |\phi_B|^2 d^2\mathbf{r} = N_B/N_A$. The parameters g_{ij} are defined as $g_{AA} = N_A u_{AA}$, $g_{BB} = N_A u_{BB}$, and $g_{AB} = N_A u_{AB}$. Finally, μ_A and μ_B are the chemical potentials of the two components.

To solve Eqs. (5) we make use of a fourth-order split-step Fourier method within an imaginary-time propagation approach [14]. Starting with an initial state with some given angular momentum, the imaginary-time propagation drives the system along the dispersion relation $E(L)$ until it finds a local minimum. If $E(L)$ has such local minima, the final state may be a metastable one. Otherwise, the initial state decays to the non-rotating ground state of the system. One should note that the dissipation of the angular momentum L is inherent to the diffusive character of this method, and it does not contradict the fact that the Hamiltonian commutes with the operator of the angular momentum, since the imaginary-time propagation operator is not unitary, and therefore does not satisfy Heisenberg's equation of motion [15].

The two methods mentioned above complement each other: the diagonalization gives the full dispersion relation $E(L)$ for any fixed angular momentum $L\hbar$, but due to numerical limitations in diagonalizing matrices of large size, one has to restrict the number of particles, as well as the values of the interaction strength. The mean-field Gross-Pitaevskii approach, on the other hand, does not have these limitations, but does not allow us to evaluate the whole dispersion relation $E(L)$ – at least in a straightforward way, but rather its local/absolute minima. Finally, due to its mean-field character, possible correlations between the atoms in certain limiting cases are not captured within this approximation, although they are not expected to be important in the problem that we consider here.

IV. RESULTS

A. Deviation from one-dimensional motion and metastability

We start with the case of a single component, i.e., when the total number of atoms $N = N_A + N_B$ is equal to N_A. We evaluate the minimum interaction strength $g_{\rm min}$ necessary for the system to support persistent currents as a function of the width of the annulus, or equivalently as a function of the confinement frequency ω. As we argued earlier, for large values of ω, the motion becomes quasi-one-dimensional, while as ω decreases, the motion becomes two-dimensional. We solve Eqs. (5) and also diagonalize the Hamiltonian numerically for several values of ω. The results of both calculations are shown in Fig. 2, represented by (black) circles (mean-field) and (red) crosses (diagonalization). As seen from this plot, the results obtained from the two approaches are in good agreement with each other.

At this point it is instructive to see how these data compare with the analytical result of a purely one-dimensional model. To reduce the two-dimensional problem into an effectively one-dimensional one, at least in the limit where the width of the annulus (set by the oscillator length) is much smaller than its radius R_0, one may start from the initial expression for the energy and integrate over the radial degrees of freedom [16]. To simplify this calculation, we assume that the density in the transverse direction is nonzero only for $R_0 - a_{\rm osc}/2 \leq \rho \leq R_0 + a_{\rm osc}/2$, where R_0 is the radius of the annulus and $a_{\rm osc}$ is the oscillator length corresponding to ω. In this limit, the order parameter may be written in a product form,

$$\phi_A(\rho,\theta) = R_A(\rho)\,\Theta_A(\theta). \tag{6}$$

Assuming the above factorization, one may start from the two-dimensional problem and derive the following one-dimensional nonlinear equation

$$-\frac{\hbar^2}{2MR_0^2}\frac{\partial^2\Theta_A(\theta)}{\partial\theta^2} + \frac{g}{a_{\rm osc}R_0}|\Theta_A(\theta)|^2\Theta_A(\theta) = \mu_A\Theta_A(\theta), \tag{7}$$

where the coefficient of the nonlinear term involves the integral $\int |R_A(\rho)|^4\,\rho d\rho$. According to previous studies [17, 18], Eq. (7) implies that the minimum value of the coupling g for metastability of currents with one unit of circulation, i.e., with $2\pi\hbar/M$, is (in the limit $R_0 \gg a_{\rm osc}$)

$$g_{\rm min} \approx \frac{3\pi}{2}\frac{\hbar^2}{M}\frac{a_{\rm osc}}{R_0} = \frac{3\pi}{2}\frac{\hbar^{5/2}}{M^{3/2}}\frac{1}{R_0\sqrt{\omega}}\,, \tag{8}$$

i.e., it scales as $\omega^{-1/2}$. Clearly the numerical prefactor in the above expression depends on the form of the order parameter in the transverse direction $R(\rho)$. If we define $g_0 \equiv \hbar^{5/2}/(M^{3/2}\omega_0^{1/2}R_0)$, this expression may be written in the more convenient form

$$\frac{g_{\rm min}}{g_0} = \frac{3\pi}{2}\sqrt{\frac{\omega_0}{\omega}}\,. \tag{9}$$

Within this simplified model, the obtained power-law dependence of $g_{\rm min}$ scaling as $\omega^{-1/2}$ is in agreement with the numerical results plotted in Fig. 2. This figure shows that $g_{\rm min}$ indeed increases linearly as a function of $(\omega/\omega_0)^{-1/2}$ for strong confinement in the transverse direction, when the motion is quasi-one-dimensional. From the numerical data we also see that for $\omega/\omega_0 \lesssim 1$, $g_{\rm min}$ grows faster, as the extra degrees of freedom associated with the motion in the transverse direction start to play a role. We also notice that for small values of ω, when the confinement becomes weak, the maximum value of the confining potential at the center of the trap decreases. For example, for $\omega/\omega_0 \sim 0.25$, the density of the system is already substantial at the center of the trap, and the deviations from quasi-one-dimensional motion are very pronounced.

B. Population imbalance and metastability

We now turn to the question of metastability in a two-component system. Again, we study the minimum interaction strength for the existence of metastable flow when the atoms are confined in a (two-dimensional) annular trap. To do this, we take $R_0/a_0 = 4$ as before, and consider a fixed and relatively weak confinement $\omega/\omega_0 = 1$, varying $x_A \equiv N_A/(N_A + N_B)$. This can be done easily within the Gross-Pitaevskii scheme, where one can choose any value for the relative population N_A/N_B, but not within the diagonalization approach, where one has to specify the (integer) particle numbers N_A and N_B, and therefore the values of x_A are more restricted. In addition, in order to achieve small steps in x_A, the number of particles has to be fairly large, which results in Hamiltonian matrices of large size, making it hard to diagonalize numerically.

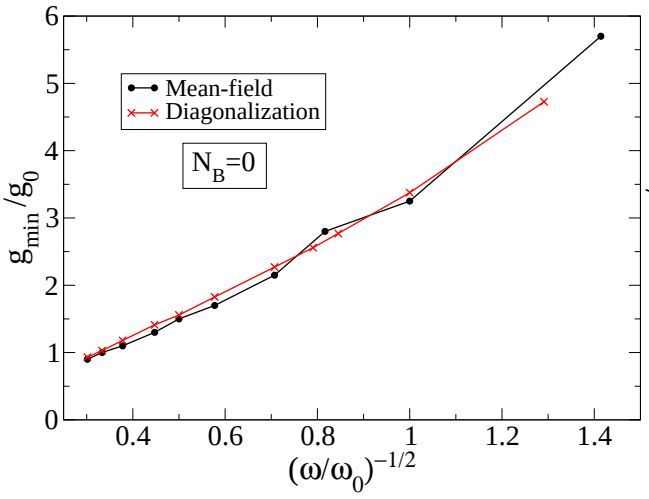

FIG. 2: (Color online) Minimum interaction strength $g_{\rm min}/g_0$ for the existence of persistent currents, as a function of $(\omega/\omega_0)^{-1/2}$ in an annular trap with $R_0/a_0 = 4$. The (black) circles show the result from the mean-field approximation, and the (red) crosses from the diagonalization of the Hamiltonian.

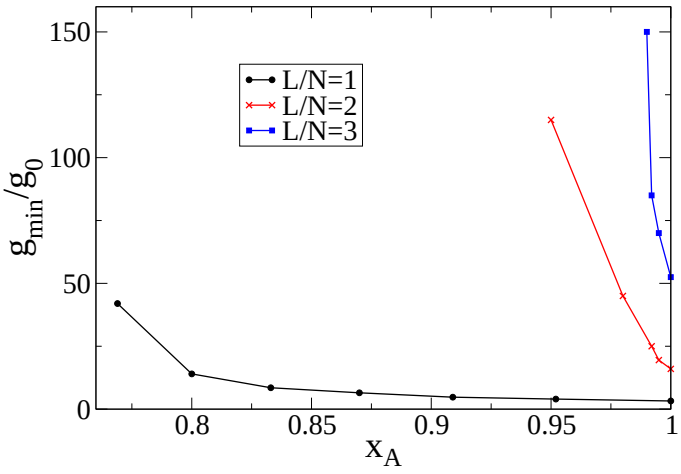

FIG. 3: (Color online) The minimum interaction strength $g_{\rm min}/g_0$ for stability of persistent currents in an annular trap with $R_0/a_0 = 4$ and $\omega/\omega_0 = 1$, as a function of the relative population x_A, obtained within the mean-field approximation. The (black) circles correspond to $L/N = 1$, the (red) crosses to $L/N = 2$, and the (blue) squares to $L/N = 3$.

As before, one can obtain a simple analytic result for $g_{\rm min}$ from the result of a strictly one-dimensional trapping potential [8]. Following the same arguments as in the previous subsection, then Eq. (7) implies that, with the assumption of a step function for the density of the gas in the transverse direction,

$$\frac{g_{\rm min}}{g_0} = \frac{3\pi}{2(4x_A - 3)}\sqrt{\frac{\omega_0}{\omega}}, \qquad (10)$$

which clearly reduces to Eq. (9) when $x_A = 1$. According to this simplified model, $g_{\rm min}$ diverges at $x_A = 3/4$ and thus metastability cannot exist for $x_A \leq 3/4$.

In Fig. 3 we show the numerical results that we obtain for the minimum interaction strength necessary for the existence of metastable states as a function of x_A, within the mean-field approximation. The (black) circles correspond to a value of the angular momentum per particle L/N equal to unity. Our calculations indicate a divergence of $g_{\rm min}$ for sufficiently small values of x_A, pretty much like the one-dimensional case, where this divergence occurs at $x_A = 3/4$. On the other hand, metastability takes place at a stronger interaction strength than in the purely one-dimensional case. Therefore, the deviation from this limit works against the stability of the currents. This result is consistent with the general statement that metastability of the superflow is not possible in trapping potentials which decrease monotonically with the distance from the center of the trap [19].

What has been mentioned so far has to do with values of the circulation equal to one unit, i.e., equal to $2\pi\hbar/M$. According to Ref. [8], in the strictly one-dimensional problem persistent currents with circulation higher than one unit are stable only in the single-component case, i.e., for $x_A = 1$ (or equivalently $N_B = 0$). Interestingly, unlike the one-dimensional case, our mean-field calculations show that persistent currents with a value of the circulation which is higher than one unit are stable for finite admixtures of a second component. This result is shown in Fig. 3 in the two higher curves, represented as (red) crosses, and (blue) squares, corresponding to $L/N = 2$ and $L/N = 3$, respectively.

The two limiting cases of strong and weak confinement are worth commenting on: as one approaches the one-dimensional limit, i.e., when ω increases, the two curves corresponding to higher values of the circulation approach infinity more rapidly, eventually becoming vertical, as in the purely one-dimensional case. Thus, metastability with $L/N = 2$ or $L/N = 3$ is not possible in this limit, in agreement with the results of Ref. [8]. Metastability is not possible, when the confinement becomes very weak, either, i.e., when the width of the annulus gets large, and the gas has a significantly nonzero density at the center of the trap. In other words, the two curves have an infinite slope in the two limiting cases (of small and large values of ω), but have a finite slope for intermediate values, indicating the stability of persistent currents in this regime.

While the behavior of the system looks similar in both limits, the underlying physical origin of the non-monotonic behavior of the slope of these curves is different in the two extremes. In the limit of small ω, this is due to the fact that metastability is absent in an almost homogeneous gas [19]. In the opposite limit of large ω, it is the one-dimensionality of the problem that causes this effect [8].

The results that we have obtained from the numerical

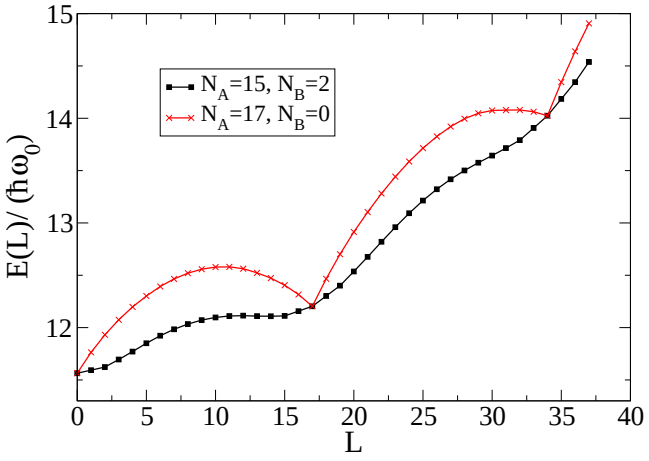

FIG. 4: (Color online) The dispersion relation $E(L)$ obtained from the diagonalization of the Hamiltonian, in a (two-dimensional) annular trap, with $N = 17$ atoms, $\omega/\omega_0 = 1$, $R_0/a_0 = 4$, and $g/g_0 = 30$. The (red) crosses show the single-component case, with $N_A = 17$ and $N_B = 0$ ($x_A = 1$), while the (black) squares correspond to a two-component system, with $N_A = 15$ and $N_B = 2$ ($x_A \approx 0.88$). While in the first case there are two local minima in $E(L)$ at $L/N = 1$ and $L/N = 2$, in the second case there is only one minimum, around $L/N = 1$.

diagonalization of the Hamiltonian are shown in Fig. 4 and are consistent with those of the mean-field approximation. Figure 4 shows the dispersion relation, i.e., the lowest eigenvalue of the Hamiltonian for each value of L, with $x_A = 1$ (red crosses) and $x_A \approx 0.88$ (black squares). More specifically, we have considered $N = 17$ atoms, with $N_A = 17$ and $N_B = 0$ in the one case, and $N_A = 15$ and $N_B = 2$ atoms in the other one. In this calculation the single-particle basis includes all the states with $|m| \leq 5$, and we consider the same parameters as before, with $R_0/a_0 = 4$, $\omega/\omega_0 = 1$, and $g/g_0 = 30$.

The dispersion relation $E(L)$ in the case of a single component has two local minima, at $L/N = 1$ and $L/N = 2$, showing that persistent currents are stable in both cases. This is consistent with the result obtained from the mean-field calculations shown in Fig. 3. On the other hand, in the case of two components, $E(L)$ has only one local minimum around $L/N = 1$. Again, this is consistent with the result of Fig. 3, since for the corresponding values of x_A and $g_{\rm min}/g_0$, only the state with $L/N = 1$ is metastable.

V. SUMMARY AND CONCLUSIONS

According to the present study, Bose-Einstein condensed atoms which move in annular traps offer a very interesting system for the study of persistent currents.

In principle one could investigate a surface in a three-dimensional phase diagram showing the minimum interaction strength for stable currents as function of both the confinement strength ω, which determines the deviation from purely-one-dimensional motion, and the population imbalance x_A. Given the size and the numerical effort of such a calculation, we have instead restricted ourselves to certain parts of this diagram, and in particular we have investigated two different questions.

Firstly, we considered the case of one component, and showed that as the width of the annulus becomes larger, and thus there are deviations from the strictly-one-dimensional motion, the critical coupling $g_{\rm min}$ that is necessary to achieve metastability increases. This result is consistent with the fact that a necessary condition for metastability is that the confining potential – and as a result the particle density – does not decrease monotonically from the center of the trap; in the picture of vortex dynamics, there is a force acting on the vortex that is associated with the rotational motion of the superfluid, which is in the opposite direction of the gradient of the single-particle density distribution.

Secondly, we investigated the case of a mixture of two components, in a fixed annular potential. We found that $g_{\rm min}$ which corresponds to persistent currents with one unit of circulation increases with the addition of the second component. Also, we found a similar behavior as in the one-dimensional problem, where $g_{\rm min}$ diverges at $x_A = 3/4$. Thus, the main effect of the finite width of the annulus is a relative increase in the critical coupling.

On the other hand, a novel result that is absent in the one-dimensional case is the stability of persistent currents with circulation for the larger component which is higher than one unit. When the motion is one-dimensional, $g_{\rm min}$ is infinite, and there are no stable currents. As the width of the annulus increases, these currents become stable for interaction strengths which are sufficiently strong, but finite. When the annulus becomes even wider, $g_{\rm min}$ becomes infinite again. Therefore, the effect of the deviation from the one-dimensional motion is rather dramatic in this case.

From the above results it is clear that the phase diagram $g_{\rm min} = g_{\rm min}(\omega, x_A)$ has an interesting structure and that the physics of persistent currents of Bose-Einstein condensed gases trapped in annular potentials is very rich. With the recent progress in building such trapping potentials in the laboratory, it will be of much interest to investigate all these effects also experimentally.

VI. ACKNOWLEDGEMENTS

This work was financed by the Swedish Research Council. The collaboration is part of the NordForsk Nordic network “Coherent Quantum Gases - From Cold Atoms to Condensed Matter”. GMK acknowledges useful discussions with M. Magiropoulos and J. Smyrnakis.

[1] A. J. Leggett, Rev. Mod. Phys. **73**, 307 (2001).

[2] S. Gupta, K. W. Murch, K. L. Moore, T. P. Purdy, and D. M. Stamper-Kurn, Phys. Rev. Lett. **95**, 143201 (2005).

[3] S. E. Olson, M. L. Terraciano, M. Bashkansky, and F. K. Fatemi, Phys. Rev. A **76**, 061404(R) (2007).

[4] C. Ryu, M. F. Andersen, P. Clad, V. Natarajan, K. Helmerson, and W. D. Phillips, Phys. Rev. Lett. **99**, 260401 (2007).

[5] K. Henderson, C. Ryu, C. MacCormick, and M. G. Boshier, New J. Phys. **11**, 043030 (2009).

[6] I. Lesanovsky and W. von Klitzing, Phys. Rev. Lett. 99, 083001 (2007).

[7] K. Kärkkäinen, J. Christensson, G. Reinisch, G. M. Kavoulakis, and S. M. Reimann, Phys. Rev. A **76**, 043627 (2007).

[8] J. Smyrnakis, S. Bargi, G. M. Kavoulakis, M. Magiropoulos, K. Kärkkäinen, and S. M. Reimann, Phys. Rev. Lett. **103**, 100404 (2009).

[9] P. Mason and N. G. Berloff, Phys. Rev. A **79**, 043620 (2009).

[10] I. Lesanovsky and W. von Klitzing, Phys. Rev. Lett. **98**, 050401 (2007).

[11] J. Brand, T. J. Haigh, and U. Zülicke, Phys. Rev. A **80**, 011602 (2009).

[12] F. Malet, G. M. Kavoulakis, and S. M. Reimann, Phys. Rev. A **81**, 013630 (2010).

[13] C. Lanczos, J. Res. Natl. Bur. Stand. **45**, 255 (1950).

[14] S. A. Chin and E. Krotscheck, Phys. Rev. E **72**, 036705 (2005).

[15] B. H. Bransden and C. J. Joachain, *Introduction to quantum mechanics*, Longman (1989).

[16] A. D. Jackson, G. M. Kavoulakis, and C. J. Pethick, Phys. Rev. A **58**, 2417 (1998).

[17] R. Kanamoto H. Saito, and M. Ueda, Phys. Rev. A **68**, 043619 (2003).

[18] G. M. Kavoulakis, Phys. Rev. A **69**, 023613 (2004).

[19] K. Kärkkäinen, J. Christensson, G. Reinisch, G. M. Kavoulakis, and S. M. Reimann, Phys. Rev. A **76**, 043627 (2007).